AD A102295

LEVEL II

(4)

ACOUSTIC RADIATION AND DIFFRACTION FROM CONVEX AND CONCAVE DOMES

Hideyo Suzuki

Technical Memorandum
File No. TM 81-110
March 21, 1981
Contract No. N00024-79-C-6043

Copy No. 7

DTIC
ELECTE
AUG 0 3 1981
S D
F

The Pennsylvania State University
Intercollege Research Programs and Facilities
APPLIED RESEARCH LABORATORY
Post Office Box 30
State College, PA 16801

DTIC FILE COPY

APPROVED FOR PUBLIC RELEASE
DISTRIBUTION UNLIMITED

NAVY DEPARTMENT

NAVAL SEA SYSTEMS COMMAND

81 7 31 007

(9) Technical report period ending Aug 81

UNCLASSIFIED

SECURITY CLASSIFICATION OF THIS PAGE (When Data Entered)

(14) ARL/PSU

REPORT DOCUMENTATION PAGE

READ INSTRUCTIONS BEFORE COMPLETING FORM

1. REPORT NUMBER: TM-81-110
2. GOVT ACCESSION NO.: AD-A102 295
3. RECIPIENT'S CATALOG NUMBER:

4. TITLE (and Subtitle): (6) ACOUSTIC RADIATION AND DIFFRACTION FROM CONVEX AND CONCAVE DOMES
5. TYPE OF REPORT & PERIOD COVERED: Ph.D, Thesis, August 1981
6. PERFORMING ORG. REPORT NUMBER: TM 81-110

7. AUTHOR(s): (10) Hideyo Suzuki
8. CONTRACT OR GRANT NUMBER(s): (15) N00024-79-C-6043

9. PERFORMING ORGANIZATION NAME AND ADDRESS:
The Pennsylvania State University
Applied Research Laboratory, P. O. Box 30
State College, PA 16801

10. PROGRAM ELEMENT, PROJECT, TASK AREA & WORK UNIT NUMBERS: (11) 21 Mar 81

11. CONTROLLING OFFICE NAME AND ADDRESS:
Naval Sea Systems Command
Department of the Navy
Washington, DC 20362

12. REPORT DATE: March 21, 1981
13. NUMBER OF PAGES: 145 pages & figures

14. MONITORING AGENCY NAME & ADDRESS (if different from Controlling Office): 12 63

15. SECURITY CLASS. (of this report): Unclassified, Unlimited
15a. DECLASSIFICATION/DOWNGRADING SCHEDULE:

16. DISTRIBUTION STATEMENT (of this Report)

Approved for public release, distribution unlimited,
per NSSC (Naval Sea Systems Command), 6/23/81.

17. DISTRIBUTION STATEMENT (of the abstract entered in Block 20, if different from Report)

18. SUPPLEMENTARY NOTES

19. KEY WORDS (Continue on reverse side if necessary and identify by block number)

acoustic, radiation, diffraction

20. ABSTRACT (Continue on reverse side if necessary and identify by block number)

The effects of the diaphragm shape of a loudspeaker on the radiation and diffraction characterisitcs are discussed using convex and concave domes in an infinite baffle. The least square error method, one of the weighted residual methods, is employed as the mathematical tool for the solution of the problems.

The results show that these characteristics are highly dependent on the shape of the diaphragm, even if it vibrates like a piston. The response

DD FORM 1 JAN 73 1473 EDITION OF 1 NOV 65 IS OBSOLETE

UNCLASSIFIED

SECURITY CLASSIFICATION OF THIS PAGE (When Data Entered)

391 997

of the concave dome has a wide peak due to the cavity resonance, resulting in higher radiation efficiency. The convex dome has lower on-axis pressure response in the same region due to the dispersion of energy to the off-axis direction.

The diffraction of sound from a concrete ring source by the convex and concave domes is also investigated in order to discuss the interaction between the loudspeaker units of a complete system. The convex dome has much larger diffraction effects than the concave dome, especially in the high-frequency region. It is shown that even the concave dome produces a discernible amount of amplitude distortion of sound radiated from an adjacent source.

The radiation and diffraction phenomena are well explained by the use of a graphical representation of the energy flow and pressure distribution.

Accession For
NTIS GRA&I
DTIC TAB
Unannounced
Justification
By
Distribution/
Availability Codes
Avail and/or
Dist Special
A

ABSTRACT

The effects of the diaphragm shape of a loudspeaker on the radiation and diffraction characteristics are discussed using convex and concave domes in an infinite baffle. The least square error method, one of the weighted residual methods, is employed as the mathematical tool for the solution of the problems.

The results show that these characteristics are highly dependent on the shape of the diaphragm, even if it vibrates like a piston. The response of the concave dome has a wide peak due to the cavity resonance, resulting in higher radiation efficiency. The convex dome has lower on-axis pressure response in the same region due to the dispersion of energy to the off-axis direction.

The diffraction of sound from a concentric ring source by the convex and concave domes is also investigated in order to discuss the interaction between the loudspeaker units of a complete system. The convex dome has much larger diffraction effects than the concave dome, especially in the high-frequency region. It is shown that even the concave dome produces a discernible amount of amplitude distortion of sound radiated from an adjacent source.

The radiation and diffraction phenomena are well explained by the use of a graphical representation of the energy flow and pressure distribution.

TABLE OF CONTENTS

		Page
ABSTRACT		iii
LIST OF FIGURES		vi
LIST OF SYMBOLS		xii
ACKNOWLEDGMENTS		xv
CHAPTER		
I	INTRODUCTION	1
	1.1 Background	1
	1.2 Previous Studies	2
	1.3 Statement of the Problem	6
II	RADIATION FROM CONVEX AND CONCAVE DOMES	8
	2.1 Geometrical Model	8
	2.1.1 Convex Dome	8
	2.1.2 Concave Dome	10
	2.2 Mathematical Discussions	12
	2.2.1 Basic Equations for Radiation Problem	12
	2.2.2 Least Square Error Method	13
	2.2.3 Radiation from a Convex Dome	15
	2.2.4 Radiation from a Concave Dome	18
	2.2.5 Geometrical Approximation Method	22
	2.3 Results and Discussions	24
	2.3.1 On-axis Pressure Response	24
	2.3.2 Radiation Impedance	34
	2.3.3 Phase Response	40
	2.3.4 Directivity Pattern	51
	2.3.5 Energy Flow and Pressure Distribution	65
	2.3.6 Comparison of Results with Other Methods	86
III	DIFFRACTION BY CONVEX AND CONCAVE DOMES	90
	3.1 Geometrical Model	90
	3.2 Mathematical Discussions	93
	3.2.1 Diffraction by a Convex Dome	93
	3.2.2 Diffraction by a Concave Dome	96
	3.3 Results and Discussions	100
	3.3.1 On-axis Pressure Response	100
	3.3.2 Directivity Pattern	110
	3.3.3 Energy Flow and Pressure Distribution	118

LIST OF CONTENTS (continued)

IV CONCLUSION 127

4.1 Remarks on the Mathematical Method. . . . 127
4.2 Summary of Results. 129
4.3 Future Work 131
4.3.1 Modal Vibration of a Diaphragm. . . 131
4.3.2 Diaphragm Shape other than a Dome . 131
4.3.3 Three-Dimensional Problem 132

APPENDIX A: Derivation of Equation (2.12) from Equation (2.11) 134

APPENDIX B: Another Solution to Radiation Problem from a Convex Dome. 135

APPENDIX C: Nonexistence and Nonuniqueness Problems of a Series Expansion of the Sound Field. 138

APPENDIX D: Acoustic Center of a Line Source. 141

REFERENCES 143

LIST OF FIGURES

Figure		Page
2.1	Geometry of the convex dome radiator.	9
2.2	Geometry of the concave dome radiator	11
2.3	Far-field on-axis pressure responses of a convex dome radiator.	25
2.4	Far-field on-axis pressure responses of convex and concave domes obtained by the geometrical approximation	27
2.5	Far-field on-axis pressure responses of a convex dome with H/A = 0.5 obtained by the least square error method (LSM) and the geometrical approximation method (GAM).	28
2.6	Far-field on-axis pressure responses of a convex dome with H/A = 0.75 obtained by the least square error method (LSM) and the geometrical approximation method (GAM).	29
2.7	Far-field on-axis pressure responses of a convex dome with H/A = 1.0 obtained by the least square error method (LSM) and the geometrical approximation mehtod (GAM).	30
2.8	Far-field on-axis pressure responses of a concave dome with H/A = 0.5 obtained by the least square error method (LSM) and the geometrical approximation method (GAM).	31
2.9	Far-field on-axis pressure responses of a concave dome with H/A = 0.75 obtained by the least square error method (LSM) and the geometrical approximation (GAM)	32
2.10	Far-field on-axis pressure responses of a concave dome with H/A = 1.0 obtained by the least square error method (LSM) and the geometrical approximation (GAM)	33
2.11	Radiation resistance characteristics of a convex dome and a flat piston (normalized by $\rho c \pi A^2$).	36
2.12	Radiation reactance characteristics of a convex dome and a flat piston (normalized by $\rho c \pi A^2$).	37

LIST OF FIGURES (continued)

Figure		Page
2.13	Radiation resistance characteristics of a convex dome and a flat piston (normalized by $\rho c \pi A^2$)	38
2.14	Radiation reactance characteristics of a convex dome and a flat piston (normalized by $\rho c \pi A^2$)	39
2.15	Radiation impedance characteristics of a concave dome with H/A = 0.5 (normalized by $\rho c \pi A^2$)	41
2.16	Radiation impedance characteristics of a concave dome with H/A = 0.75 (normalized by $\rho c \pi A^2$)	42
2.17	Radiation impedance characteristics of a concave dome with H/A = 1.0 (normalized by $\rho c \pi A^2$)	43
2.18	Radiation resistance characteristics of a concave dome (normalized by $\rho c \pi A^2$)	44
2.19	Phase responses of a convex dome	45
2.20	Phase responses of a concave dome	46
2.21	Acoustic center of a convex dome	49
2.22	Acoustic center of a concave dome	50
2.23	Directivity patterns of a convex dome and a flat piston at kA = 1.0	52
2.24	Directivity patterns of a convex dome and a flat piston at kA = 2.0	53
2.25	Directivity patterns of a convex dome and a flat piston at kA = 3.0	54
2.26	Directivity patterns of a convex dome and a flat piston at kA = 5.0	55
2.27	Directivity patterns of a convex dome and a flat piston at kA = 7.0	56
2.28	Directivity patterns of a convex dome and a flat piston at kA = 10.0	57

LIST OF FIGURES (continued)

Figure		Page
2.29	Directivity patterns of a concave dome and a flat piston at kA = 1.0	58
2.30	Directivity patterns of a concave dome and a flat piston at kA = 2.0	59
2.31	Directivity patterns of a concave dome and a flat piston at kA = 3.0	60
2.32	Directivity patterns of a concave dome with H/A = 1.0 at kA = 4.15	61
2.33	Directivity patterns of a concave dome and a flat piston at kA = 5.0	62
2.34	Directivity patterns of a concave dome and a flat piston at kA = 7.0	63
2.35	Directivity patterns of a concave dome and a flat piston at kA = 10.0	64
2.36	Energy flow and pressure distribution of a convex dome with H/A = 0.5 at kA = 1.0 . . .	67
2.37	Energy flow and pressure distribution of a convex dome with H/A = 0.5 at kA = 3.0 . . .	68
2.38	Energy flow and pressure distribution of a convex dome with H/A = 0.5 at kA = 10.0 . . .	69
2.39	Energy flow and pressure distribution of a convex dome with H/A = 0.75 at kA = 1.0 . . .	70
2.40	Energy flow and pressure distribution of a convex dome with H/A = 0.75 at kA = 3.0 . . .	71
2.41	Energy flow and pressure distribution of a convex dome with H/A = 0.75 at kA = 10.0 . .	72
2.42	Energy flow and pressure distribution of a convex dome with H/A = 1.0 at kA = 1.0 . . .	73
2.43	Energy flow and pressure distribution of a convex dome with H/A = 1.0 at kA = 3.0 . . .	74
2.44	Energy flow and pressure distribution of a convex dome with H/A = 1.0 at kA = 10.0 . . .	75

LIST OF FIGURES (continued)

Figure		Page
2.45	Energy flow and pressure distribution of a concave dome with H/A = 0.5 at kA 1.0	76
2.46	Energy flow and pressure distribution of a concave dome with H/A = 0.5 at kA = 3.0 . . .	77
2.47	Energy flow and pressure distribution of a concave dome with H/A = 0.5 at kA = 10.0 . .	78
2.48	Energy flow and pressure distribution of a concave dome with H/A = 0.75 at kA = 1.0 . .	79
2.49	Energy flow and pressure distribution of a concave dome with H/A = 0.75 at kA = 3.0 . .	80
2.50	Energy flow and pressure distribution of a concave dome with H/A = 0.75 at kA = 10.0 . .	81
2.51	Energy flow and pressure distribution of a concave dome with H/A = 1.0 at kA = 1.0 . . .	82
2.52	Energy flow and pressure distribution of a concave dome with H/A = 1.0 at kA = 3.0 . . .	83
2.53	Energy flow and pressure distribution of a concave dome with H/A = 1.0 at kA = 4.15 . .	84
2.54	Energy flow and pressure distribution of a concave dome with H/A = 1.0 at kA = 10.0 . .	85
2.55	Far-field on-axis pressure responses of a convex dome and an oblate spheroid.	87
2.56	Far-field on-axis pressure responses of a concave dome obtained by the least square error method (LSM) and the finite element method (FEM).	89
3.1	Geometry of a ring source with a concentric convex dome in an infinite baffle	91
3.2	Geometry of a ring source with a concentric concave dome in an infinite baffle.	92
3.3	Far-field on-axis pressure responses of a ring source with a concentric convex dome for H/A = 0.5 and A_1/A = 1.5	101

LIST OF FIGURES (continued)

Figure		Page
3.4	Far-field on-axis pressure responses of a ring source with a concentric convex dome with H/A = 0.75 and A_1/A = 1.5	102
3.5	Far-field on-axis pressure responses of a ring source with a concentric convex dome with H/A = 1.0 and A_1/A = 1.5	103
3.6	Far-field on-axis pressure responses of a ring source with a concentric concave dome with H/A = 0.5 and A_1/A = 1.5	104
3.7	Far-field on-axis pressure responses of a ring source with a concentric concave dome with H/A = 0.75 and A_1/A = 1.5	105
3.8	Far-field on-axis pressure responses of a ring source with a concentric concave dome with H/A = 1.0 and A_1/A = 1.5	106
3.9	Far-field on-axis pressure responses of a ring source with a concentric concave dome with H/A = 0.5 and A_1/A = 2.0	107
3.10	Far-field on-axis pressure responses of a ring source with a concentric concave dome with H/A = 0.75 and A_1/A = 2.0	108
3.11	Far-field on-axis pressure responses of a ring source with a concentric concave dome with H/A = 1.0 and A_1/A = 2.0	109
3.12	Differences of the far-field on-axis pressure responses of a ring source with a concentric concave dome with A_1/A = 1.5 when H/A is changed by $\pm$0.02 from H/A = 0.5	111
3.13	Directivity patterns of a ring source with a concentric convex dome and a flat piston for H/A = 1.0 and A_1/A = 1.5 at kA = 1.6 . .	112
3.14	Directivity patterns of a ring source with a concentric convex dome and a flat piston for H/A = 1.0 and A_1/A = 1.5 at kA = 7.5 . .	113
3.15	Directivity pattern of a ring source with a concentric convex dome for H/A = 1.0 and A_1/A = 1.5 at kA = 12.0	114

LIST OF FIGURES (continued)

Figure		Page
3.16	Directivity patterns of a ring source with a concentric concave dome and a flat piston for H/A = 1.0 and A_1/A = 1.5 at kA = 1.2 . .	115
3.17	Directivity patterns of a ring source with a concentric concave dome and a flat piston for H/A = 1.0 and A_1/A = 1.5 at kA = 4.6 . .	116
3.18	Directivity patterns of a ring source with a concentric concave dome and a flat piston for H/A = 1.0 and A_1/A = 1.5 at kA = 10.0 . .	117
3.19	Energy flow and pressure distribution of a ring source with a concentric convex dome for H/A = 1.0 and A_1/A = 1.5 at kA = 1.6 . .	119
3.20	Energy flow and pressure distribution of a ring source with a concentric convex dome for H/A = 1.0 and A_1/A = 1.5 at kA = 7.4 . .	120
3.21	Energy flow and pressure distribution of a ring source with a concentric convex dome for H/A = 1.0 and A_1/A = 1.5 at kA = 12.0 . .	121
3.22	Energy flow and pressure distribution of a ring source with a concentric concave dome for H/A = 1.0 and A_1/A = 1.5 at kA = 1.2 . .	122
3.23	Energy flow and pressure distribution of a ring source with a concentric concave dome for H/A = 1.0 and A_1/A = 1.5 at kA = 4.6 . .	123
3.24	Energy flow and pressure distribution of a ring source with a concentric concave dome for H/A = 1.0 and A_1/A = 1.5 at kA = 10.0 . .	124
3.25	Energy flow and pressure distribution of the sound field in a rectangular room consisting of (3,1,0) and (1,2,0) modes . . .	126

LIST OF SYMBOLS

A	radius of the dome
A_1	radius of the ring source
A( )	amplitude function
H	height of the dome
H( )	transfer function
I_o, I_x, I_z	intensity
Im	imaginary part
J	error function
L	operator of the boundary condition
O, O_1	origin of coordinate system
P( )	prescribed pressure distribution on the radiator surface
P_n( ), P_n'( )	Legendre function of the first kind and order n, and its derivative
Q	source strength per unit length
R	radius of the sphere
Re	real part
R_1	distance from the origin O_1 to the ring source
S, $S^{(1)}$, $S^{(2)}$	surface where the boundary condition is imposed
U( )	prescribed velocity distribution on the radiator surface
U_o	amplitude of the velocity
a_n	unknown coefficient
c	sound velocity of the fluid
d, d_1 d_2	distance function
dS	element of surface integration

LIST OF SYMBOLS (continued)

e	basis of natural logarithm
f, $f^{(1)}$, $f^{(2)}$	prescribed function of the boundary condition
$h_n(\ )$, $h_n'(\ )$	spherical Hankel function of the second kind and order n, and its derivative
i	imaginary unit
$j_n(\ )$, $j_n'(\ )$	spherical Bessel function of order n, and its derivative
k	wavenumber
ℓn	natural logarithm
log	common logarithm
l_x, l_y	lengths of two-dimensional room
m, n	orders of functions and unknown coefficients
$\bar{n}$	unit outward normal to the surface
$n_n(\ )$, $n_n'(\ )$	spherical Neumann function of order n, and its derivative
$p(\ )$	pressure distribution in the field
p_n	n^{th} component of the pressure distribution
$q(\ )$	weighting function
r, r', r_1, r_2, f	radius of the spherical coordinate system
$\bar{u}(\ )$	vector field of particle velocity
$u_B(\ )$	velocity distribution on the opening of the cavity
u_n	n^{th} component of the velocity distribution
(x,y,z)	rectangular coordinate system
z_o	distance between O and O_1
z_r	radiation impedance

LIST OF SYMBOLS (continued)

$\Psi_n(\ )$	function defined by $L\psi_n(\ )$
ζ	point on the boundary surface
θ_o	cone angle of the dome
$\theta, \theta', \theta_1, \theta_2$	cone angle of the spherical coordinate system
ξ	field point
ρ	density of the medium
ρ_m	density of the material
$\phi, \phi', \phi_1, \phi_2$	azimuthal angle of the spherical coordinate system
$\phi(\ )$	phase response
$\psi(\ )$	velocity potential in the field
$\psi_n(\ )$	n^{th} component of the velocity potential
ω, ω'	angular frequency
∇	gradient operator
∇^2	Laplacian operator
∂	differentiator
$*$	complex conjugate

ACKNOWLEDGMENTS

The author wishes to thank Dr. Jiri Tichy, Chairman of the Graduate Program in Acoustics, for his constant advice and encouragement throughout this work.

The author is deeply indebted to Dr. Francis H. Fenlon, Associate Professor of Engineering Science, and to Dr. William Thompson, Jr., Associate Professor of Acoustical Mechanics, for their invaluable advice and suggestions. The author greatly appreciate the constructive criticism of this work by Dr. Vernon H. Neubert, Professor of Engineering Mechanics, and Dr. Alan D. Stuart, Research Associate in the Applied Research Laboratory.

Special appreciation goes to Karen W. Gottschall for her dedication and assistance to the author in fulfilling the requirements for the doctoral degree. The author wishes to thank Dorothy L. Tindall and the students in the graduate Program in Acoustics for editing and improving the manuscript.

This research was supported by the Applied Research Laboratory of The Pennsylvania State University under Contract with the U.S. Naval Sea Systems Command.

CHAPTER I

INTRODUCTION

1.1 Background

The cone-type loudspeaker has been used since the birth of the direct radiator loudspeaker. The reason for this is the mechanical strength against the force given through the voice-coil due to its diaphragm shape. A paper cone, because of its satisfactory properties such as relatively large Young's modulus-to-density ratio (E/ρ_m) and high loss factor, has been used as the main loudspeaker diaphragm of the direct radiator loudspeaker. But as far as paper being used as a diaphragm material, E/ρ_m does not have enough margin for us to try a flat or a very shallow diaphragm.

The situation has been changed, however, since composite materials with large E/ρ_m have come into use. With these materials, it has become possible to try any kind of diaphragm shape, even the flat diaphragm. At this point, we naturally come to the question, "What is the best shape for a radiator?" The diaphragm shape has effects on both the vibration characteristics and the radiation characteristics. These latter effects, however, have not had much attention paid to them up until now. This is our motivation to investigate the relation between the convex or concave diaphragm in an infinite baffle and its radiation

characteristics.

Other interesting phenomena are found in the interactions between loudspeaker units in a loudspeaker system. The sound emitted from a high-frequency unit is diffracted by a (normally concave) low-frequency unit. This effect causes the modification of the on- and off-axis pressure responses of the high-frequency unit. This diffraction is also responsible for an amplitude-modulated distortion of the high-frequency sound when the diaphragm of the low-frequency unit vibrates with a large excursion. These static and dynamic interactions between each unit of the loudspeaker system are important topics that need investigation if improvements on loudspeaker design are to be made. Another example of this kind of phenomenon is the diffraction of noise by a convex or a concave object on a plane. The diffraction of noise will change the pressure distribution around the object, and if the noise source is close to this object, it may also change the total radiated power from the noise source. Thus, the diffraction of sound from a source adjacent to a convex or a concave object in an infinite baffle are of great interest.

1.2 Previous Studies

The radiation problems from convex and concave objects are quite different from each other in the way they are solved. The radiation from a convex object in an

infinite baffle is equivalent to the radiation from a radiator with a symmetric radiator in the other semi-infinite space. On the other hand, the radiation problem from a concave dome in an infinite baffle must be solved in a semi-infinite space. The studies on the radiation from a radiator of finite size in an infinite space are reviewed first.

The radiation from a complete sphere or spheroid is the one to which the method of separation of variables is applicable. The solution to this kind of problem is found in many books such as [1]-[5]. One of the interesting researches in this field was achieved by Ikegaya [6]. As one of his problems, he investigated the radiation from an oblate spheroid, assuming that it can be well approximated by a portion of a sphere in an infinite baffle. The results show that the on-axis response is highly dependent on the height-to-radius ratio. These results are compared with our results later.

Three distinct methods of integral forms have been reported to obtain numerical solutions of the problems of acoustic radiation from an arbitrary body, the simple source method, the surface Helmholtz integral equation, and the internal Helmholtz integral equation. The simple source method was employed by Chen and Schweikert [7], and McCormick and Baron [8]. Chen and Schweikert, assuming a distribution of simple sources over the radiator surface, gave the formulation of the radiation problem from a shell

in an infinite medium. McCormick and Baron utilized dynamic influence coefficients from the vibration in vacuum of the shell and a potential source theory approach for the fluid to discuss the radiation from a cylindrical shell of finite length. Chertock [9] investigated the sound radiation from a body of arbitrary shape using the surface Helmholtz integral equation. The third method was used by Copley [10], who adopted the internal Helmholtz integral equation which results when the field point lies within the surface of the radiator. As Copley [11] and Schenck [12] pointed out, however, the first two methods fail to provide unique solutions when the frequency is approximately equal to any of the characteristic frequencies. Schenck, showing that the third method is subject to similar difficulties and has undesirable computational characteristic, proposed a modified Helmholtz integral equation formulation in the same paper.

A quite different approach was applied on the radiation problem from a finite cylinder by Williams, Parke, Moran, and Sherman [13]. They expressed the pressure field in terms of spherical wave functions with unknown coefficients. Then, using the least square error method, the unknown coefficients were determined from the boundary condition. The same method was used to solve a radiation problem of a piston set in a sphere by Thompson and Skudrzyk [14]. Fenlon [15] discussed the radiation field at the surface of a finite cylinder, applying the method of weighted residuals

on the internal Helmholtz integral equation. Hunt, Knittel, and Barach [16] employed the finite element method for the vibrational characteristics of the elastic body and the acoustic pressure field enclosing the radiator. They used the analytical method to obtain the boundary conditions for this mathematical model.

To the author's knowledge, very few studies on the radiation from a concave object in an infinite baffle have been discussed. Ohie, Suzuki, and Shindo [17] discussed the radiation from a concave sound source in an infinite baffle, where the space inside the truncated cone was approximated by the stairwise combination of thin cylinders, and cylindrical wave functions were used in each cylinder. The same kind of problem was investigated by Shindo, Kyono, Yashima, Yamabuchi, and Kagawa [18] using the finite element method. The same method was used by Sakai, Kyono, Morita, Yamabuchi, and Kagawa [19] for the investigation of radiation from a horn loudspeaker.

Problems of acoustic diffraction or scattering by a sphere, an infinite cylinder, or a spheroid are found in many articles such as [20]-[25], in which the analytical method is applicable. Another technique, the integral equation approach, has been used by Burke, Miller, Poggie, Pjerrou, Maxum, and Meecham [26] for the scattering by an elastic body. Hunt, Knittel, Nichols, and Barach [27] used the finite element approach to acoustic scattering from an elastic circular plate. Most of these problems, however,

deal with the diffraction or scattering of a plane wave, which are different from the problem of interest.

As it was shown above, the finite element method has been used for both problems of radiation from convex and concave radiators. The method similar to the one used in [13], however, will be employed for the present radiation and diffraction problems since it is quite close to the analytical method except for the way the unknown coefficients are determined.

1.3 Statement of the Problem

The main object lies on the general discussion of the relation between the shape of the diaphragm and its radiation and diffraction characteristics. For the generality of the discussion, it is desirable to represent the diaphragm shape as simply as possible. A portion of a sphere (which is called a "dome" hereafter) is suitable for this purpose because it is simply represented by one parameter, the height-to-radius ratio. To simplify the problem, an infinite baffle are assumed for the radiation and diffraction problems. The radiation and diffraction characteristics such as on-axis pressure response, radiation impedance, phase response, directivity pattern, and near-field sound distribution is discussed. It is reasonable to assume axisymmetry of the sound field for the radiation problem of a loudspeaker. A point source located close to a

convex or a concave dome may be a more suitable model for a three-dimensional diffraction problem. Initially, however, only an axisymmetric sound field is treated. As a sound source in the diffraction problem, an axisymmetric circular line source (which is called a "ring source" hereafter) is assumed. This makes the analysis much simpler and still gives a fundamental understanding of the problem.

The study addresses the following: (1) for the radiation problem, the effect of the height-to-radius ratio of the convex or the concave dome in an infinite baffle on its radiation characteristics; and (2) for the diffraction problem, the effect of the height-to-radius ratio of the convex or the concave dome in the infinite baffle on the radiation characteristics of the axisymmetric ring source.

CHAPTER II

RADIATION FROM CONVEX AND CONCAVE DOMES

2.1 Geometrical Model

2.1.1 Convex Dome

The first problem is to investigate the radiation phenomenon from a convex dome in an infinite baffle in the semi-infinite fluid medium with density ρ and velocity c. The existence of the infinite baffle is expressed mathematically as the boundary condition that the normal velocity on the baffle surface is equal to zero. The same boundary condition is achieved by assuming another symmetric dome on the other side and removing the infinite baffle. For the convenience of mathematical treatment, this radiator composed of these two domes in an infinite space will be used as the radiator model.

The cross section of this model is shown in Figure 2.1. The center of the radiator is the origin of the rectangular coordinate system (x,y,z). The radiator is symmetric about xy-plane and axisymmetric about the z-axis. Both domes are described as a portion of a sphere with radius R. The sphere of the right side dome has the origin O_1. The polar coordinate systems (r',θ',ϕ') with the origin O and (r,θ,ϕ) or (r_1,θ_1,ϕ_1) with the origin O_1 are used. The

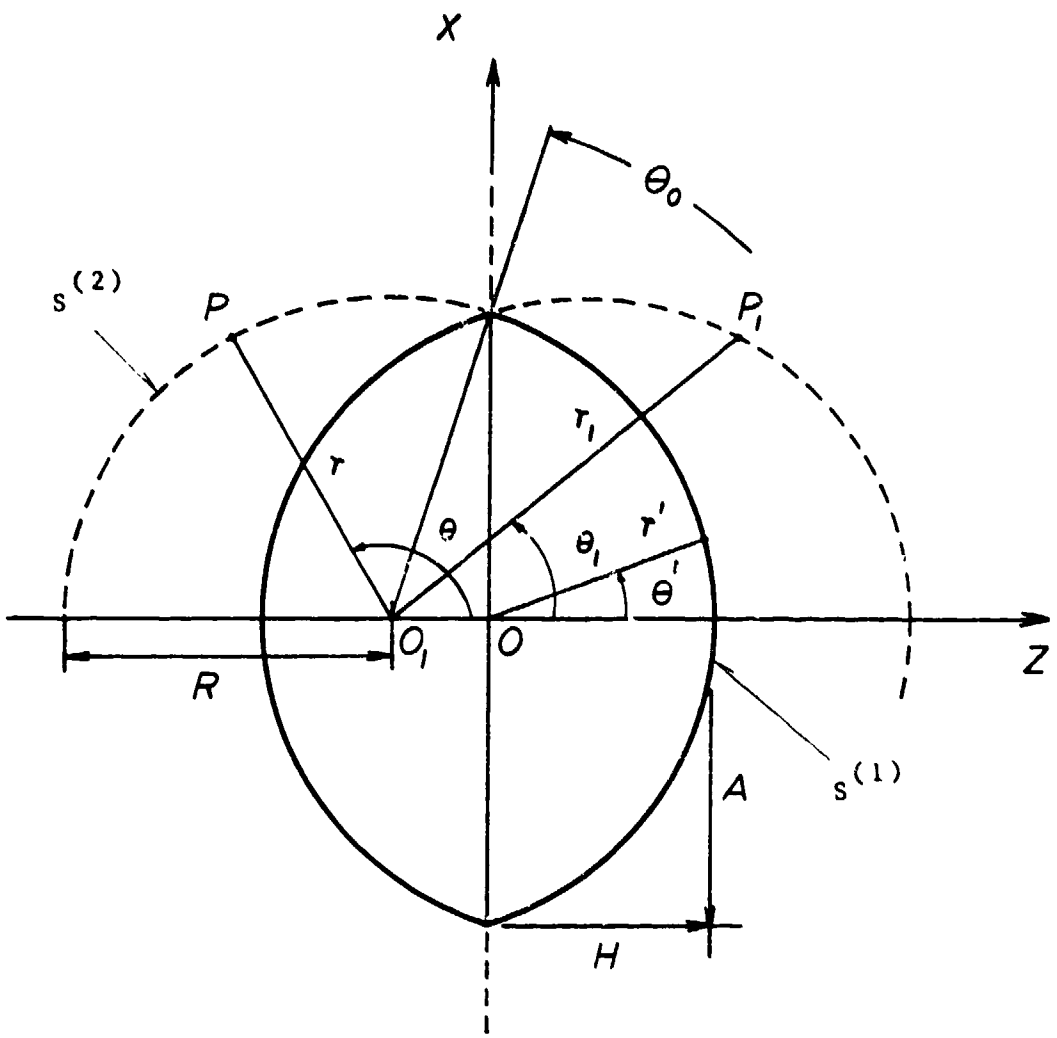

Figure 2.1 Geometry of the convex dome radiator.

area of the right side dome ($r=R$, $0\leq\theta\leq\theta_o$, $0\leq\phi\leq 2\pi$) is denoted by $S^{(1)}$, and the imaginary surface ($r=R$, $\theta_o\leq\theta\leq\pi$, $0\leq\phi\leq 2\pi$) is denoted by $S^{(2)}$. The radius and the height of the dome are A and H, respectively. The domes are assumed to vibrate sinusoidally with angular frequency ω in the z direction and with the amplitude U_o and 180 degrees out-of-phase with each other. The assumption of the piston-like motion may not be suitable for an actual loudspeaker in the high-frequency region because of the higher order modes developing on the diaphragm, but it will be beneficial for basic discussions of sound radiation.

2.1.2 Concave Dome

Figure 2.2 shows the geometry of the concave dome radiator. The xy-plane coincides with the baffle surface, and the z-axis is the axis of revolution. The dome is described as a portion of a sphere of radius R and origin O_1. The dome has the radius A and height H. The polar coordinate system (r,ϑ,ϕ) will be used for the semi-infinite space including the cavity in the baffle. The surface of the dome ($r=R$, $\theta_o\leq\theta\leq\pi$, $0\leq\phi\leq 2\pi$) is denoted by $S^{(1)}$. The points on the surface of the opening $S^{(2)}$ will be described by (r_1,θ_1,ϕ_1).

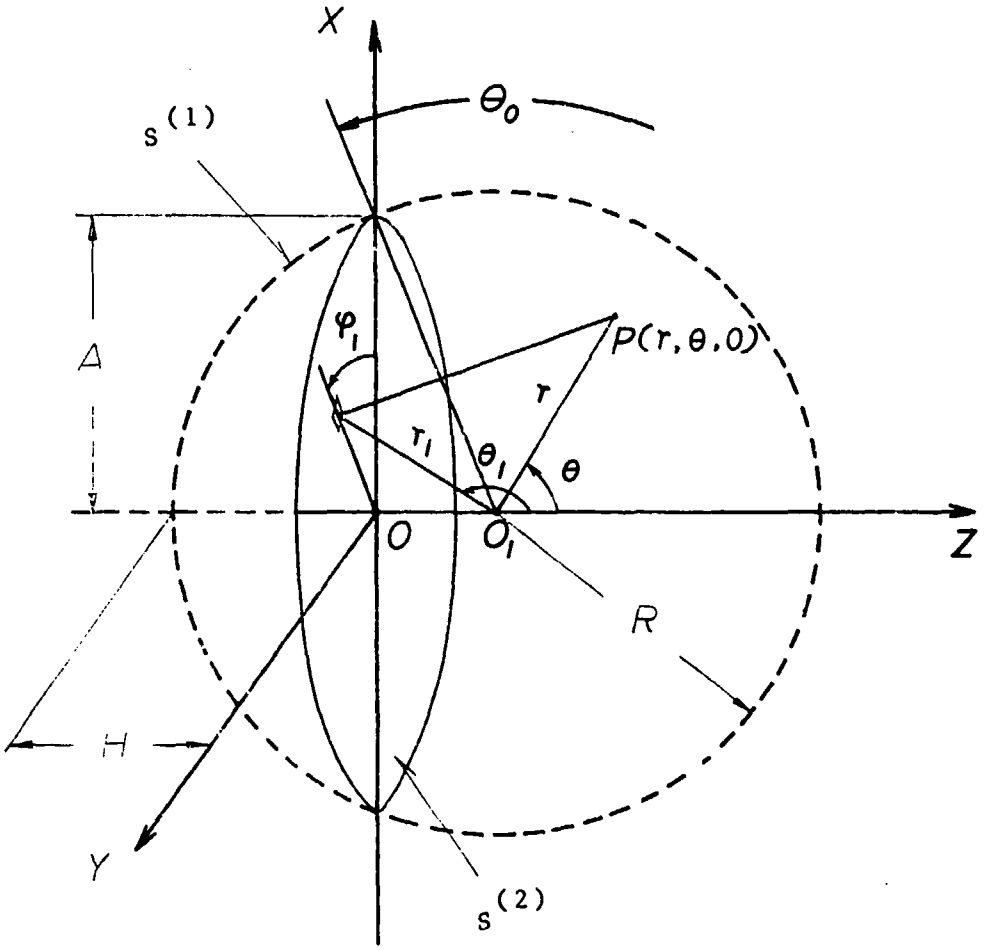

Figure 2.2 Geometry of the concave dome radiator.

2.2 Mathematical Discussions

2.2.1 Basic Equations for Radiation Problem

The sound in a fluid medium is a dynamic disturbance of the fluid which can be described by a time dependent scalar quantity like pressure or velocity potential. In linear acoustics, the wave equation of the harmonic wave propagation in the fluid is expressed by the Helmholtz equation:

$$(\nabla^2 + k^2)\, \psi(\xi) = 0 , \qquad (2.1)$$

where $\psi(\xi)$ is the velocity potential, k is the wavenumber, ∇^2 is the Laplacian operator, ξ is the field point in the acoustic medium, and the time-dependent term $e^{+j\omega t}$ is suppressed. The pressure $p(\xi)$ and the particle velocity $\bar{u}(\xi)$ are related to the velocity potential by the following equations:

$$p(\xi) = j\omega\rho\, \psi(\xi) \qquad (2.2)$$

and

$$\bar{u}(\xi) = -\nabla\, \psi(\xi) , \qquad (2.3)$$

where ∇ is the gradient operator.

The radiation problem is to find a solution to Eq. (2.1) to satisfy the appropriate boundary condition. The boundary condition on the radiator surface is expressed by

$$L\,\psi(\zeta) = f(\zeta)\ , \tag{2.4}$$

where ζ is a point on the radiator surface. The Dirichlet and Neumann boundary conditions are given by

$$L = j\omega\rho\ ;\quad f(\zeta) = P(\zeta) \tag{2.5}$$

and

$$L = -\frac{\partial}{\partial \bar{n}}\ ;\quad f(\zeta) = U(\zeta)\ , \tag{2.6}$$

respectively, where $P(\zeta)$ and $U(\zeta)$ are the pressure and the normal velocity distributions prescribed on the surface of the radiator, and $\bar{n}$ is the unit outward normal to the surface. It should be noted that Eq. (2.4) can also express the mixed boundary condition if one assumes Dirichlet and Neumann boundary conditions on the different areas of the radiator surface.

The solution of Eq. (2.1) also has to satisfy the radiation condition [28]:

$$\lim_{\hat{r}\to\infty} \int_{S_{\hat{r}}} \left| \frac{\partial}{\partial r}\, p(\xi) + jk\, p(\xi) \right|^2_{r=\hat{r}} dS = 0\ , \tag{2.7}$$

where r is the distance from the origin of coordinates to the field point, and $S_{\hat{r}}$ is the surface of a sphere of radius $\hat{r}$ centered at the origin, surrounding the field point ξ and the radiator.

2.2.2 Least Square Error Method

As it was mentioned before, one cannot apply the method of separation of variables, because there exists no appropriate coordinate system that matches the boundary of the radiator except in the case of H/A = 1.0, which corresponds to the radiation from a complete sphere. Here, the method called "least square error method" will be used extensively in the present radiation and diffraction problems [29].

The velocity potential will be expanded in the following form:

$$\psi(\xi) = \sum_{n=0}^{\infty} a_n \psi_n(\xi) , \qquad (2.8)$$

where a_n is the unknown coefficient, and the set of infinite trial functions $\psi_n(\xi)$ is considered to be capable of describing the unknown function $\psi(\xi)$ which satisfies the wave equation Eq. (2.1) and the radiation condition Eq. (2.7). When the maximum of the order n is truncated by N, the "best" approximation of the boundary condition Eq. (2.4) on the boundary S is defined as a solution with the set of unknown coefficients a_n, n = 0, 1, . . ., N that makes the following functional stationary:

$$J = \int_S q(\zeta) \left| \sum_{n=0}^{N} a_n \psi_n(\zeta) - f(\zeta) \right|^2 dS , \qquad (2.9)$$

where

$$\Psi_n(\zeta) = L\,\psi_n(\zeta) , \qquad (2.10)$$

and $q(\zeta)$ is a non-negative weighting function necessary at least for the consistency of dimensions of the integrands of Eq. (2.9) in the case of mixed boundary condition problems. The a_n is given by the condition that J is stationary, i.e., insensitive to arbitrary variations in the parameter a_n,

$$\frac{\partial}{\partial a_n} J = 0 , \quad n = 0 , 1, \ldots, N . \qquad (2.11)$$

Substituting Eq. (9) into Eq. (11), (N+1) simultaneous equations are obtained [see Appendix A]:

$$\int_S q(\zeta)\left[\sum_{n=0}^{N} a_n \Psi_n(\zeta)\Psi_m^*(\zeta)\right]dS = \int_S q(\zeta)\Psi_m^*(\zeta)f(\zeta)dS$$

$$m = 0, 1, \ldots, N , \qquad (2.12)$$

where * denotes the complex conjugate.

Thus, if the proper trial functions and expressions for the boundary condition are found, the solution of best approximation can be obtained by solving Eq. (2.12).

2.2.3 Radiation from a Convex Dome

The general discussion of the mathematical tool used for the radiation problem has been completed in the previous two sections. In order to solve the problem efficiently, it is important to use physical and mathematical intuition for the selection of appropriate trial functions and the

coordinate system. This means that the proper choice of trial functions and coordinate system enables one to approximate the boundary condition accurately enough with the smallest order of truncation N.

The direct and simple application of the previous mathematical discussion for the radiation problem by the convex dome shown in Figure 2.1 is to expand the velocity potential in terms of spherical harmonic functions with the origin at the center of the radiator. However, two basic problems are inherent with this procedure. [These are discussed in detail in Appendix B.]

Now, on the basis of this knowledge, it seems reasonable to choose the center of one of the spheres as the origin of the coordinate system. The velocity potential is expanded in terms of the infinite series such as [30]:

$$\psi(x) = \sum_{n=0}^{\infty} a_n h_n(kr) P_n(\cos\theta) , \qquad (2.13)$$

where $h_n(kr)$ is the spherical Hankel function of the second kind and order n with the suppression of the superscript (2), and $P_n(\cos\theta)$ is the Legendre function of the first kind and order n. [The validity of the expression in the form of Eq. (2.13) for Dirichlet and Neumann boundary conditions is shown in Appendix C.]

Then, the boundary condition on the radiator surface $S^{(1)}$ is given by

$$L^{(1)} = -\frac{\partial}{\partial r}\bigg|_{r=R} \qquad (2.14)$$

and

$$f^{(1)}(\zeta) = U_o \cos\theta \ . \tag{2.15}$$

Then,

$$\psi_n^{(1)}(\theta) = - k\, h_n'(kR)\, P_n(\cos\theta) \ . \tag{2.16}$$

Here, the superscript (1) or (2) indicates the functions with regard to the surface $S^{(1)}$ or $S^{(2)}$, respectively. Also, $\psi_n^{(1)}(\theta)$ and $f^{(1)}(\theta)$ are used instead of $\psi_n^{(1)}(\zeta)$ and $f^{(1)}(\zeta)$ since they are functions of θ only.

On the imaginary surface $S^{(2)}$, one can use the condition of symmetry of the sound field. The velocity potential at point P is equal to the one at point P_1, giving the relation:

$$\sum_{n=0}^{N} a_n\, h_n(kr)\, P_n(\cos\theta) = \sum_{n=0}^{N} a_n\, h_n(kr_1)\, P_n(\cos\theta_1) \ , \tag{2.17}$$

where R, θ, r_1, and θ_1 are related to each other by the following equations:

$$r_1 \cos\theta_1 = R\,(2\cos\theta_o - \cos\theta) \tag{2.18}$$

and

$$r_1 \sin\theta_1 = R \sin\theta \ , \tag{2.19}$$

and R is given by

$$R = (H^2 + A^2)/2H \ . \tag{2.20}$$

Rewriting Eq. (2.17), one obtains

$$\sum_{n=0}^{N} a_n [h_n(kR)\, P_n(\cos\theta) - h_n(kr_1)\, P_n(\cos\theta_1)] = 0 . \quad (2.21)$$

The condition of symmetry of the sound field does not give an explicit form to the operator L. But, comparing Eq. (2.21) with Eq. (2.4), one comes to the interpretation that the operator L, when applied on the velocity potential at a point, gives the difference of velocity potentials at that point and its symmetric point.

Thus, $\psi_n^{(2)}(\theta)$ and $f^{(2)}(\theta)$ can be defined such as:

$$\psi_n^{(2)}(\theta) = h_n(kr)\, P_n(\cos\theta) - h_n(kr_1)\, P_n(\cos\theta_1) \quad (2.22)$$

and

$$f^{(2)}(\theta) = 0 . \quad (2.23)$$

Applying Eqs. (2.16), (2.17), and Eqs. (2.22), (2.23) into Eq. (2.12), the set of (N+1) simultaneous equations are obtained:

$$\sum_{n=0}^{N} a_n \left[\int_{S^{(1)}} \psi_m^{(1)*}(\theta)\, \psi_n^{(1)}(\theta)\, dS + \int_{S^{(2)}} \psi_m^{(2)*}(\theta)\, \psi_n^{(2)}(\theta)\, dS \right]$$

$$= \int_{S^{(1)}} \psi_m^{(1)*}(\theta)\, f^{(1)}(\theta)\, dS , \quad m = 0, 1, \ldots, N, \quad (2.24)$$

where

$$q(\zeta) = 1.0 \quad (2.25)$$

is assumed in Eq. (2.12).

2.2.4 Radiation from a Concave Dome

In the case of radiation from a concave dome, it is impossible to get rid of the infinite baffle without changing the boundary condition. Thus, the sound field must be dealt with in a semi-infinite space. Instead, one can use the knowledge that the sound field is uniquely determined by the use of the Rayleigh integral if the normal velocity distribution on the baffle surface is given.

The velocity potential inside the sphere with the origin O_1 is expanded in terms of infinite series such as [30]:

$$\psi(x) = \sum_{n=0}^{N} a_n j_n(kr) P_n(\cos\theta) , \qquad (2.26)$$

where $j_n(kr)$ is the spherical Bessel function of the first kind and order n.

The boundary condition on the radiator surface $S^{(1)}$ is given by the same forms as Eqs. (2.14) and (2.15):

$$L^{(1)} = -\frac{\partial}{\partial r}\Big|_{r=R} \qquad (2.27)$$

and

$$f^{(1)}(\theta) = U_o \cos\theta . \qquad (2.28)$$

Thus,

$$\psi_n^{(1)}(\theta) = -k\, j_n'(kR)\, P_n(\cos\theta) \,. \tag{2.29}$$

Once the expression for the velocity potential (with unknown coefficients) inside the sphere is given, one can obtain the normal velocity distribution on the opening $S^{(2)}$ of the cavity:

$$u_B(r_1,\theta_1) = -\frac{\partial}{\partial z}\psi(r,\theta)\Big|_{\substack{r=r_1\\ \theta=\theta_1}} = -\left[\frac{\partial\psi}{\partial r}\frac{\partial r}{\partial z} + \frac{\partial\psi}{\partial\theta}\frac{\partial\theta}{\partial z}\right]_{\substack{r=r_1\\ \theta=\theta_1}} . \tag{2.30}$$

The derivatives are given from the geometry by

$$\frac{\partial r}{\partial z} = \cos\theta \tag{2.31}$$

and

$$\frac{\partial\theta}{\partial z} = -\frac{\sin\theta}{r} \,. \tag{2.32}$$

Substituting Eqs. (2.31) and (2.32) into Eq. (2.30), one obtains

$$u_B(r_1,\theta_1) = -\sum_{n=0}^{\infty} a_n[k\cos\theta_1\, j_n'(kr_1)\, P_n(\cos\theta_1) + \sin^2\theta_1\, j_n(kr_1)\, P_n'(\cos\theta_1)/r_1] \,. \tag{2.33}$$

Now, the velocity potential $\psi_u(r,\theta)$ due to $u_B(r_1,\theta_1)$ outside the cavity can be obtained using the Rayleigh integral:

$$\psi_u(r,\theta) = \frac{1}{2\pi}\int_{S^{(2)}}\left[\underline{u}_n(r_1,\theta_1)\,\frac{e^{-jkd}}{d}\right] dS\,, \qquad (2.34)$$

where

$$d = [(r\sin\theta - r_1\sin\theta_1\cos\phi_1)^2 + (r_1\sin\theta_1\sin\phi_1)^2 + (r\cos\theta - r_1\cos\theta_1)^2]^{1/2} \qquad (2.35)$$

is the distance between the point of interest $(r,\theta,0)$ and the point of surface element dS (r_1,θ_1,ϕ_1). The two velocity potentials given by Eqs. (2.26) and (2.34) must be equal to each other (potential matching) everywhere inside the sphere and outside the cavity.

It seems reasonable to impose the condition of the potential matching on the imaginary surface of the sphere. But the expansion of the form of Eq. (2.26) causes a nonuniqueness problem when the boundary condition is given on the surface of the sphere at or near its characteristic frequencies [see Appendix C]. For this reason, the opening of the cavity $S^{(2)}$ is chosen as the area on which the condition of potential matching is imposed. Then, one obtains

$$\sum_{n=0}^{N} a_n[j_n(kr)\,P_n(\cos\theta)] = -\sum_{n=0}^{N} a_n\left[\int_{S^{(2)}}\{k\cos\theta_1 j'_n(kr_1) P_n(\cos\theta_1) + \sin^2\theta_1\, j_n(kr_1)\, P'_n(\cos\theta_1)/r_1\}\left(\frac{e^{-jkd}}{2\pi d}\right) dS\right], \qquad (2.36)$$

with the relationship between r and θ such as:

$$r = -z_o/\cos\theta \ . \tag{2.37}$$

where z_o is the distance between O and O_1. Rewrite this equation,

$$\sum_{n=0}^{N} a_n[j_n(kr)\ P_n(\cos\theta) + \int_{S^{(2)}} \{k\cos\theta_1 j_n'(kr_1)\ P_n(\cos\theta_1) + \sin^2\theta_1\ j_n(kr_1)\ P_n'(\cos\theta_1)/r_1\}\ \left(\frac{e^{-jkd}}{2\pi d}\right)\ dS] = 0 \ . \tag{2.38}$$

Thus, $\psi_n^{(2)}(\theta)$ and $f^{(2)}(\theta)$ can be defined such as:

$$\psi_n^{(2)}(\theta) = [j_n(kr)\ P_n(\cos\theta) + \int_{S^{(2)}} \{k\cos\theta_1 j_n'(kr_1)\ P_n(\cos\theta_1) + \sin^2\theta_1 j_n(kr_1)\ P_n'(\cos\theta_1)/r_1\}\ \left(\frac{e^{-jkd}}{2\pi d}\right)\ dS] \tag{2.39}$$

and

$$f^{(2)}(\theta) = 0 \ . \tag{2.40}$$

Now, by the same method used in Section 2.2.3, one obtains the (N+1) simultaneous equations [again Eq. (2.25) was assumed]:

$$\sum_{n=0}^{N} a_n[\int_{S^{(1)}} \psi_m^{(1)*}(\theta)\ \psi_n^{(1)}(\theta)\ dS + \int_{S^{(2)}} \psi_m^{(2)*}(\theta)\psi_n^{(2)}(\theta)\ dS] = \int_{S^{(1)}} \psi_m^{(1)*}(\theta) f^{(1)}(\theta)\ dS \ , \quad m = 0, 1, \ldots, N. \tag{2.41}$$

2.2.5 Geometrical Approximation Method

It is well known that sound will be radiated normal to the surface of the radiator when the wavelength is much smaller than the radiator size. For higher frequencies, the geometrical approximation begins to have practical meaning. The geometrical approximation here assumes that an infinite number of point sources are distributed in such a way that they form the shape of the radiator with equal surface density in an infinite space. The on-axis sound pressure of the convex dome, which is normalized by the sound pressure due to a single point source with the same total volume velocity at the origin O, is then given by

$$p = \left[\int_0^{\theta_o} 2\pi R\sin\theta\cos\theta e^{ikR(\cos\theta-\cos\theta_o)} Rd\theta\right]/\pi R^2\sin^2\theta_o$$

$$= 2\left[e^{ikR(1-\cos\theta_o)}(ikR - 1) + (1 - \cos\theta_o \cdot ikR)/\sin^2\theta_o(ikR)^2\right] . \quad (2.42)$$

The expression for the concave dome is the same except that the phase response has the opposite sign. The results obtained with this method will be compared with exact solutions.

2.3 Results and Discussions

The calculations were made for three different height/radius ratios such that H/A = 0.5, 0.75, and 1.0. The frequency range was from kA = 0.1 to 10.0. The accuracy of the results was confirmed by verifying the degree of matching of velocity and velocity potential. Except in the vicinity of the rim of the dome, the differences were less than a few percent. The weighting function $q(\zeta)$ in Eq. (2.12) was kept equal to unity all through the calculations, because varying it did not give any significant improvement in accuracy. The maximum order of N was 40 for kA = 10.0.

2.3.1 On-axis Pressure Response

The far-field on-axis pressure response of a convex dome normalized to the pressure response of a flat piston with same volume velocity are shown in Figure 2.3, for H/A = 0.5, 0.75, and 1.0. When H/A is equal to 0.5, the response shows a meaningful decrease from about kA = 0.5, and reaches to the -3.5dB line around kA = 2.0. For H/A = 0.75 and 1.0, minimum levels in the middle frequency region (say, kA = 0.5 - 5.0) are -6.5dB and -9dB, respectively. This effect of the diaphragm shape on the pressure response is essential when a dome-type loudspeaker is designed. For a dome-type loudspeaker with a 1cm radius, the range from kA = 0.5 to 5.0 corresponds to the frequency range from 2.7kHz to 27kHz. This range includes the reproduction range of a

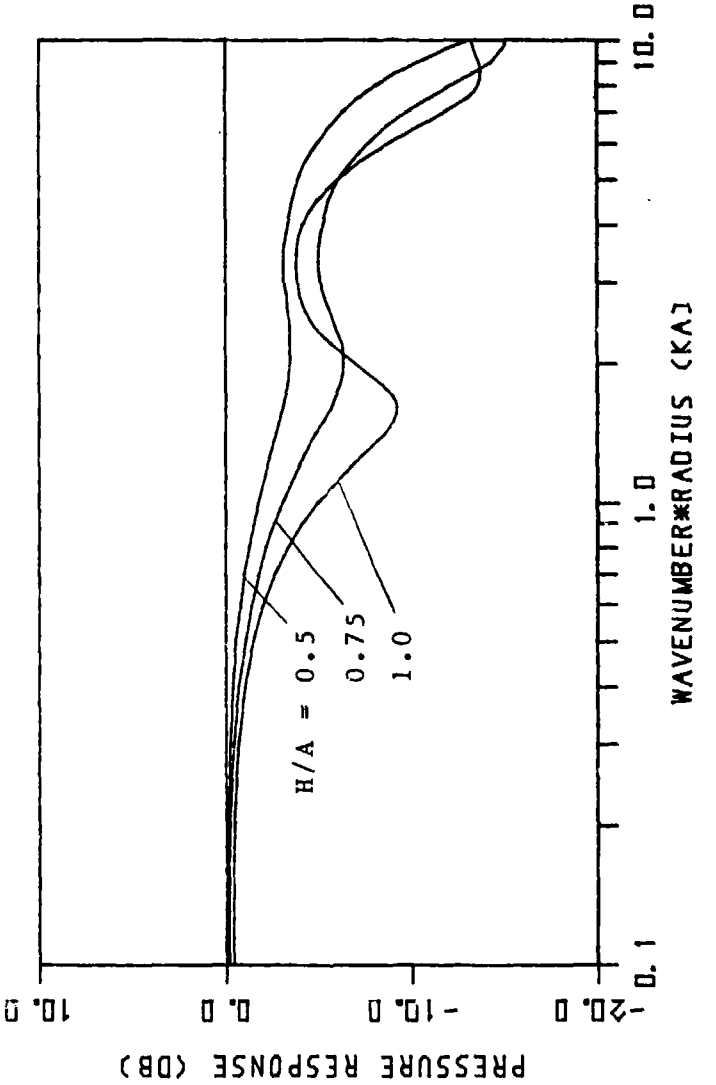

Figure 2.3 Far-field on-axis pressure responses of a convex dome radiator.

dome-type loudspeaker, which may have the H/A ratio of about 0.75. This means that the achieved pressure response is much lower than the one estimated from the assumption of a flat piston. This kind of discrepancy is usually encountered when a dome-type loudspeaker is designed.

It is meaningful to compare the pressure response with results obtained by the geometrical approximation method, which are shown in Figure 2.4. All three responses begin to roll off from about kA = 3.0 at the rate of -6dB/oct., but with different undulations. As the H/A ratio becomes smaller, the fluctuation becomes larger. In Figures 2.5-2.7, two responses obtained by the least square error method (LSM) and the geometrical approximation method (GAM) are compared for each H/A ratio. Figures show that the geometrical approximation gives a fairly good estimation of the true response in the high-frequency region. Especially for H/A = 1.0, the difference is less than 1dB above kA = 4.0.

The results of the concave dome are shown in Figures 2.8-2.10. Contrary to the results of the convex dome, the pressure response of the concave dome has a wide peak around kA = 1.0 - 1.5 for H/A = 1.0 - 0.5. This region is included in the reproduction range of an actual cone-type loudspeaker. For H/A = 0.5, the peak level is about 4dB. This kind of resonance effect is not clearly observed in the pressure responses of an actual loudspeaker. Two reasons for this can be considered. The first one is that the

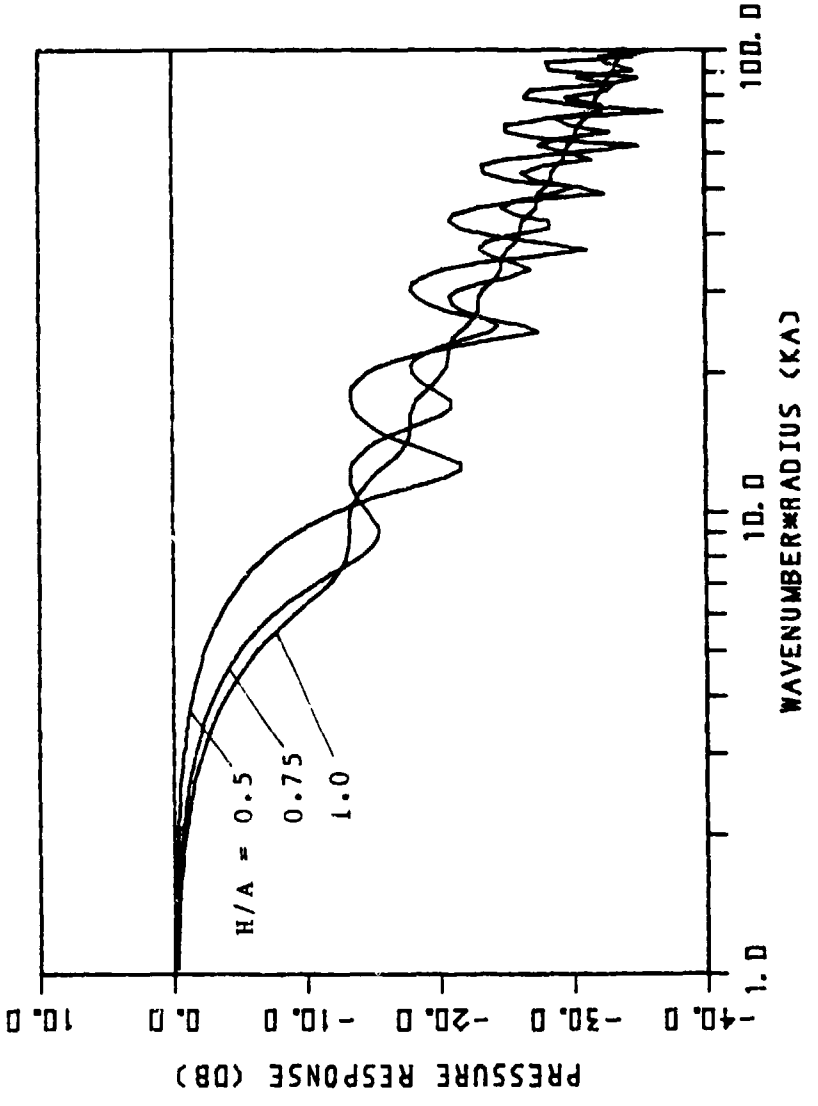

Figure 2.4 Far-field on-axis pressure responses of convex and concave domes obtained by the geometrical approximation.

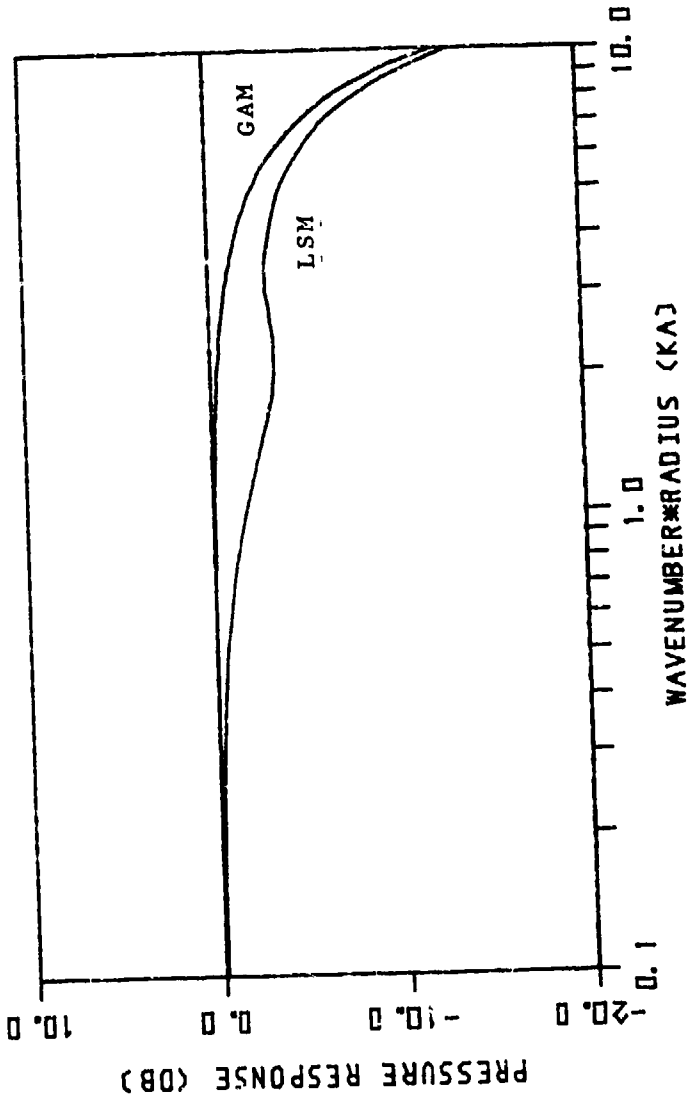

Figure 2.5 Far-field on-axis pressure responses of a convex dome with H/A = 0.5 obtained by the least square error method (LSM) and the geometrical approximation method (GAM).

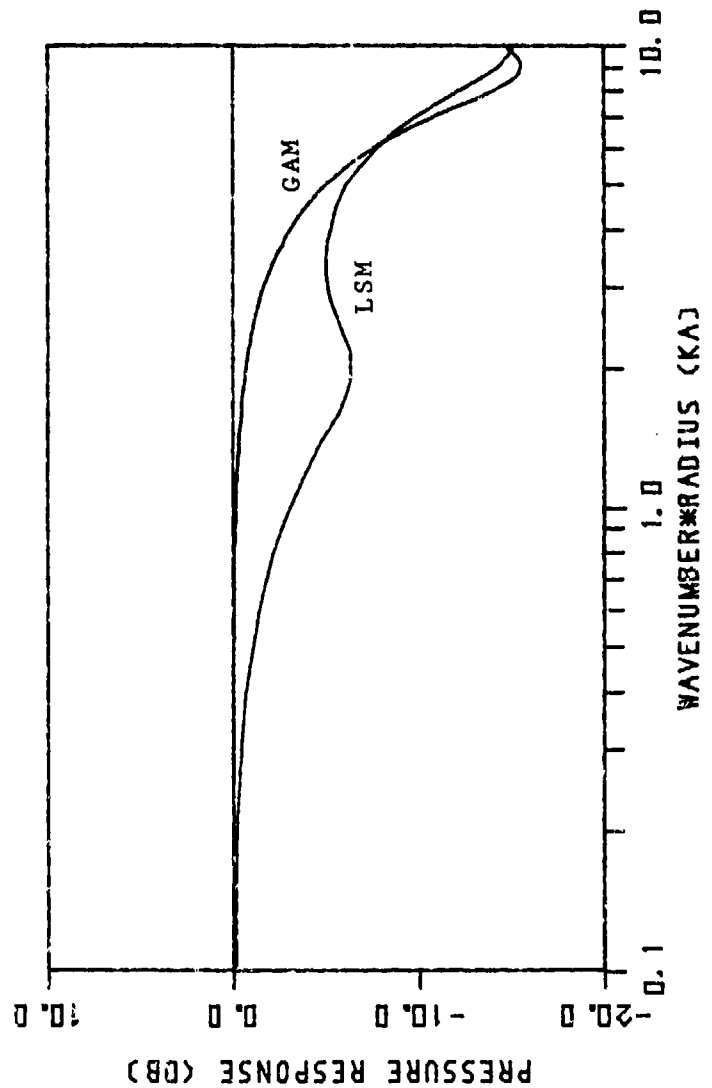

Figure 2.6 Far-field on-axis pressure responses of a convex dome with H/A = 0.75 obtained by the least square error method (LSM) and the geometrical approximation method (GAM).

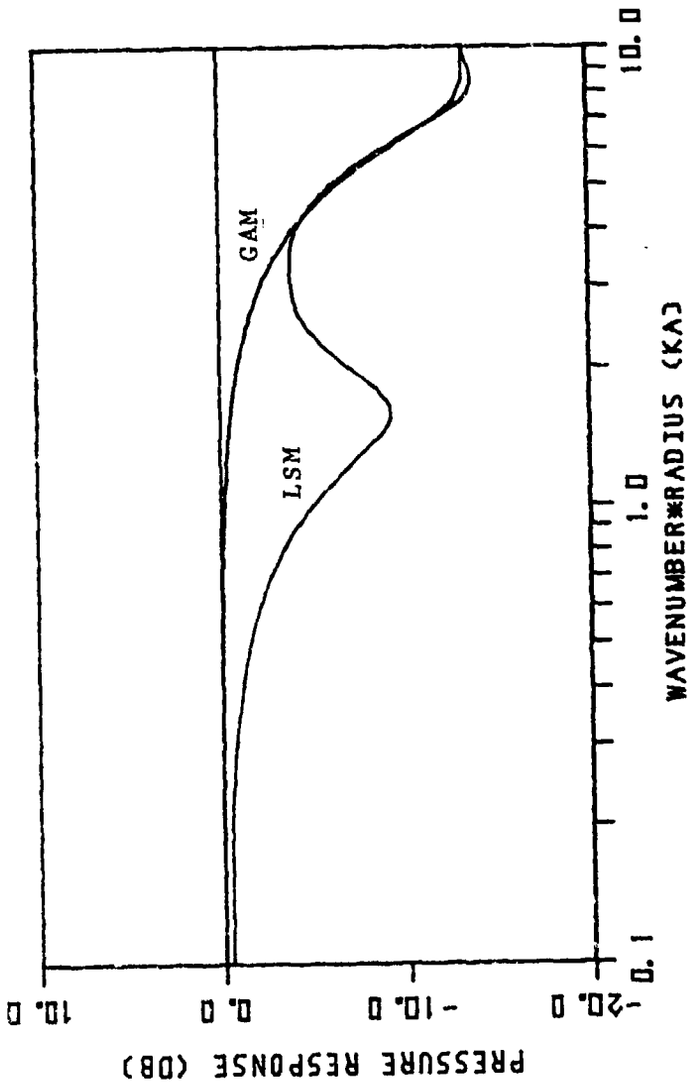

Figure 2.7 Far-field on-axis pressure responses of a convex dome with H/A = 1.0 obtained by the least square error method (LSM) and the geometrical approximation mehtod (GAM).

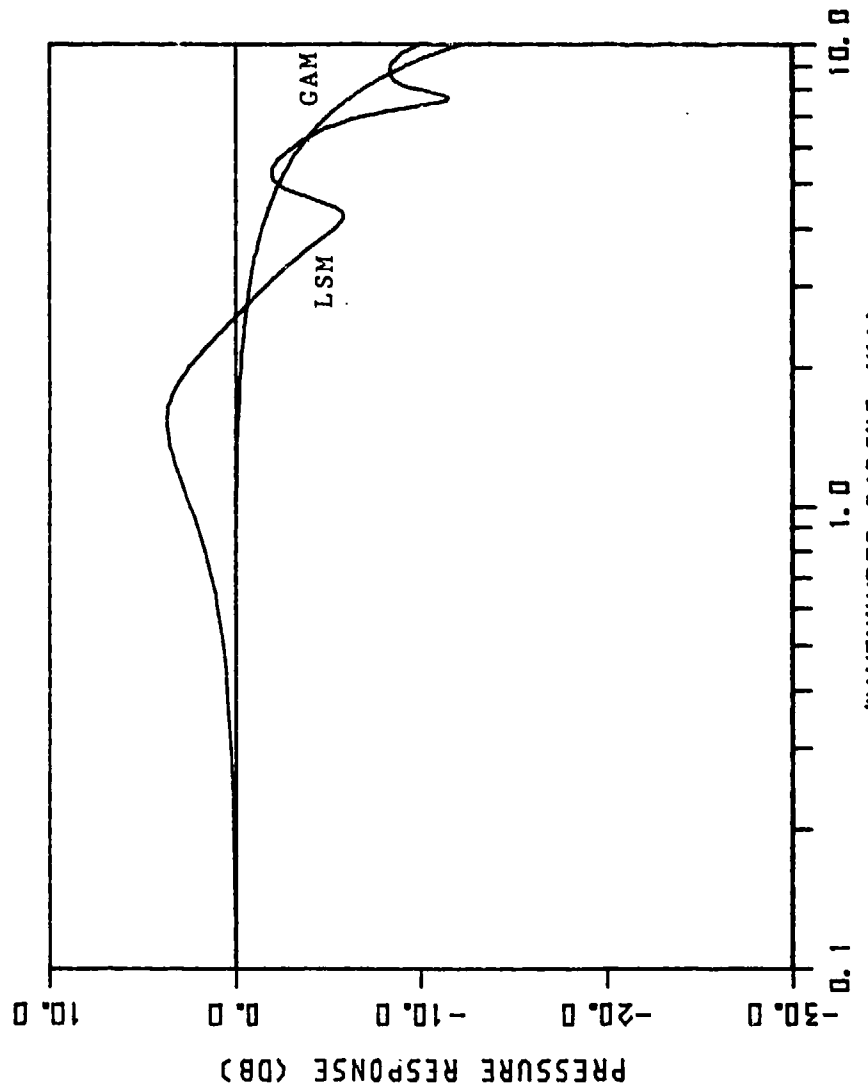

Figure 2.8 Far-field on-axis pressure responses of a concave dome with H/A = 0.5 obtained by the least square error method (LSM) and the geometrical approximation method (GAM).

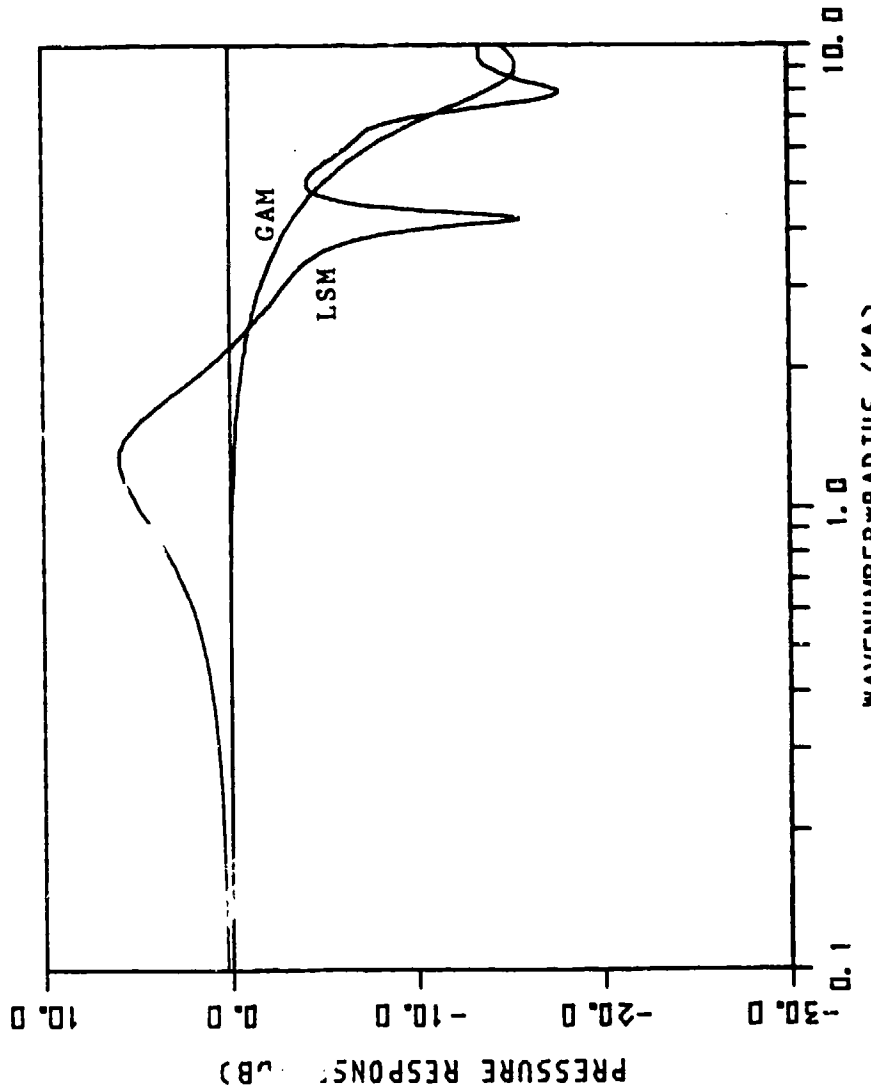

Figure 2.9 Far-field on-axis pressure responses of a concave dome with H/A = 0.75 obtained by the least square error method (LSM) and the geometrical approximation (GAM).

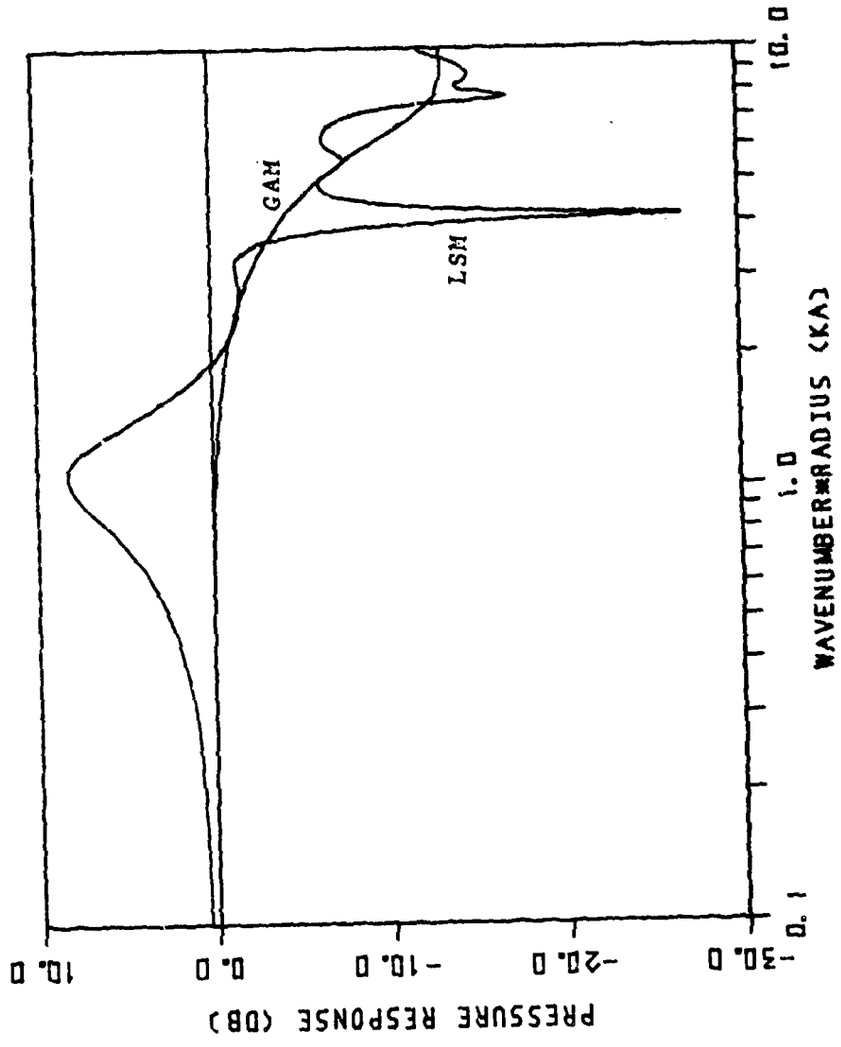

Figure 2.10 Far-field on-axis pressure responses of a concave dome with H/A = 1.0 obtained by the least square error method (LSM) and the geometrical approximation (GAM).

actual cone diaphragm may break up around this frequency region. The second one is that the inductance of the voice-coil reduces the driving force in the same region. For the concave dome, the geometrical approximation gives a rough estimation of the true response.

The above discussion shows that the total range may be divided into three regions. The region in which the response is almost equal to that of a flat piston is the low-frequency region (approximately $kA \leq 0.5$). In the high-frequency region (approximately $kA \geq 5.0$), the response can be estimated by the geometrical approximation method. In the range between these two regions, the response must be obtained by an exact method.

The fact that responses of the convex and concave domes are intrinsically different may mean that the sound quality of them may also have basic differences.

2.3.2 Radiation Impedance

The normalized radiation impedance is defined by the following equation:

$$z_r = \{\tfrac{1}{2} \int_{S(1)} p(\zeta)u^*(\zeta)dS\}/\{\tfrac{1}{2} \rho c\pi A^2 U_o^2\} \quad . \qquad (2.43)$$

The numerator of this equation is the total power (complex), and the denominator is the effective radiated power from a radiator with velocity U_o and constant radiation impedance $\rho c\pi A^2$. The real part (Re) of z_r is the normalized

radiation resistance, and the imaginary part (Im) is the normalized radiation reactance.

The radiation impedance characteristics of the convex dome are shown in Figures 2.11 and 2.12. The radiation resistance of the convex dome is smaller than that of the flat piston with the same radius, and decreases as the height of the dome increases. The radiation resistance of a flat piston fluctuates above kA = 2.0, while its pressure response stays constant. On the other hand, for the same frequency region, the radiation resistance of the convex dome is constant even if its on-axis pressure response varies.

In order to discuss the frequency response of the radiated power, the radiation impedances were plotted on a logarithmic scale in Figures 2.13 and 2.14. When the diaphragm is driven with constant acceleration with respect to frequency, the velocity decreases by 6dB/oct. If the response of $10\log(z_r)$ increases by 6dB/oct., the radiated power remains constant. As Figure 2.13 shows, the flat piston has the closest radiation resistance to the line with a 6dB/oct. slope. As the H/A ratio increases, the convex dome reduces its range of the constant power response. For H/A = 0.5, the radiated power at kA = 2.0 is about 5dB lower than the level in the low-frequency range. The radiation reactance of the convex dome has a slope of +3dB/oct. and -3dB/oct. in the low- and high-frequency region, respectively, and always positive (mass-like).

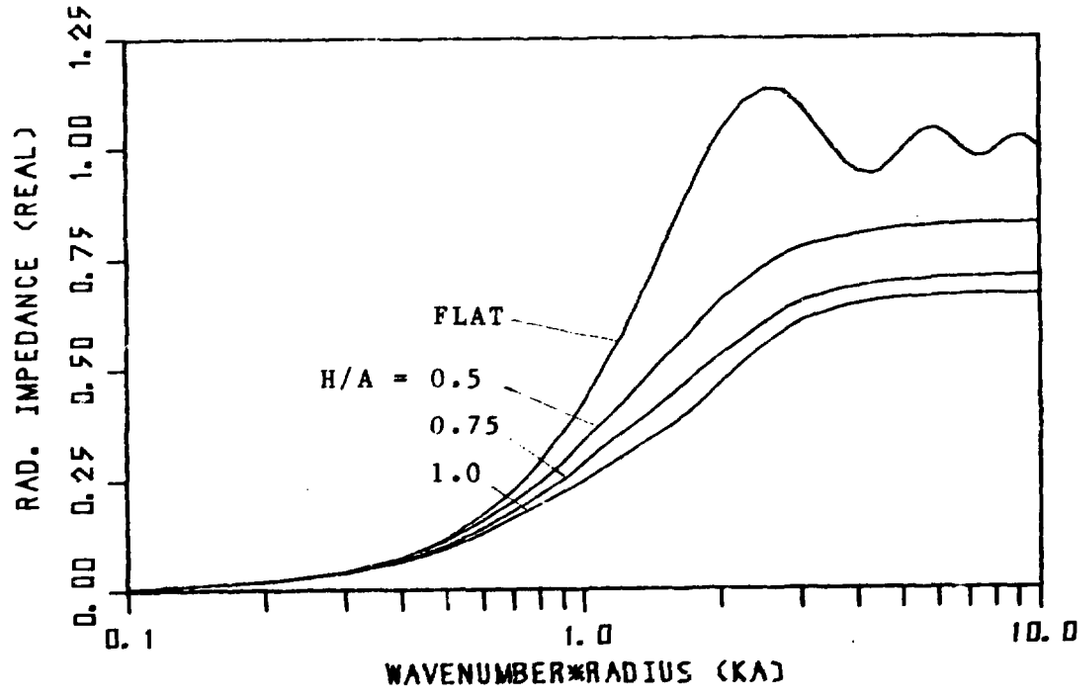

Figure 2.11 Radiation resistance characteristics of a convex dome and a flat piston (normalized by $\rho c \pi A^2$).

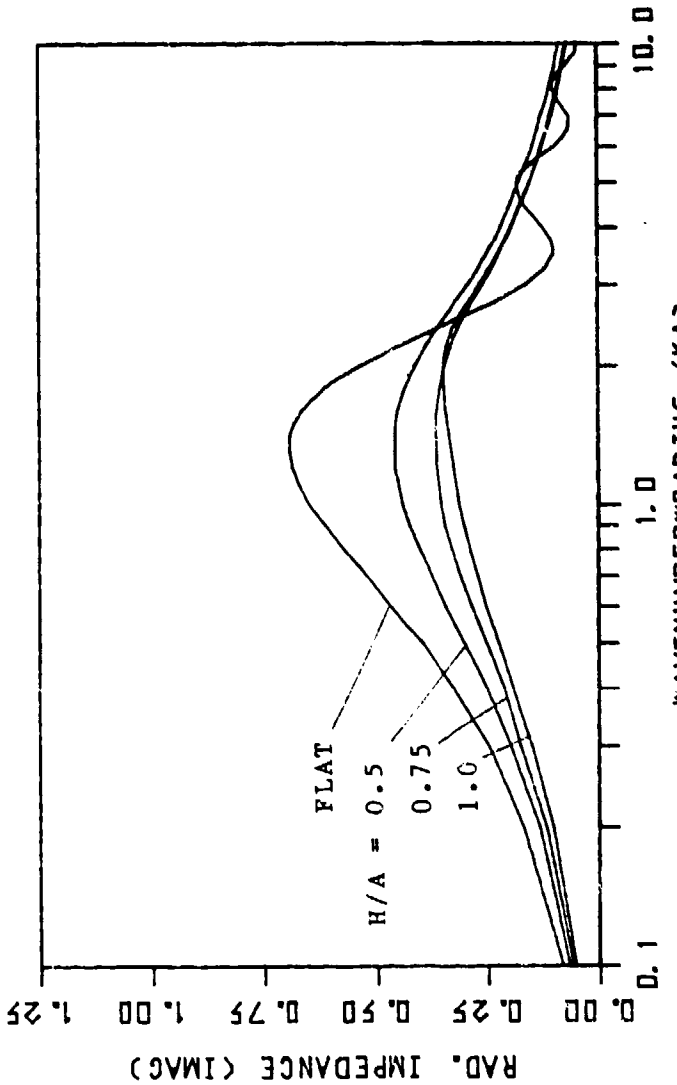

Figure 2.12 Radiation reactance characteristics of a convex dome and a flat piston (normalized by $\rho c \pi A^2$).

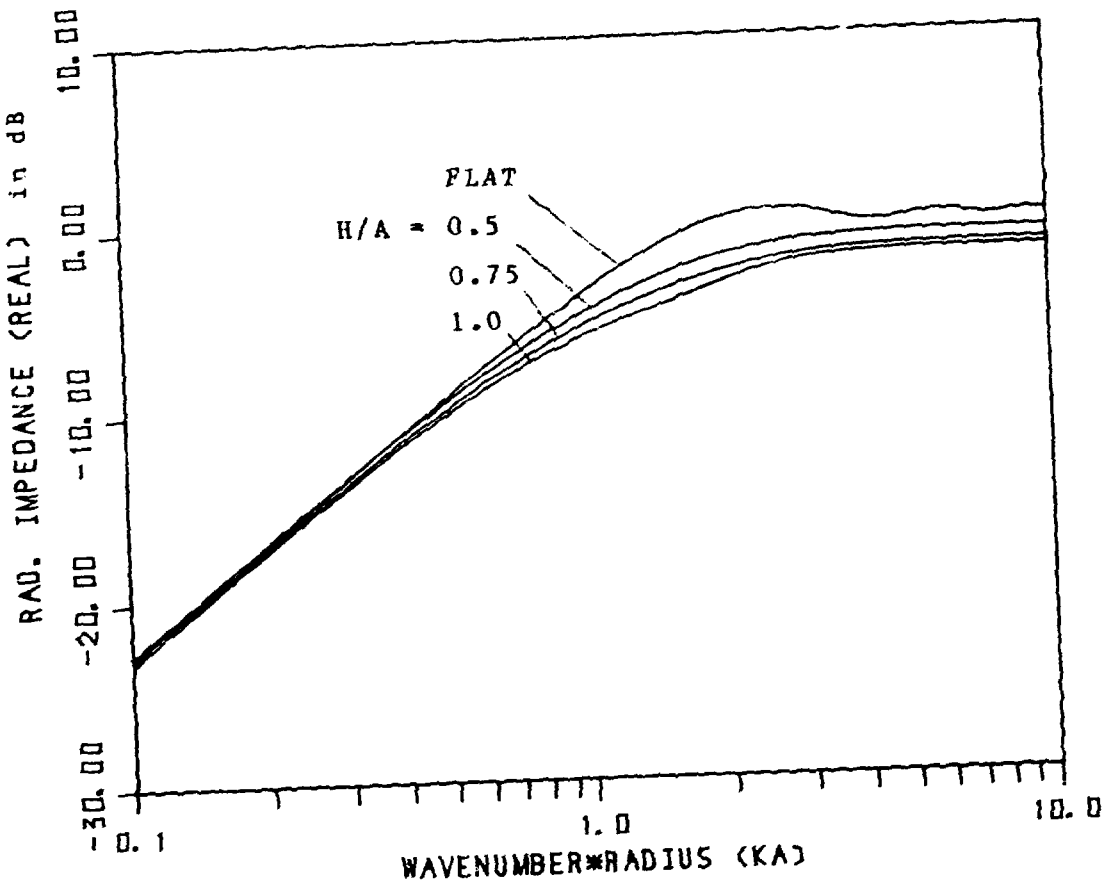

Figure 2.13 Radiation resistance characteristics of a convex dome and a flat piston (normalized by $\rho c \pi A^2$).

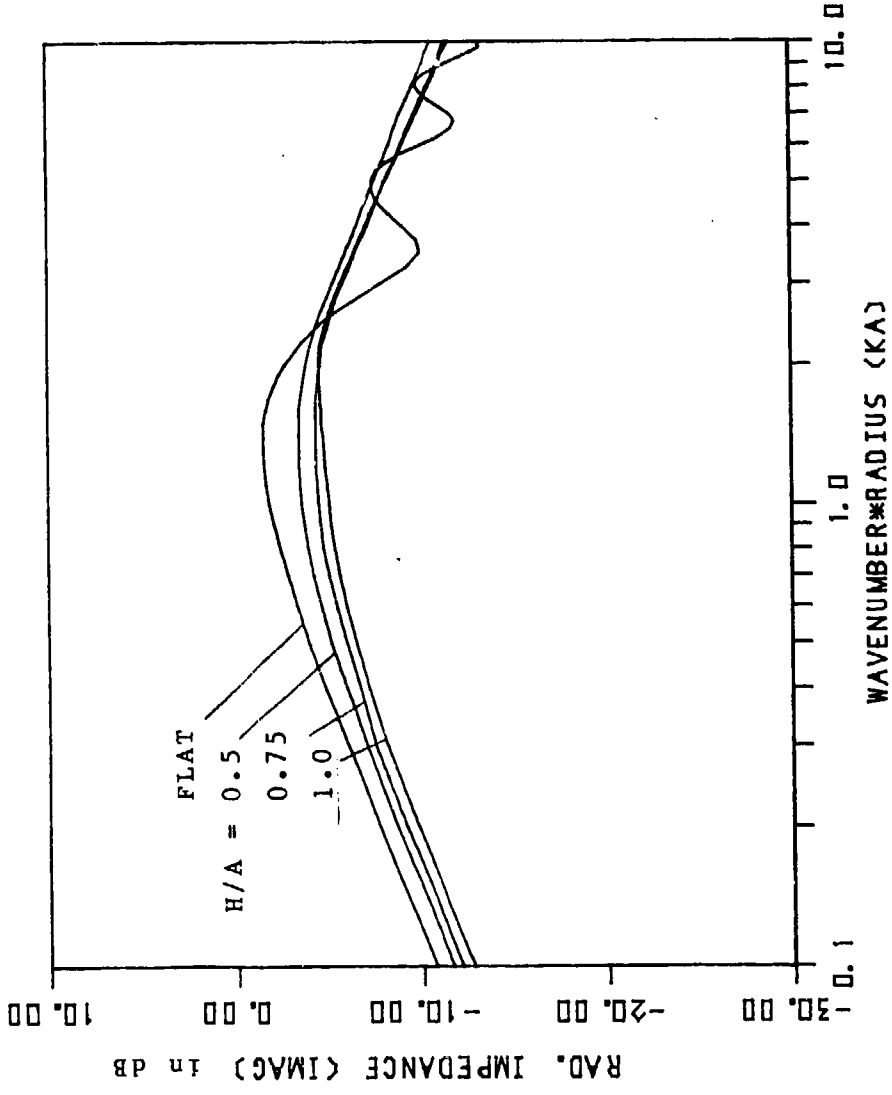

Figure 2.14 Radiation reactance characteristics of a convex dome and a flat piston (normalized by $\rho c \pi A^2$).

The radiation impedances of the concave dome are shown in Figures 2.15-2.17. Radiation resistance of the concave dome is much larger than that of the flat piston and the convex dome in the region $kA \leq 3.0$. This can be explained as a resonance effect of the cavity. The frequency of the maximum resistance is slightly higher than that of the maximum pressure response. The radiation reactance is zero at these frequencies, and mostly negative (spring-like) above those frequencies.

The plot of the radiation resistance on a logarithmic scale is shown in Figure 2.18. The 6db/oct. line stays between the curves of the flat piston and concave dome with $H/A = 0.5$. Thus, if the acceleration of a diaphragm is constant with respect to frequency and if the diaphragm stays like a piston, the widest range of constant radiated power is achieved by a concave dome with H/A ratio somewhere between 0.0 and 0.5. The radiation mass loaded on the concave radiator is almost equal to the sum of the mass of the fluid inside the cavity and the radiation mass of a flat piston with the same radius ($= 0.85 \rho\pi A^3$).

2.3.3 Phase Response

The far-field on-axis phase responses of the convex and concave domes, which are normalized to the phase response of an on-axis point source on the baffle, are shown in Figures 2.19-2.20, respectively. The phase responses of the convex and concave domes increase or decrease

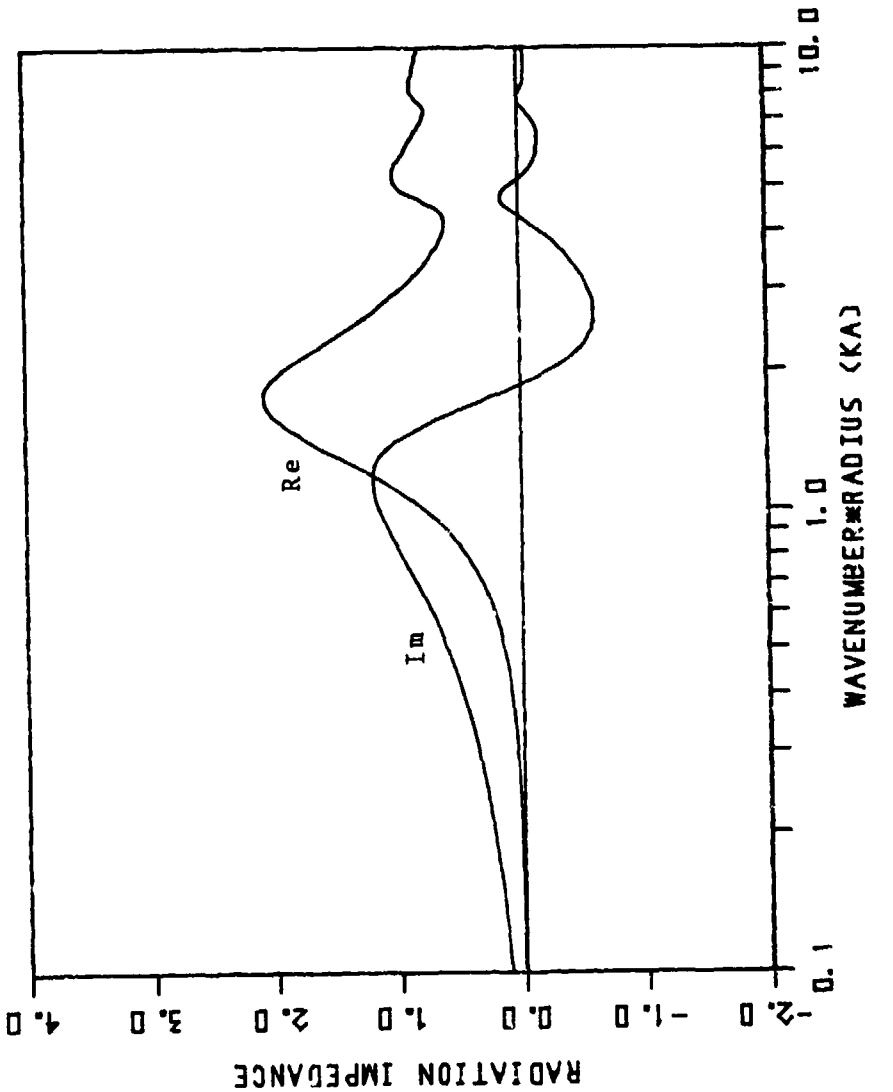

Figure 2.15 Radiation impedance characteristics of a concave dome with H/A = 0.5 (normalized by $\rho c \pi A^2$).

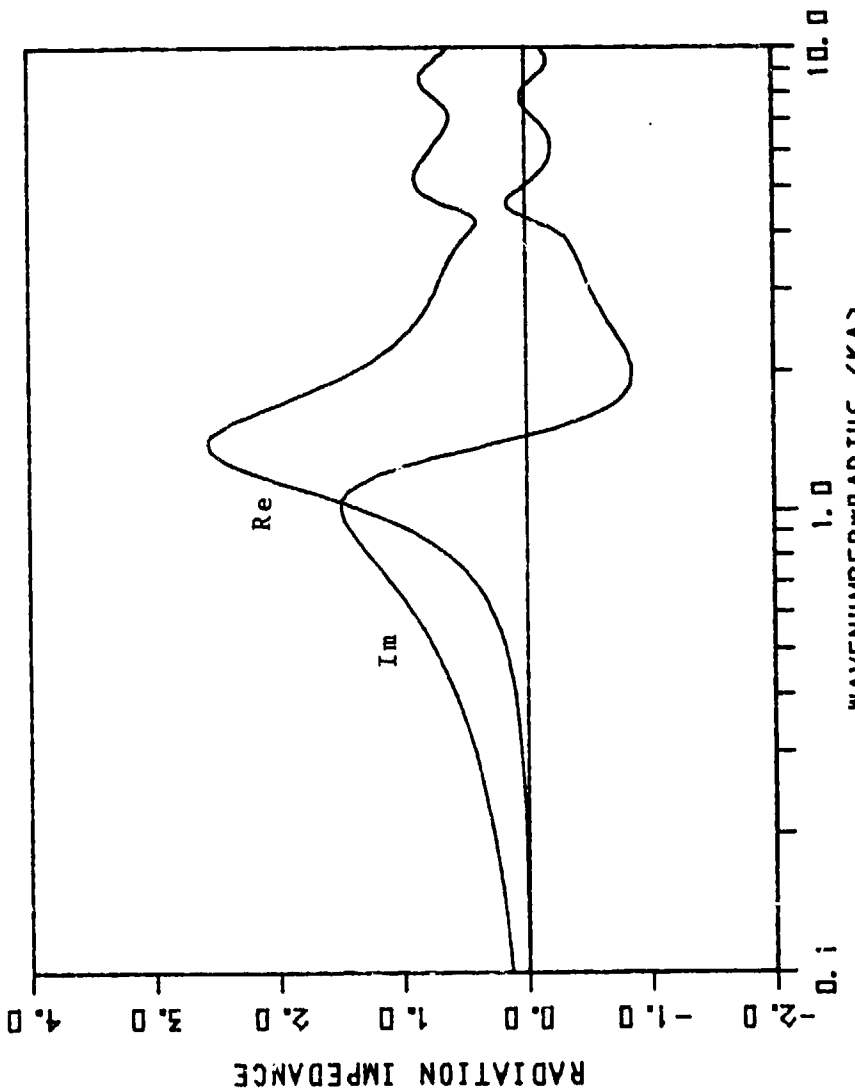

Figure 2.16 Radiation impedance characteristics of a concave dome with H/A = 0.75 (normalized by $\rho c \pi A^2$).

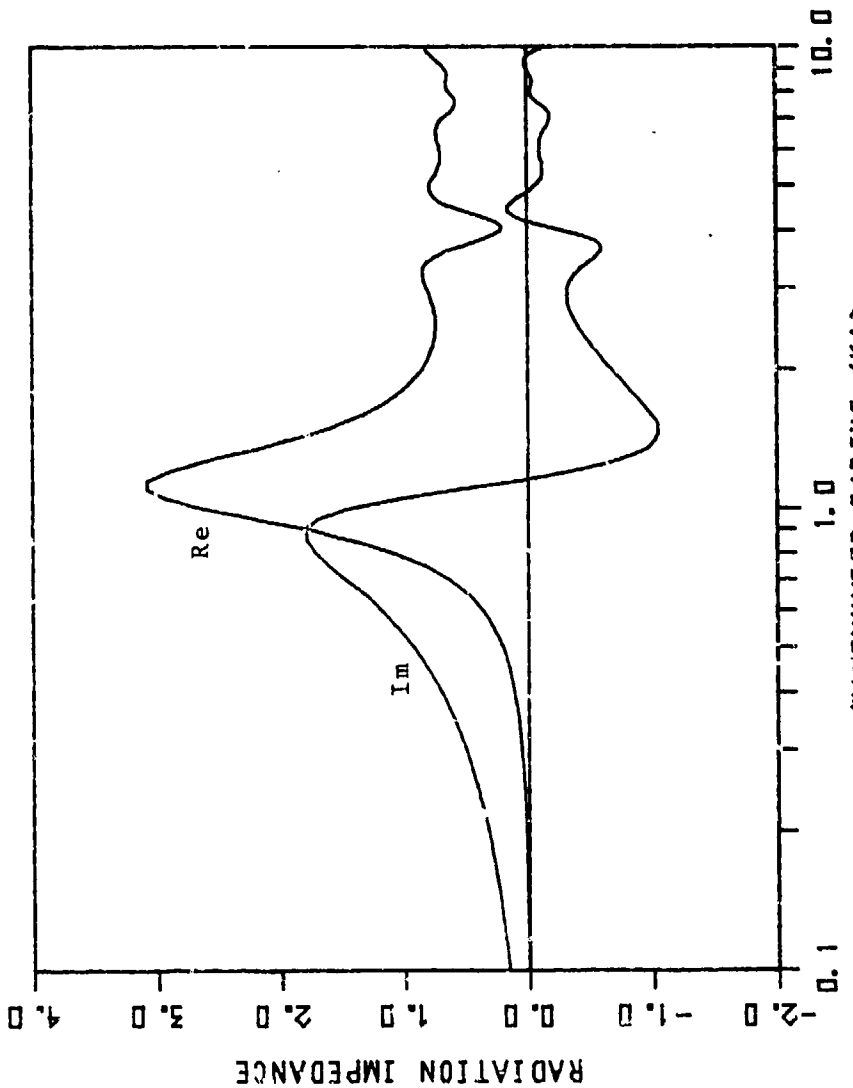

Figure 2.17 Radiation impedance characteristics of a concave dome with H/A = 1.0 (normalized by $\rho c \pi A^2$).

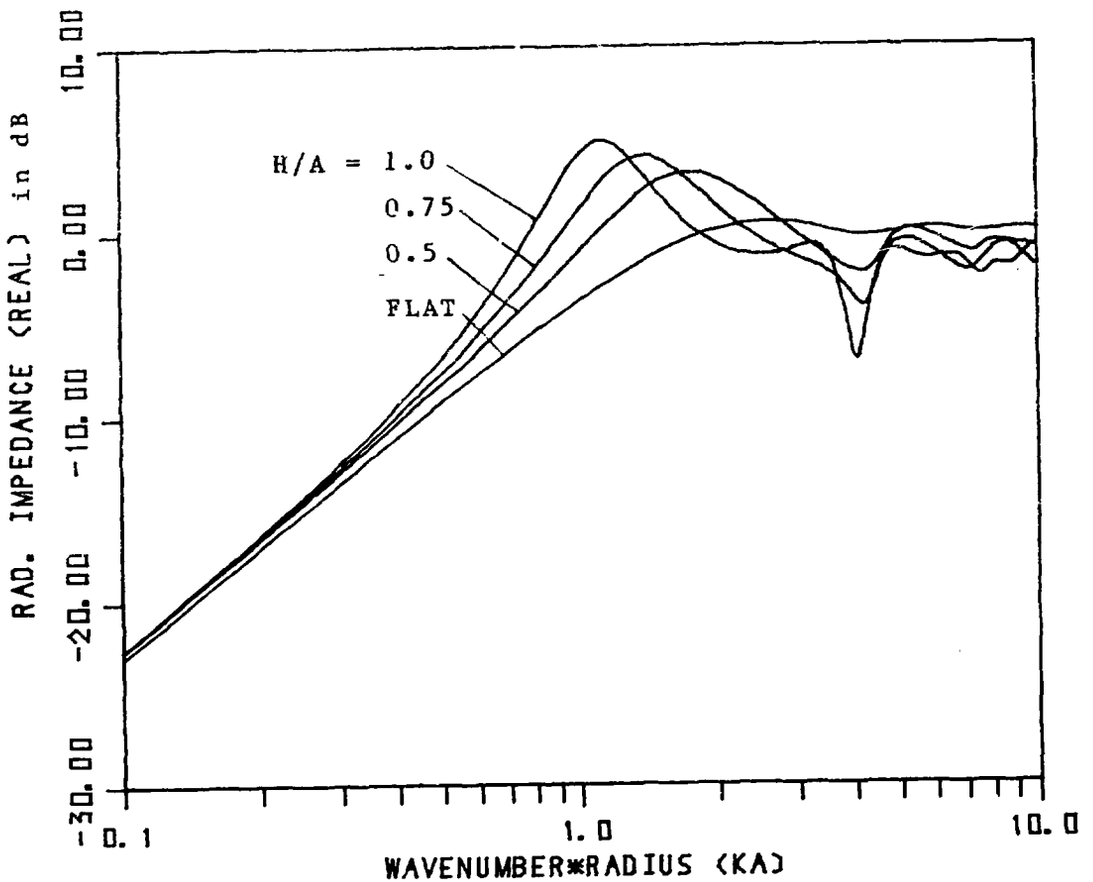

Figure 2.18 Radiation resistance characteristics of a concave dome (normalized by $\rho c \pi A^2$).

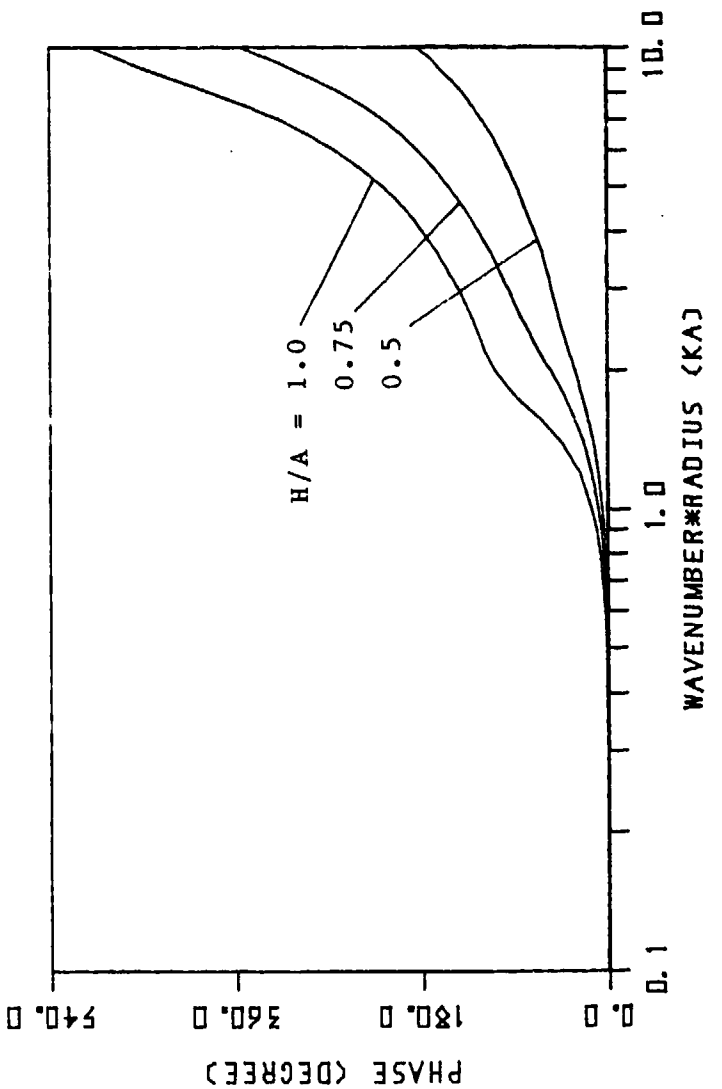

Figure 2.19 Phase responses of a convex dome.

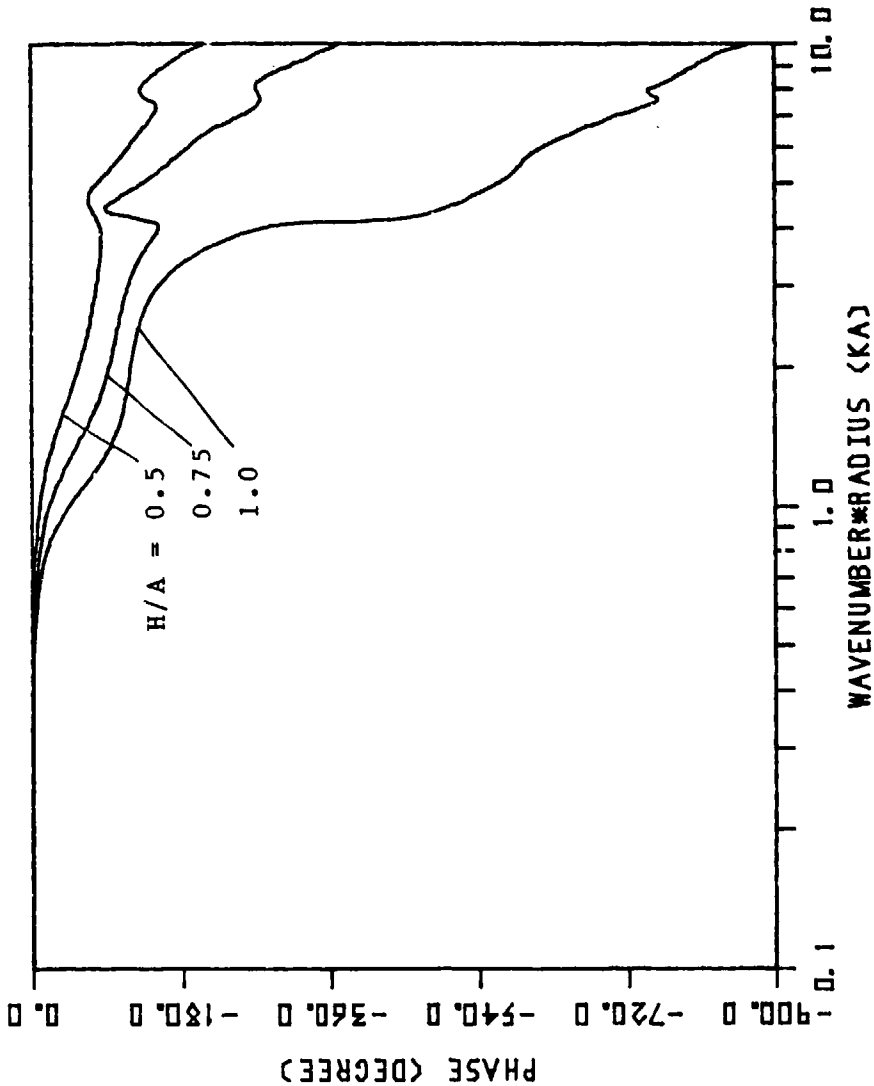

Figure 2.20 Phase responses of a concave dome.

respectively as the frequency increases. It is interesting to separate the total phase response into two parts, i.e., the minimum phase response obtained from the amplitude response through a Hilbert transform and the remaining phase response. The transfer function of the loudspeaker can therefore be represented by the following form:

$$H(\omega) = A(\omega)e^{i\phi_{min}(\omega)}e^{i\phi_{allpass}(\omega)} . \qquad (2.44)$$

The non-minimum phase response $\phi_{allpass}(\omega)$ is important because, even if the pressure response is ideally equalized by a minimum phase network, it still remains as the factor which causes a time delay.

The response $\phi_{min}(\omega)$ is obtained from the Hilbert transform [31],

$$\phi_{min}(\omega) = \int_{-\infty}^{\infty} \ell nA(\omega')d\omega'/(\omega' - \omega)\pi . \qquad (2.45)$$

For the exact solution of Eq. (2.45), one must know the pressure response $A(\omega)$ over the entire region of ω. But the range actually known is from kA = 0.1 to 10.0. For kA = 10.0 to 819.1, the pressure responses were calculated by the geometrical approximation method. This frequency region was sufficient to obtain the required precision of $\phi_{min}(\omega)$ in the frequency range from kA = 0.1 to 10.0. Then, $\phi_{allpass}(\omega)$ is obtained by

$$\phi_{allpass}(\omega) = \phi_{total}(\omega) - \phi_{min}(\omega) . \qquad (2.46)$$

By dividing Eq. (2.46) by k, one obtains the corresponding distance due to the phase delay, which will be referred to here as the "acoustic center". The characteristics of the acoustic center for various values of H/A are shown in Figures 2.21-2.22. The results in the low-frequency region are not quite correct because of using the discrete Fourier transform with the frequency interval of 0.1 to calculate Eq. (2.45). Also, a small error in the phase response can cause relatively large fluctuations in this region. The result for the concave dome with H/A = 1.0 is not shown because of the difficulty of taking into account the sharp dip of the pressure response around kA = 4.15.

It is interesting to note that the position of the acoustic center of a convex dome is constant and equal to H over the entire frequency range from kA = 0.1 to 10.0. The same result is obtained from the purely geometrical approximation. The reason for the existence of the acoustic center at the front of the source is shown in Appendix D for the case of a line source as an example.

The position of the acoustic center of the concave dome is also constant except in the very high-frequency region, and is located between the baffle surface and the top of the dome. The results of Figures 2.21-2.22 are very important because they show the location of the source after the equalization of the pressure response. The equalized responses of the convex and concave domes are nondispersive in the range used for an actual loudspeaker.

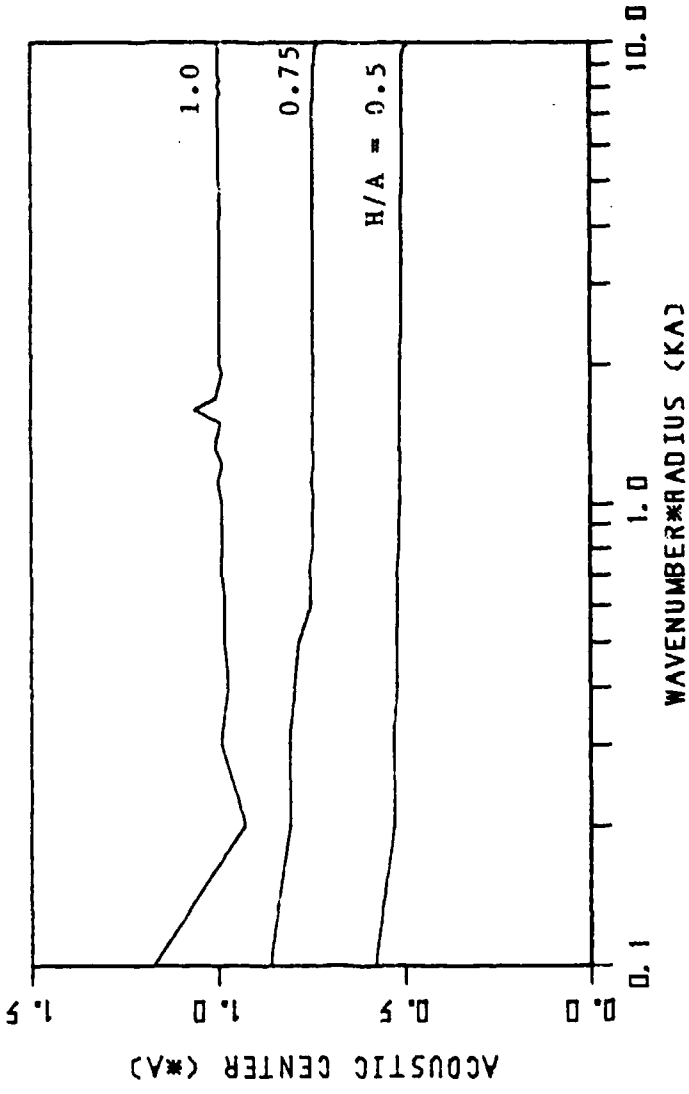

Figure 2.21 Acoustic center of a convex dome.

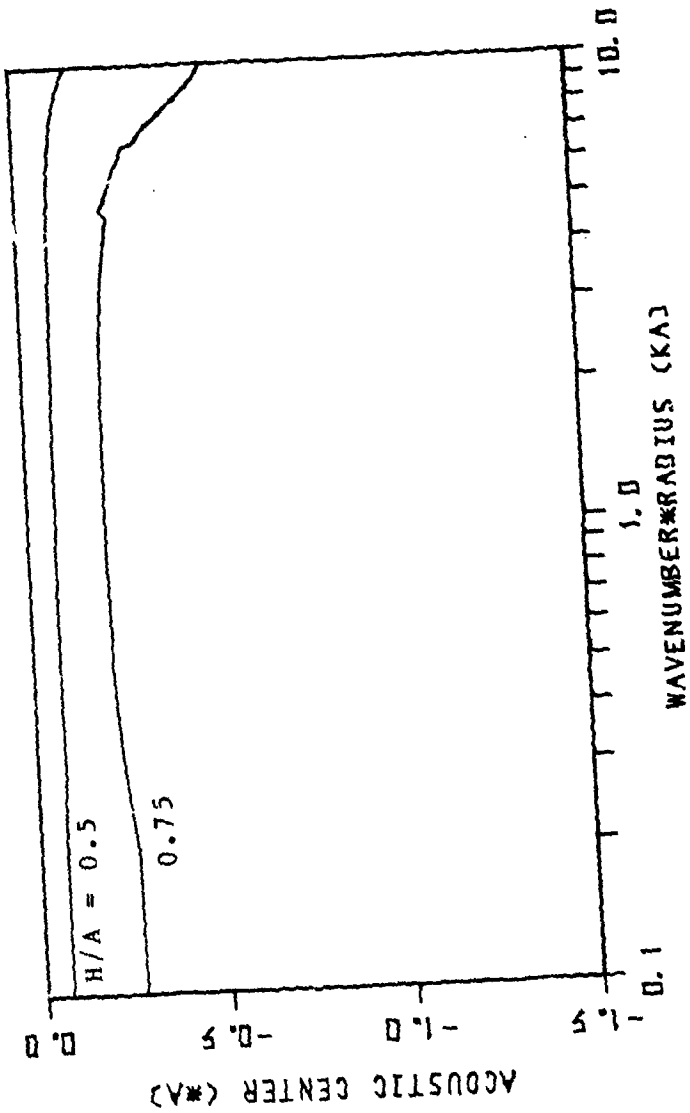

Figure 2.22 Acoustic center of a concave dome.

2.3.4 Directivity Pattern

The directivity pattern is one of the most important characteristics of a transducer. If one knows both the on-axis pressure level and the directivity pattern at a specific frequency, total radiated power and the radiation impedance at that frequency can be calculated.

Directivity patterns of the convex dome are shown in Figures 2.23-2.28, along with those of a flat piston. The on-axis pressures are lower than the 90-degree off-axis pressures for the convex domes with H/A = 1.0 or 0.75, and at kA = 1.0 and 2.0. From this frequency region, the convex dome has a wider directivity pattern than the flat piston. The convex dome has the narrowest directivity pattern around kA = 5.0 (Figure 2.26). Again, at higher frequencies, lower on-axis pressure responses than the off-axis pressure responses are observed (Figures 2.27 and 2.28).

Figures 2.29-2.35 show the directivity patterns of a concave dome. The concave dome has almost the same directivity patterns as the flat piston until about kA = 3.0. Figure 2.32 shows the directivity pattern at kA = 4.15, which is the frequency at which the on-axis pressure response has a sharp dip (Figure 2.10). The on-axis pressure is much lower than the 66-degree off-axis pressure. This results suggests that the normal velocity distribution on the opening of the cavity is not in a uniform phase. In the higher frequency region, the directivity pattern of a

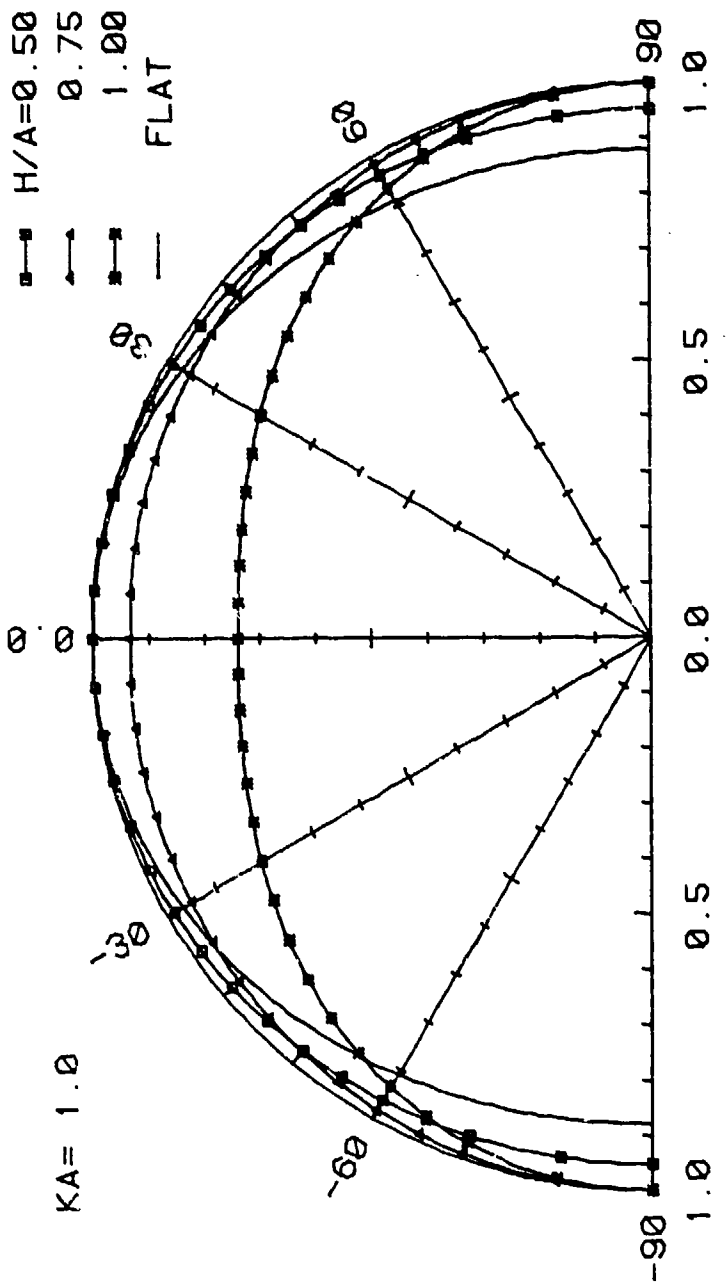

Figure 2.23 Directivity patterns of a convex dome and a flat piston at kA = 1.0.

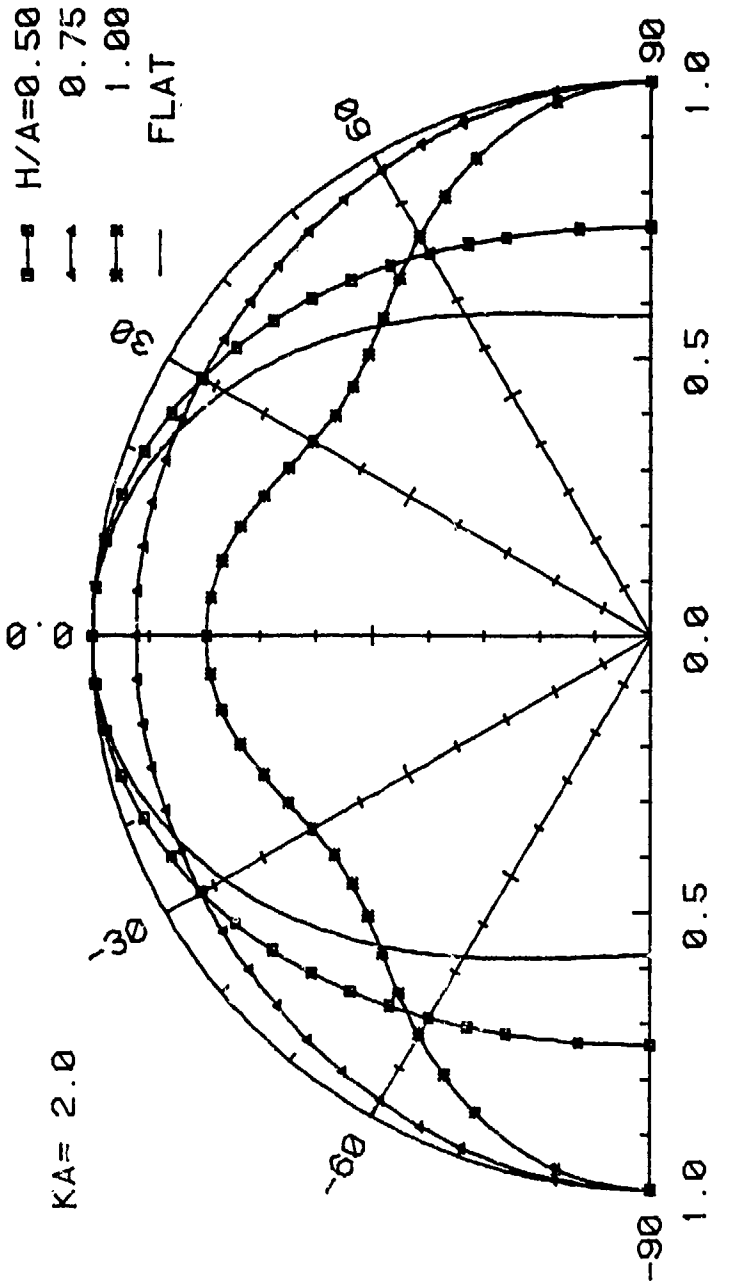

Figure 2.24 Directivity patterns of a convex dome and a flat piston at kA = 2.0.

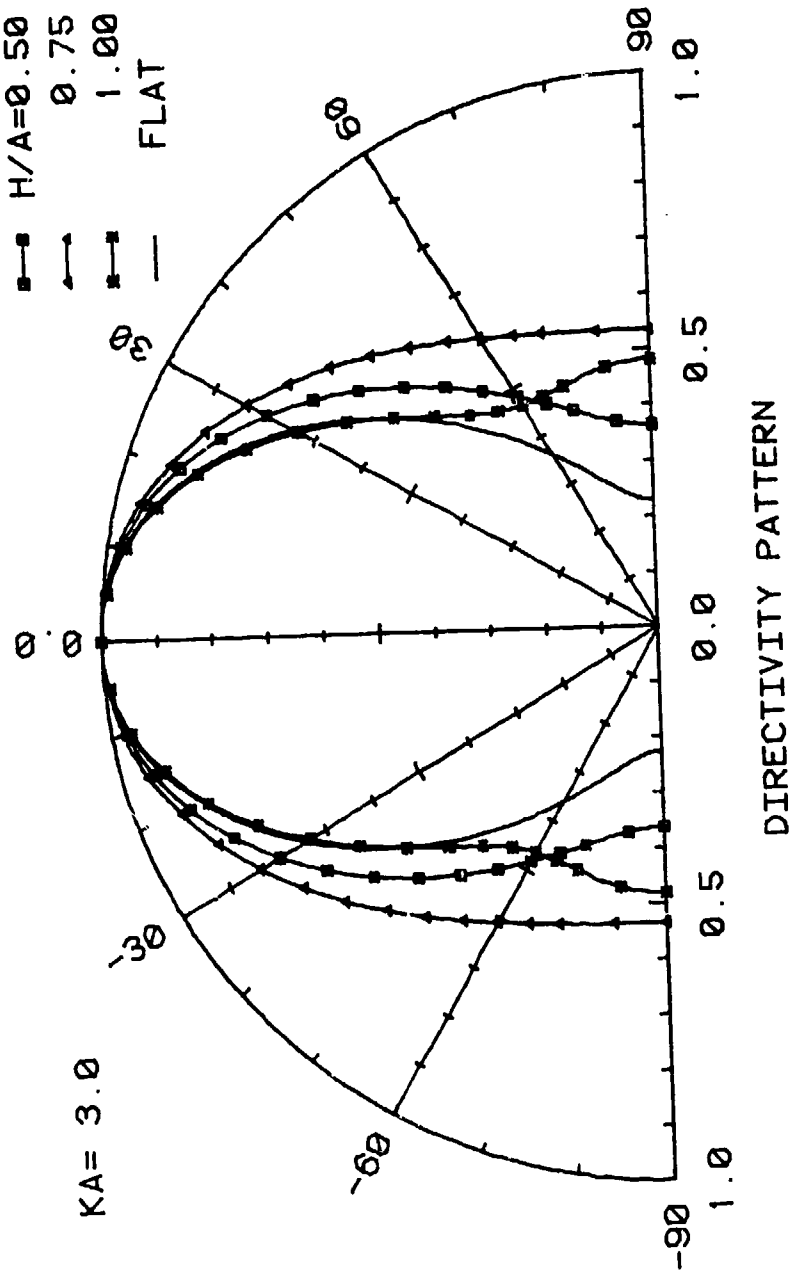

Figure 2.25 Directivity patterns of a convex dome and a flat piston at kA = 3.0.

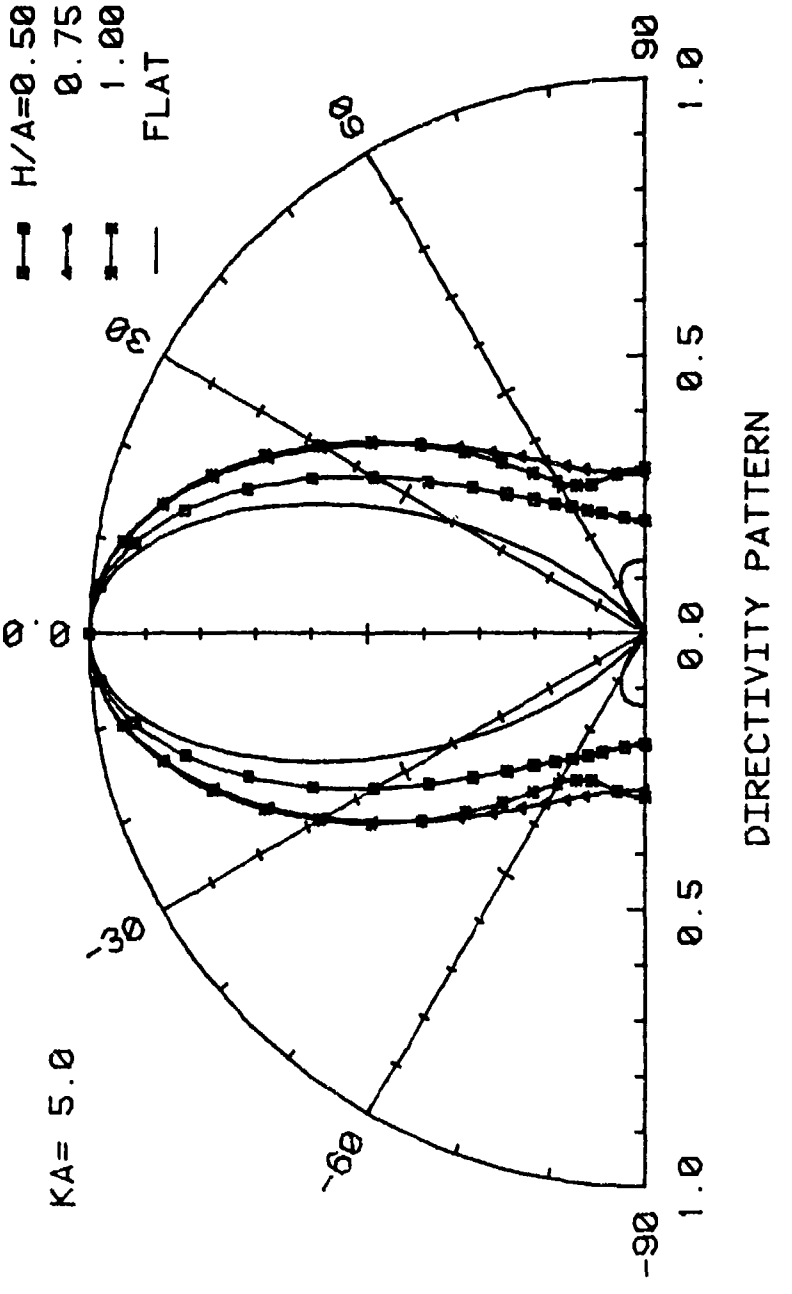

Figure 2.26 Directivity patterns of a convex dome and a flat piston at kA = 5.0.

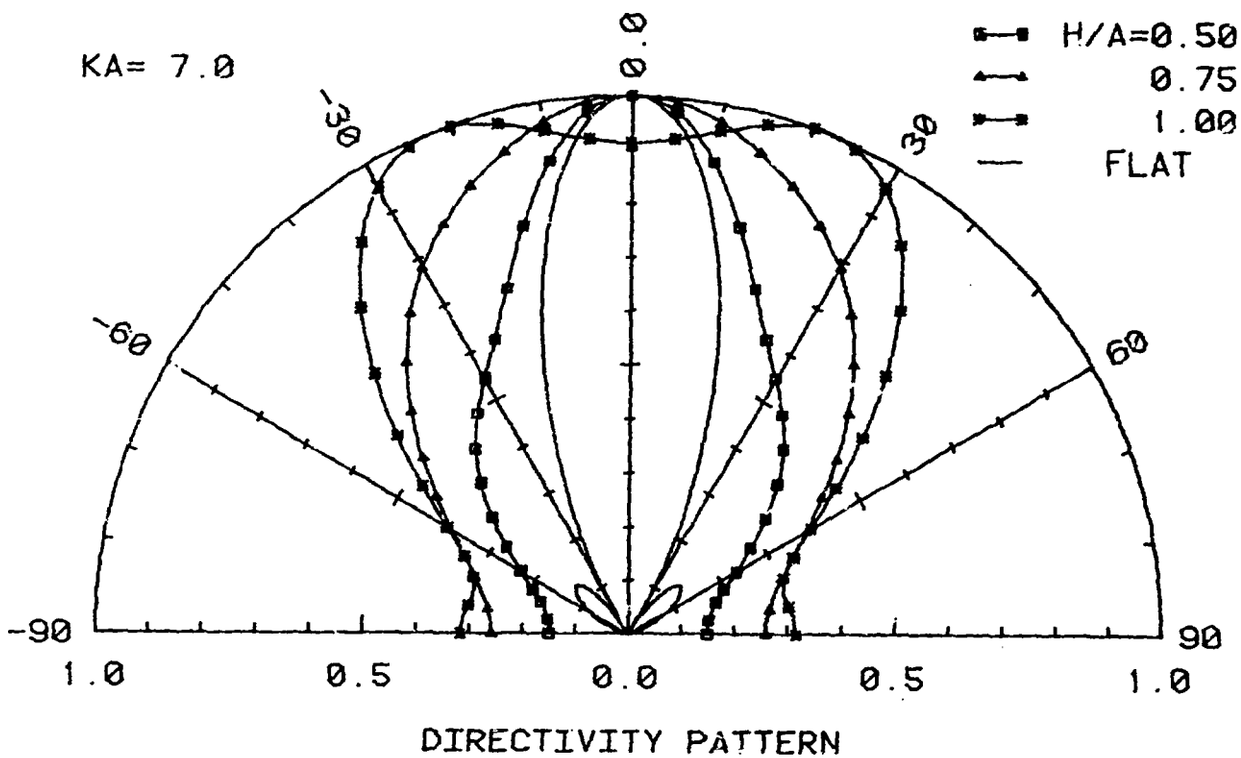

Figure 2.27 Directivity patterns of a convex dome and a flat piston at kA = 7.0.

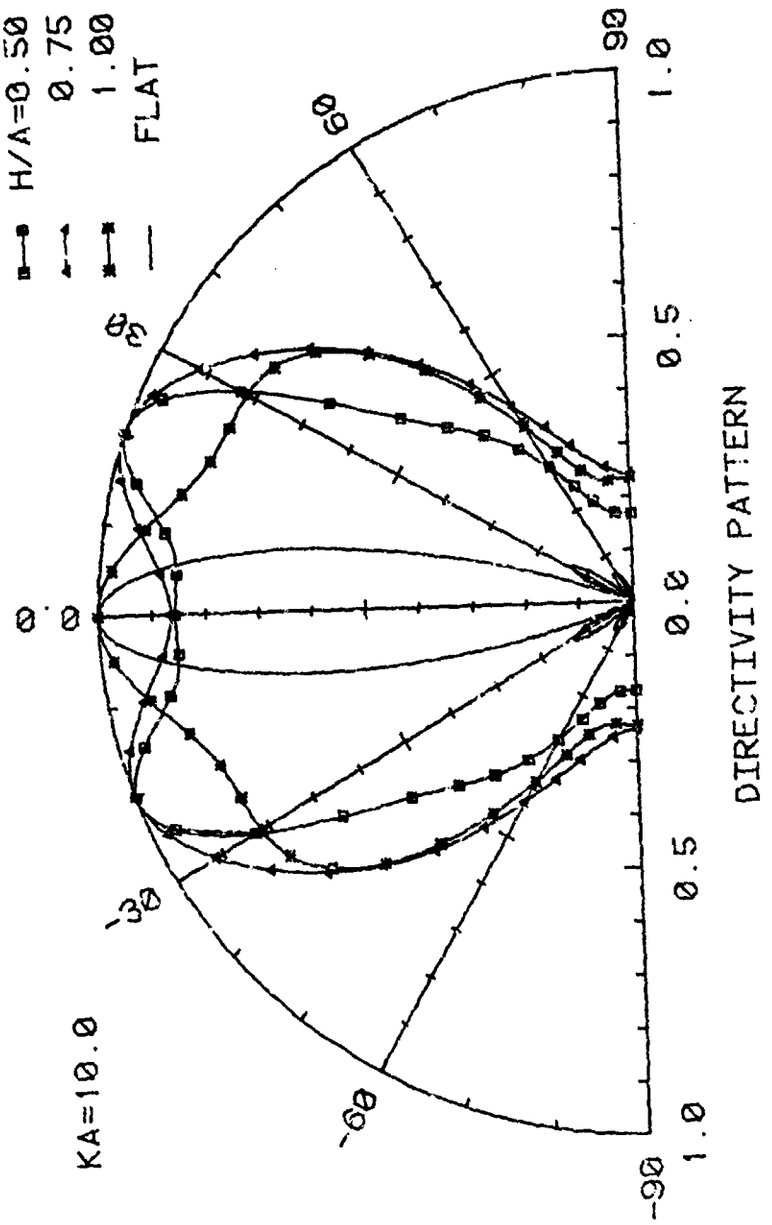

Figure 2.28 Directivity patterns of a convex dome and a flat piston at kA = 10.0.

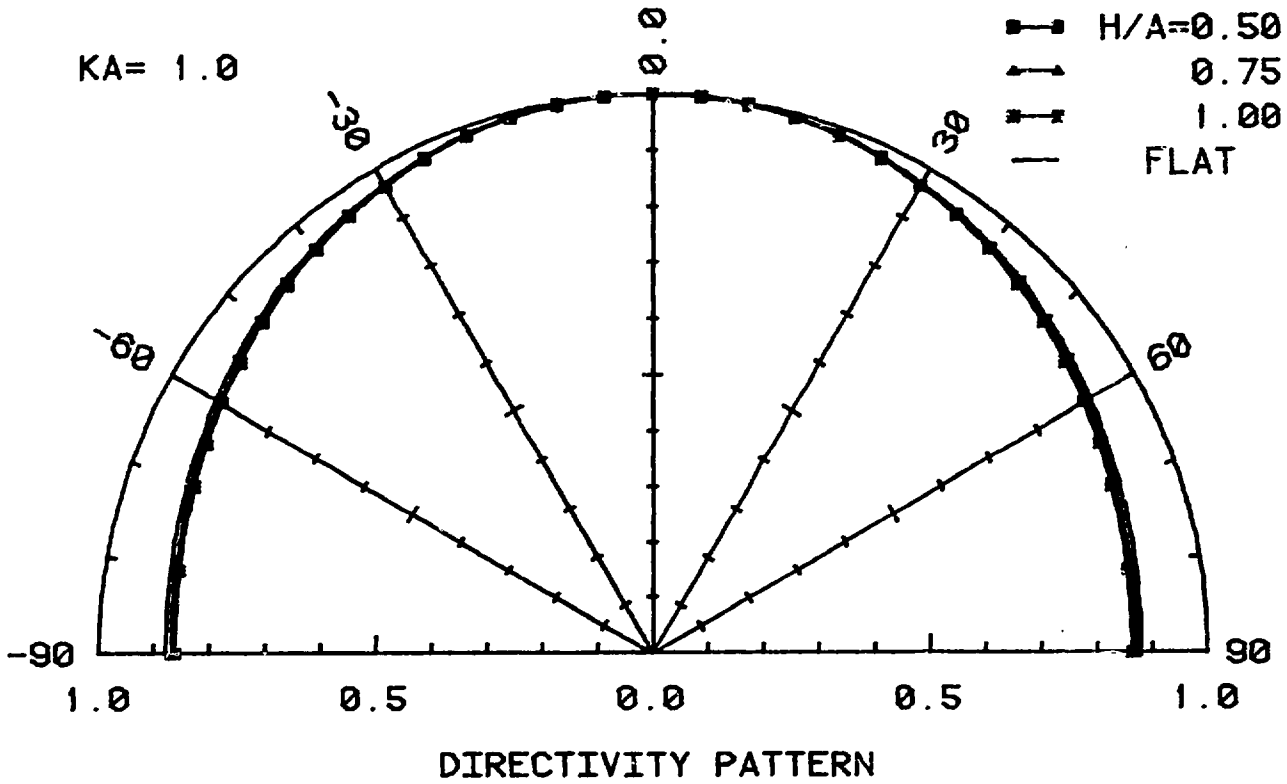

Figure 2.29 Directivity patterns of a concave dome and a flat piston at kA = 1.0.

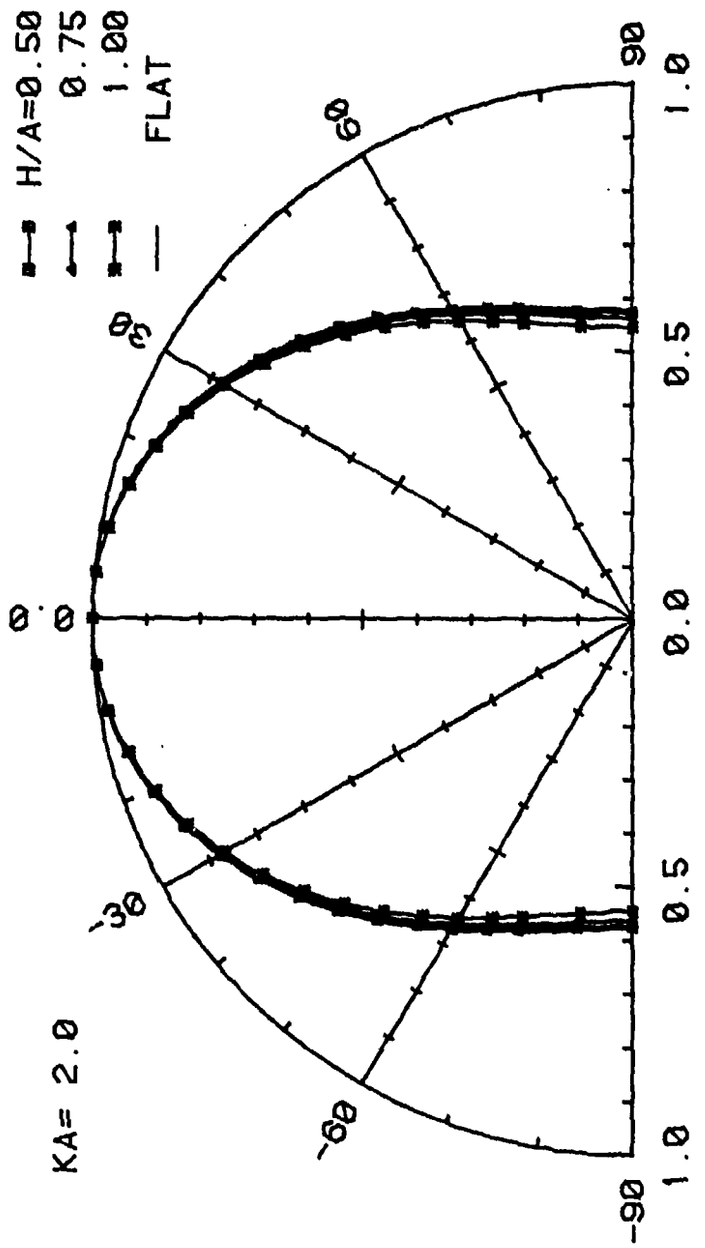

Figure 2.30 Directivity patterns of a concave dome and a flat piston at kA = 2.0.

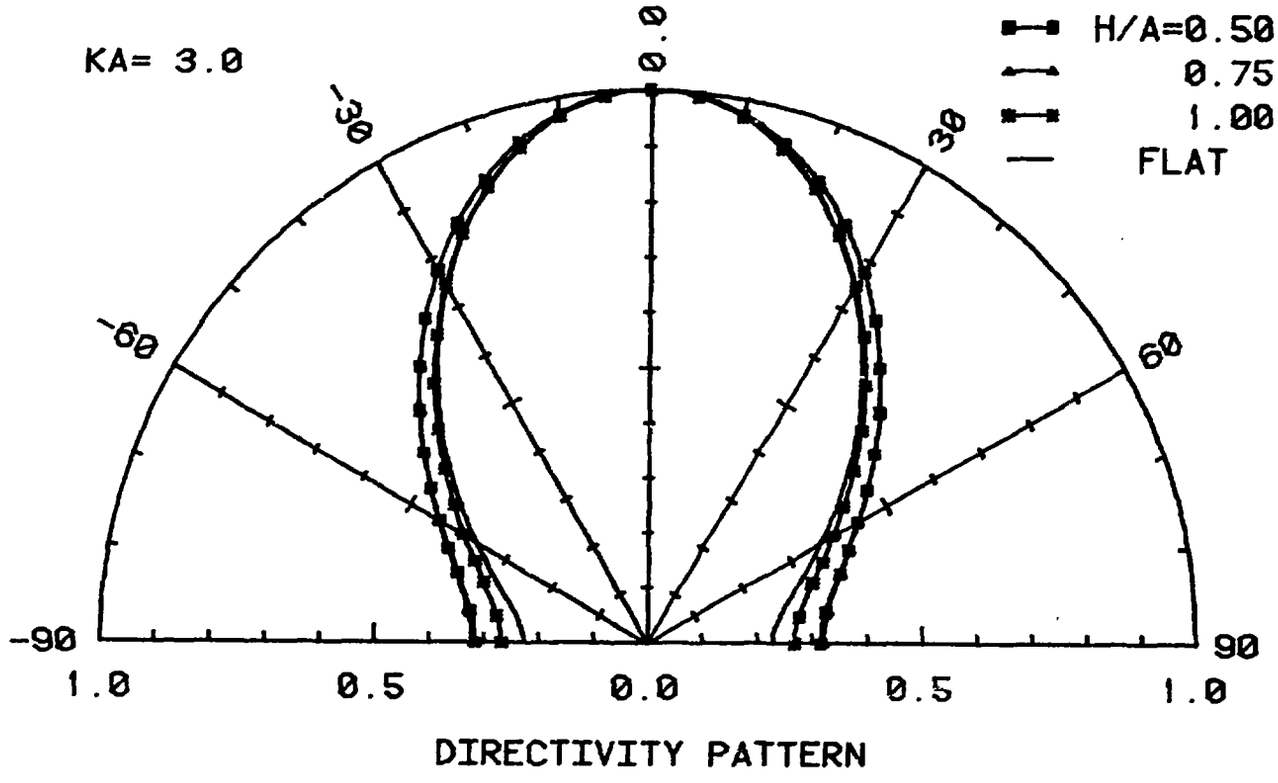

Figure 2.31 Directivity patterns of a concave dome and a flat piston at kA = 3.0.

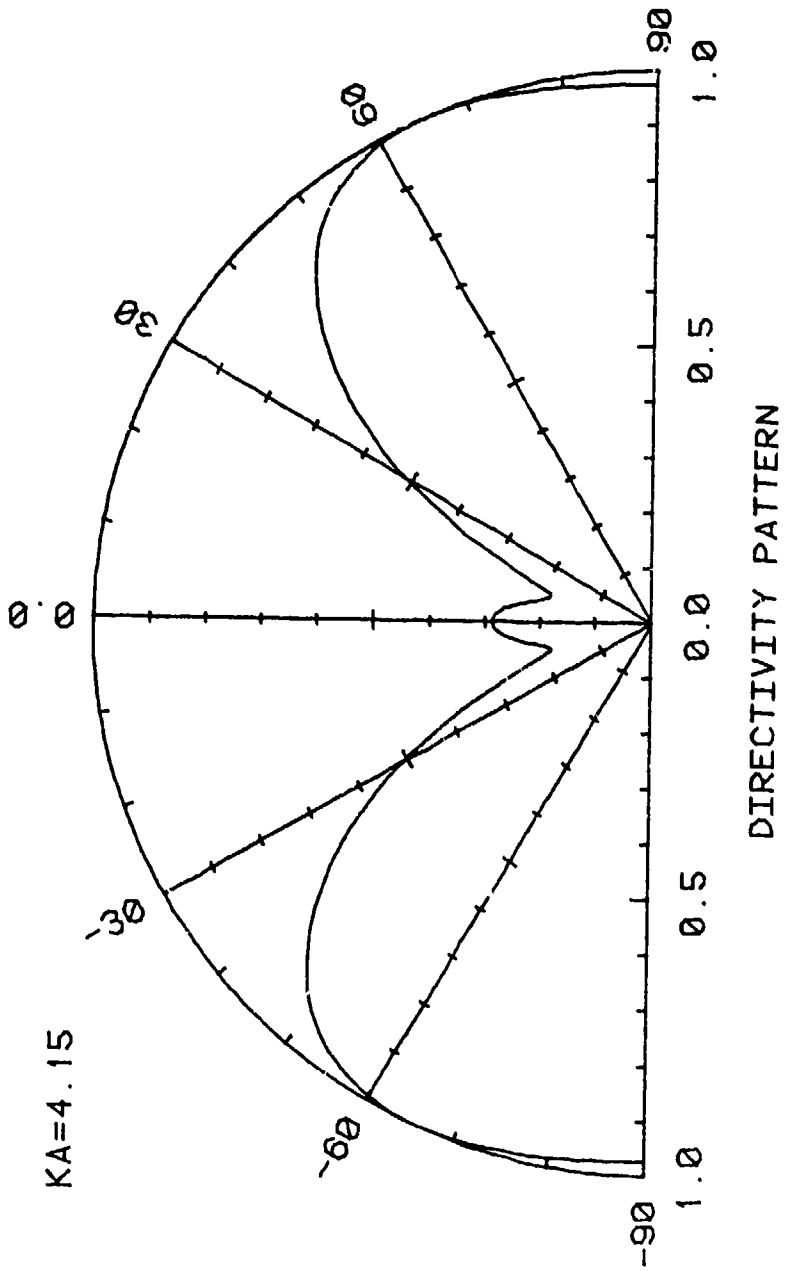

Figure 2.32 Directivity patterns of a concave dome with H/A = 1.0 at kA = 4.15.

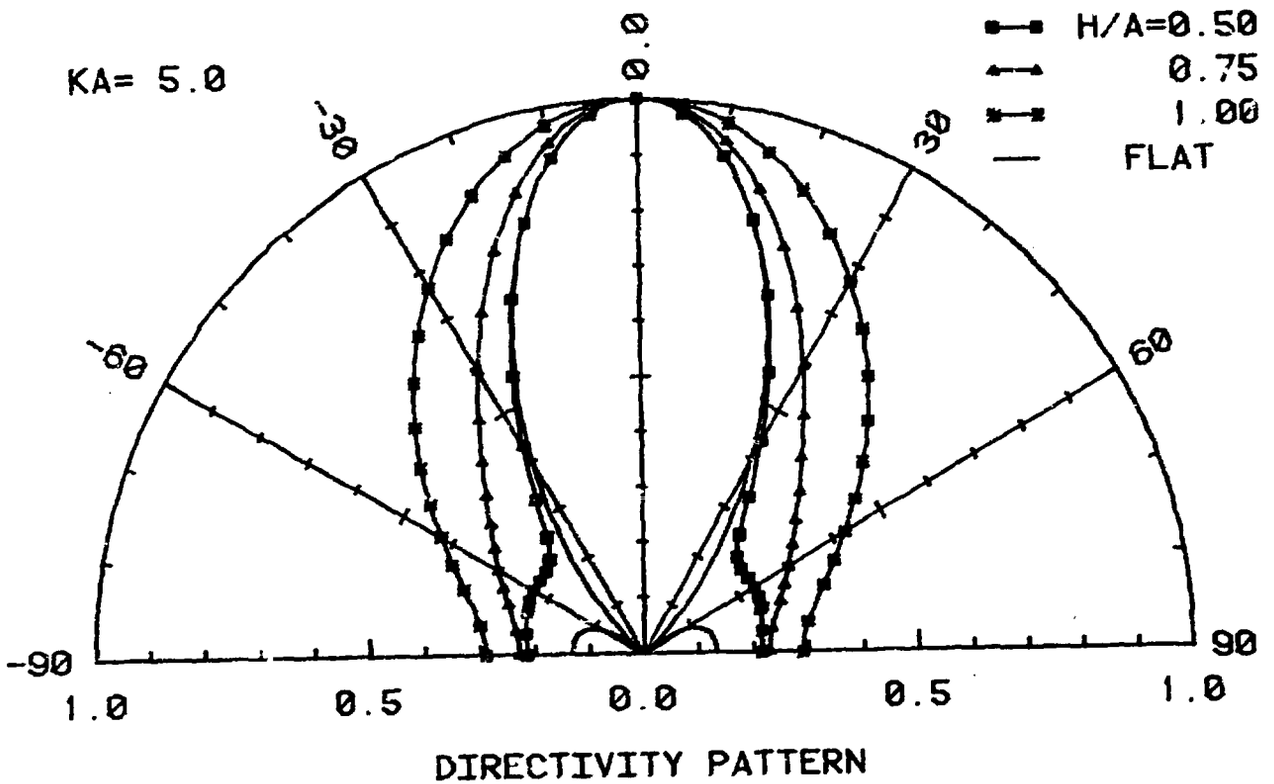

Figure 2.33 Directivity patterns of a concave dome and a flat piston at kA = 5.0.

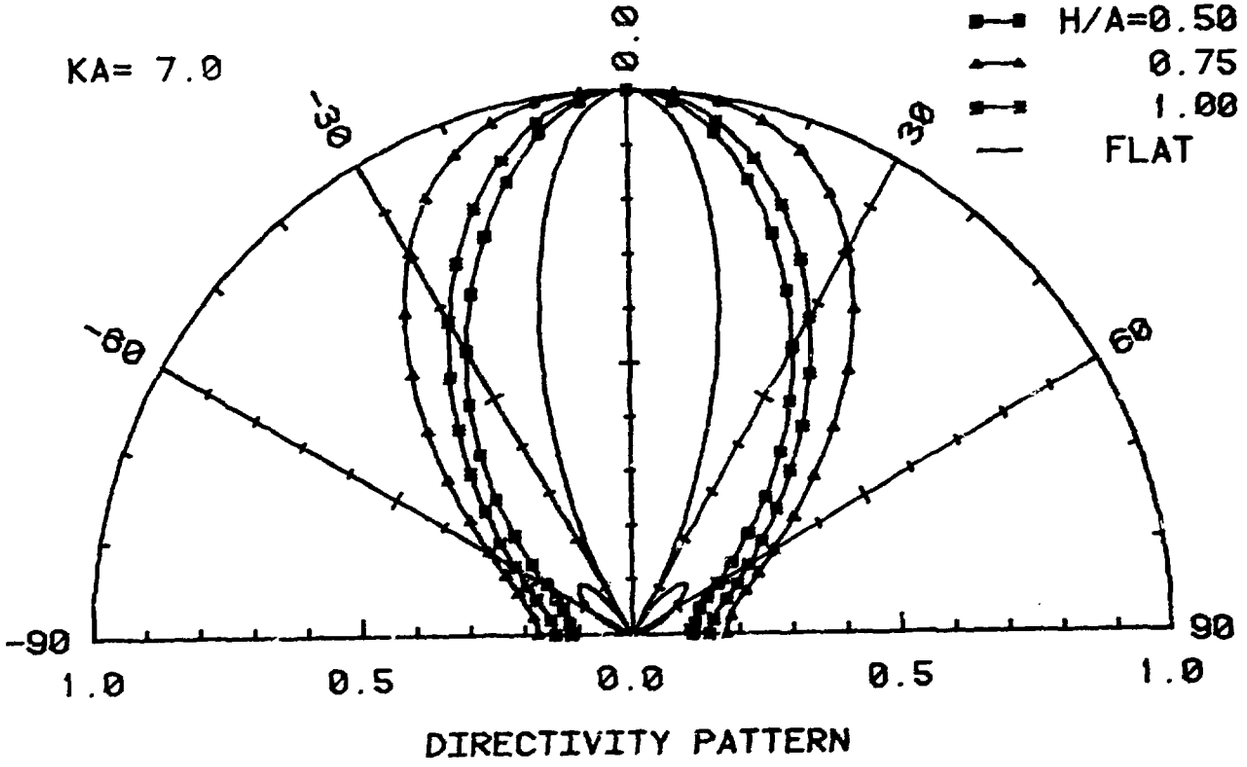

Figure 2.34 Directivity patterns of a concave dome and a flat piston at kA = 7.0.

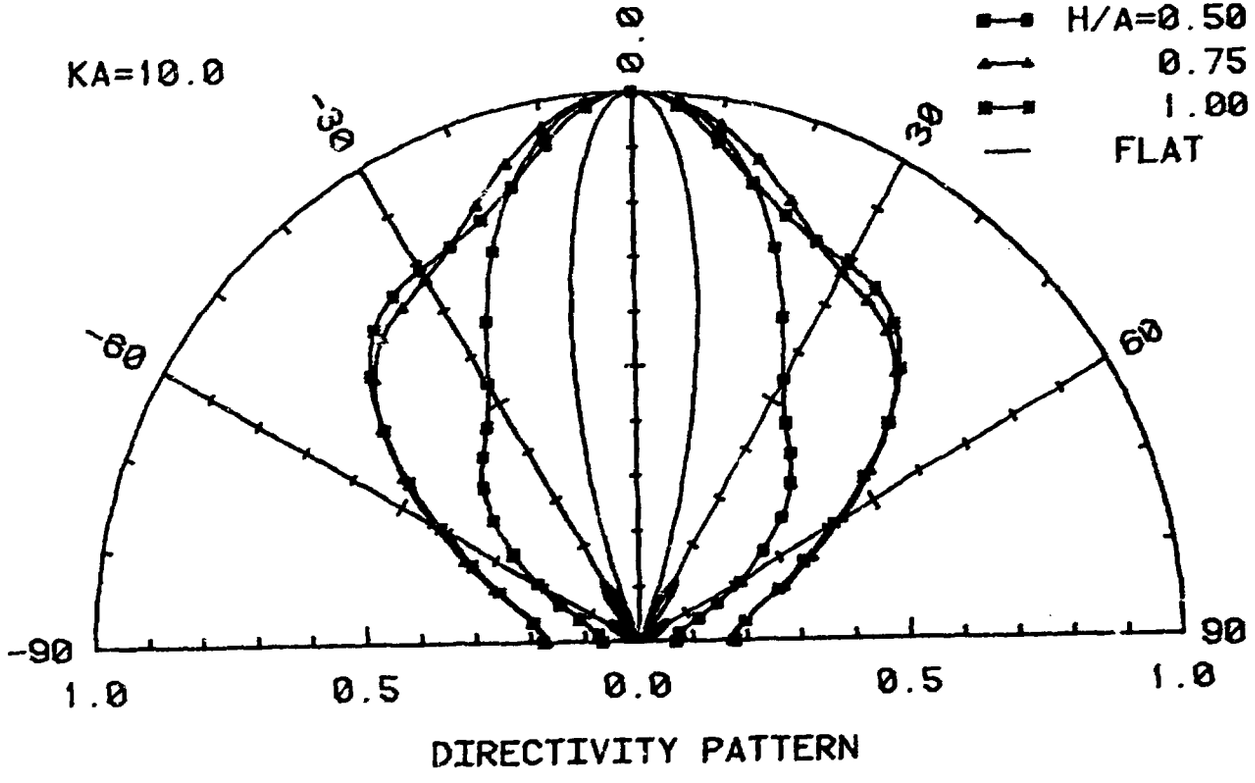

Figure 2.35 Directivity patterns of a concave dome and a flat piston at kA = 10.0.

concave dome has similar properties to those of the convex dome. Neither dome shows zero pressure at any angle. As a practical point of view, it should be mentioned that the convex dome has wider directivity than the concave dome or the flat piston in the frequency range normally used for the loudspeaker.

2.3.5 Energy Flow and Pressure Distribution

Besides the sound pressure, the important and interesting quantity used to describe the sound field is the energy flow. Therefore, the sound intensity was calculated and the results are presented for some H/A values.

The x and z components of intensity in the field are defined as

$$I_{x,z} = \mathrm{Re}[p\, u^*_{x,z}] / 2 \,. \qquad (2.47)$$

Then, the direction of the particle motion and the intensity I_o in that direction are given, respectively, by

$$\theta = \tan^{-1}(I_x/I_z) \qquad (2.48)$$

and

$$I_o = (I_x^2 + I_z^2)^{1/2} \,. \qquad (2.49)$$

These two values are simply described by an arrow with its direction and length.

The graphs of energy flow and pressure distribution of the convex dome for several H/A values are shown in Figures

2.36-2.44. The arrow shows the relative amplitude proportional to $(I_o)^{1/2}$ and the direction of I_o at the point of the tail of the arrow. The size of the circle is proportional to the absolute value of the pressure at its center. For the convex dome with H/A = 1.0 at kA = 1.0 (Figure 2.42), the energy tends to flow from the high-pressure region (near axis) to the low-pressure region (off-axis) on the surface of the radiator. As a consequence, at distances greater than approximately 3 radiator radii, the on-axis sound pressure is smaller than the 90-degree off-axis sound pressure. As the frequency increases, the energy starts to be radiated normal to the surface, and the bundle of energy is confined near the axis.

The pressure distribution and the energy flow of the concave dome are shown in Figures 2.45-2.54. The energy radiated from the concave dome with H/A = 1.0 at frequency kA = 1.0 (Figure 2.51) flows along the axis inside the cavity. The pressure is constant along the opening of the cavity, but decreases along the axis even inside the cavity. This shows that the effect of the cavity cannot be represented by a simple lumped compliance in the analog circuit. At kA = 3.0 (Figure 2.52), the pressure along the opening is not constant, and the energy flow is not parallel to the axis anymore. The graph at kA = 4.15 (Figure 2.53) shows some interesting results. The energy radiated from some area of the radiator surface goes around about 360 degrees inside the cavity, and goes out to semi-infinite

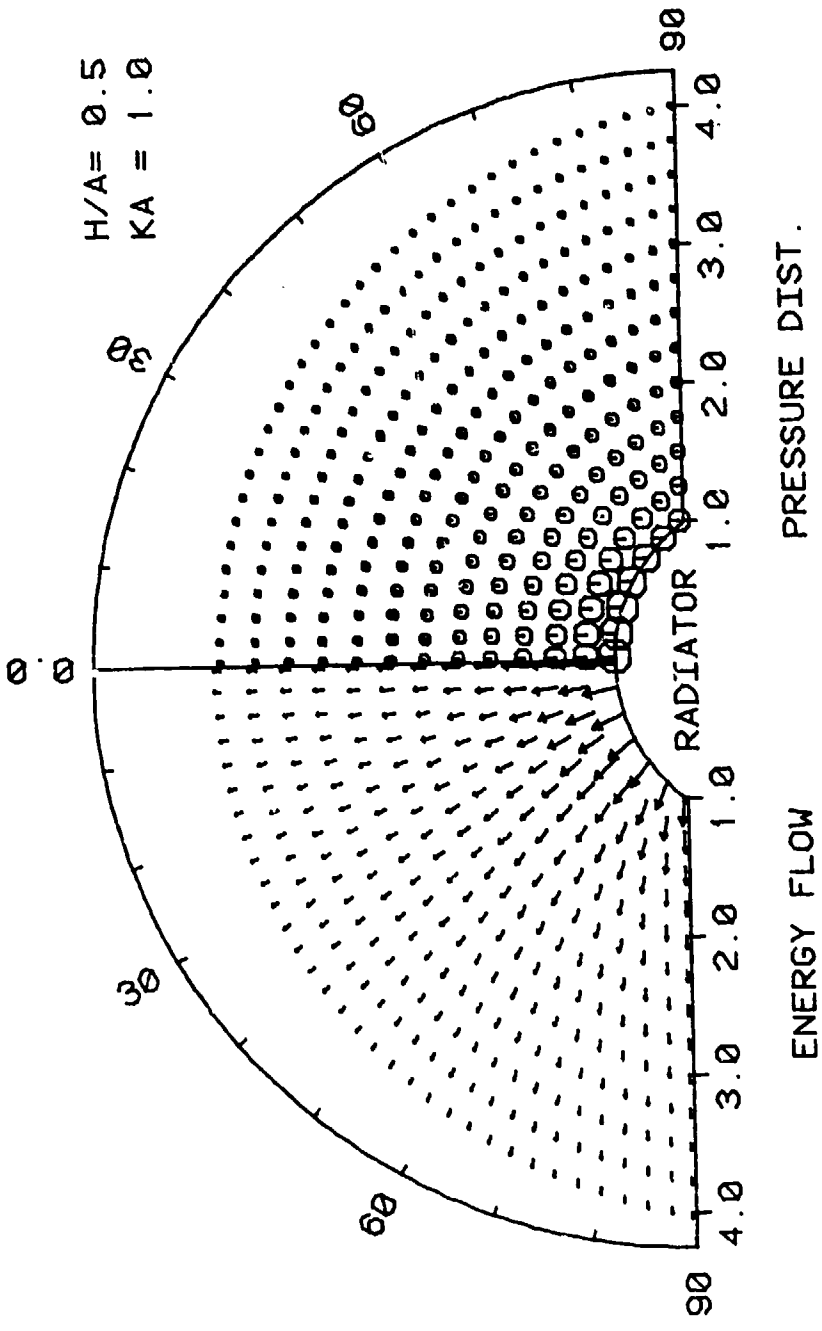

Figure 2.36 Energy flow and pressure distribution of a convex dome with H/A = 0.5 at kA = 1.0.

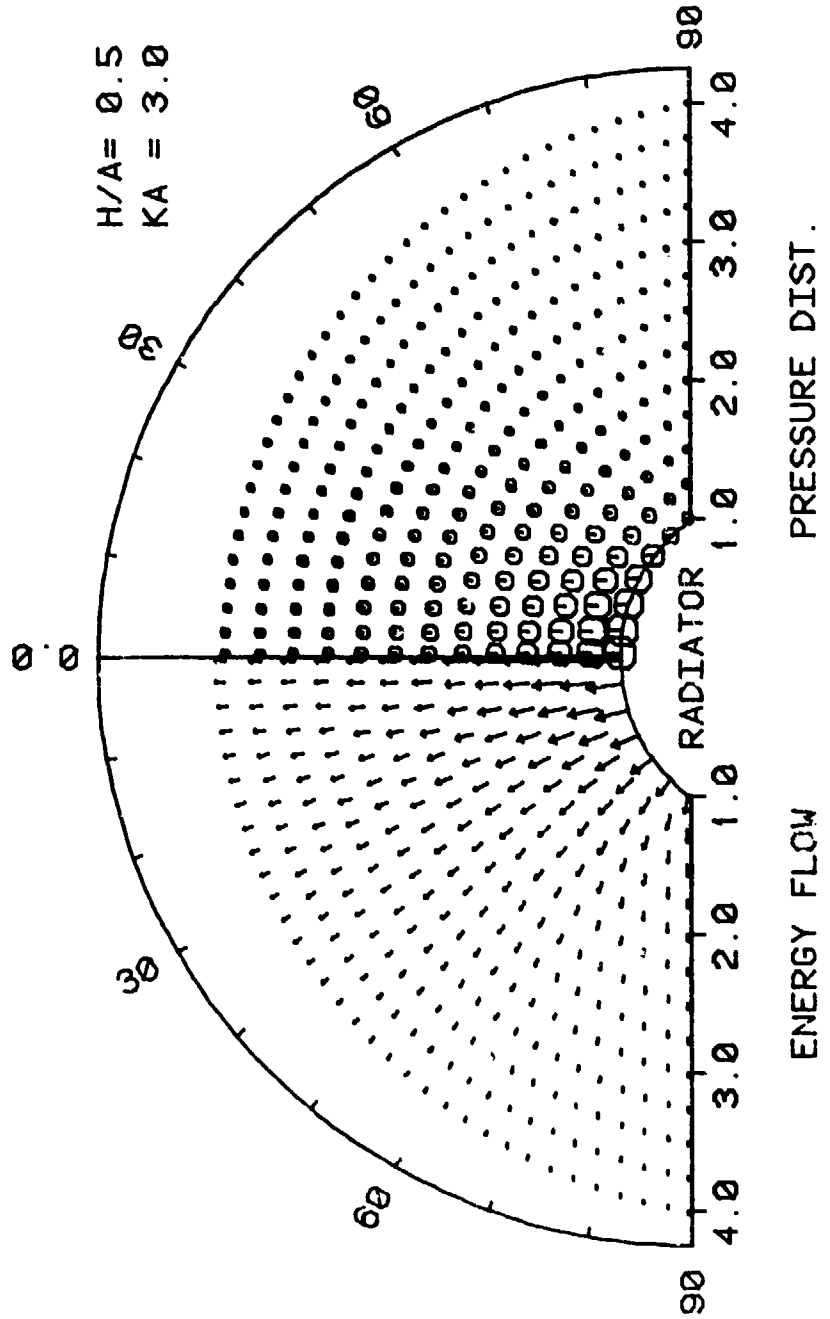

Figure 2.37 Energy flow and pressure distribution of a convex dome with H/A = 0.5 at kA = 3.0.

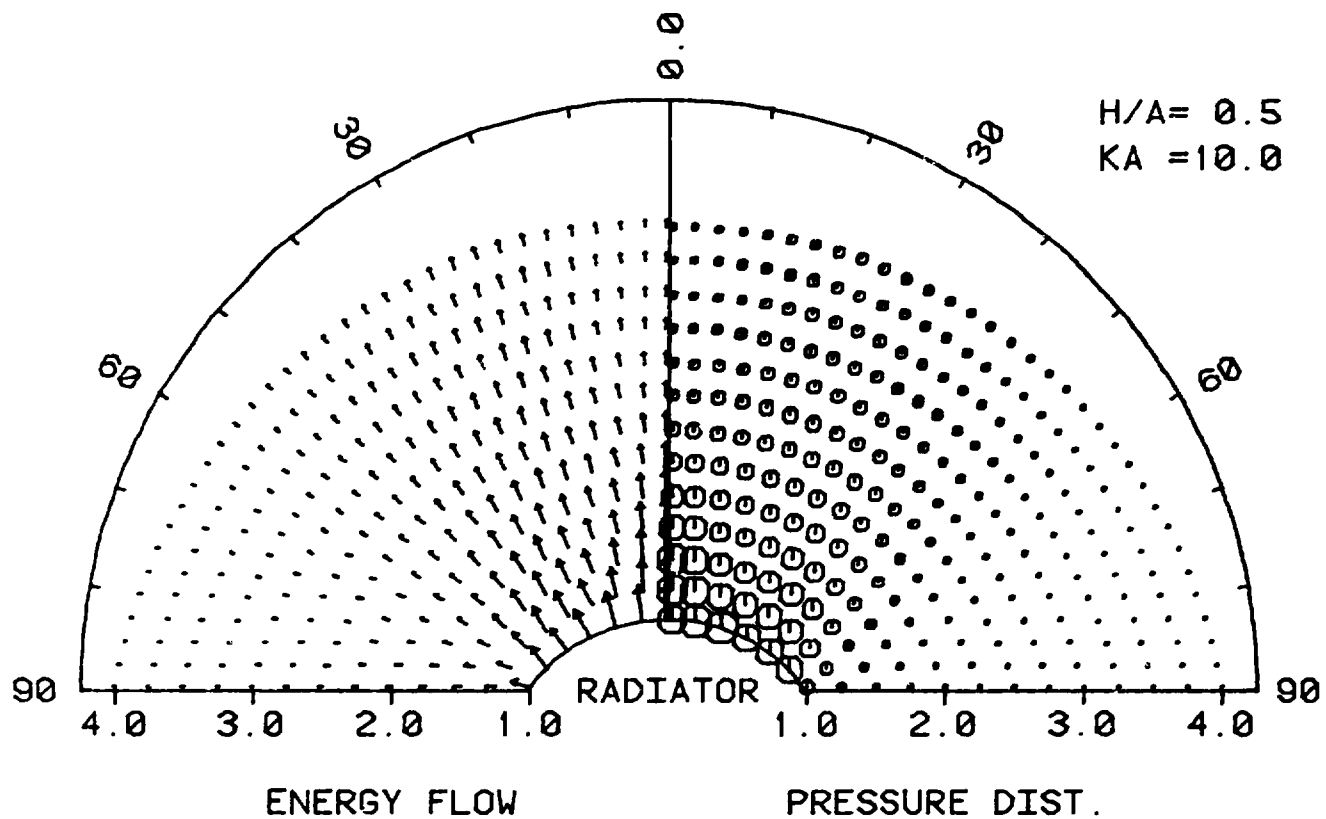

Figure 2.38 Energy flow and pressure distribution of a convex dome with H/A = 0.5 at kA = 10.0.

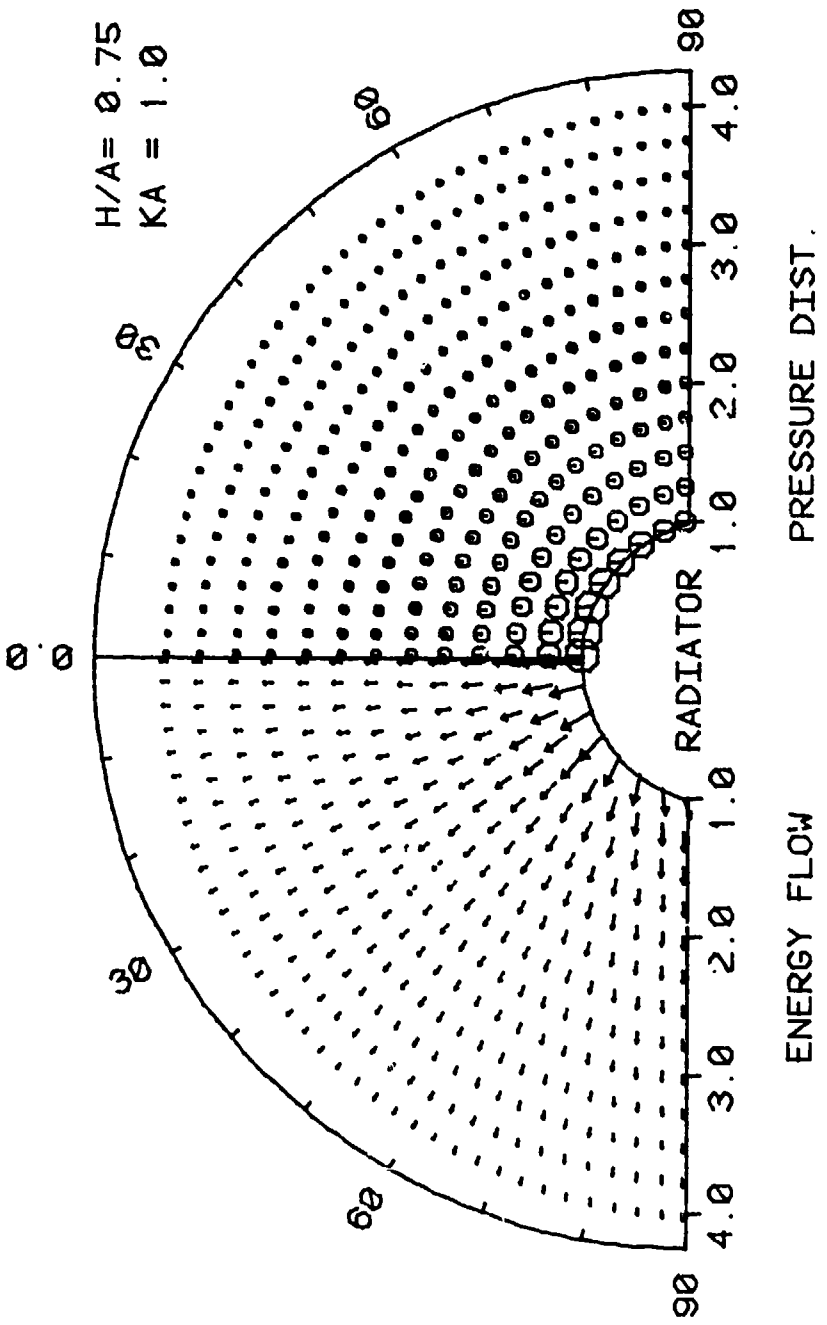

Figure 2.39 Energy flow and pressure distribution of a convex dome with H/A = 0.75 at kA = 1.0.

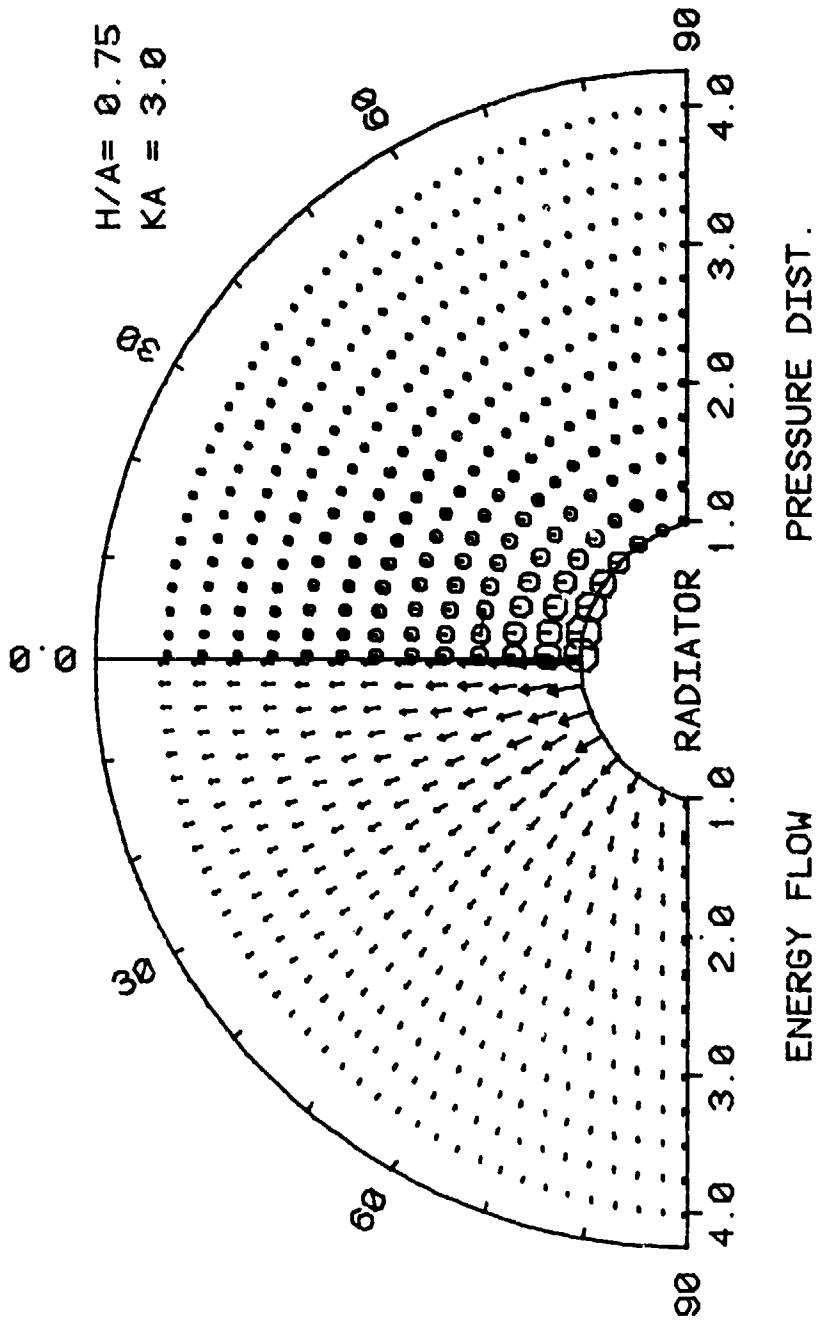

Figure 2.40 Energy flow and pressure distribution of a convex dome with H/A = 0.75 at kA = 3.0.

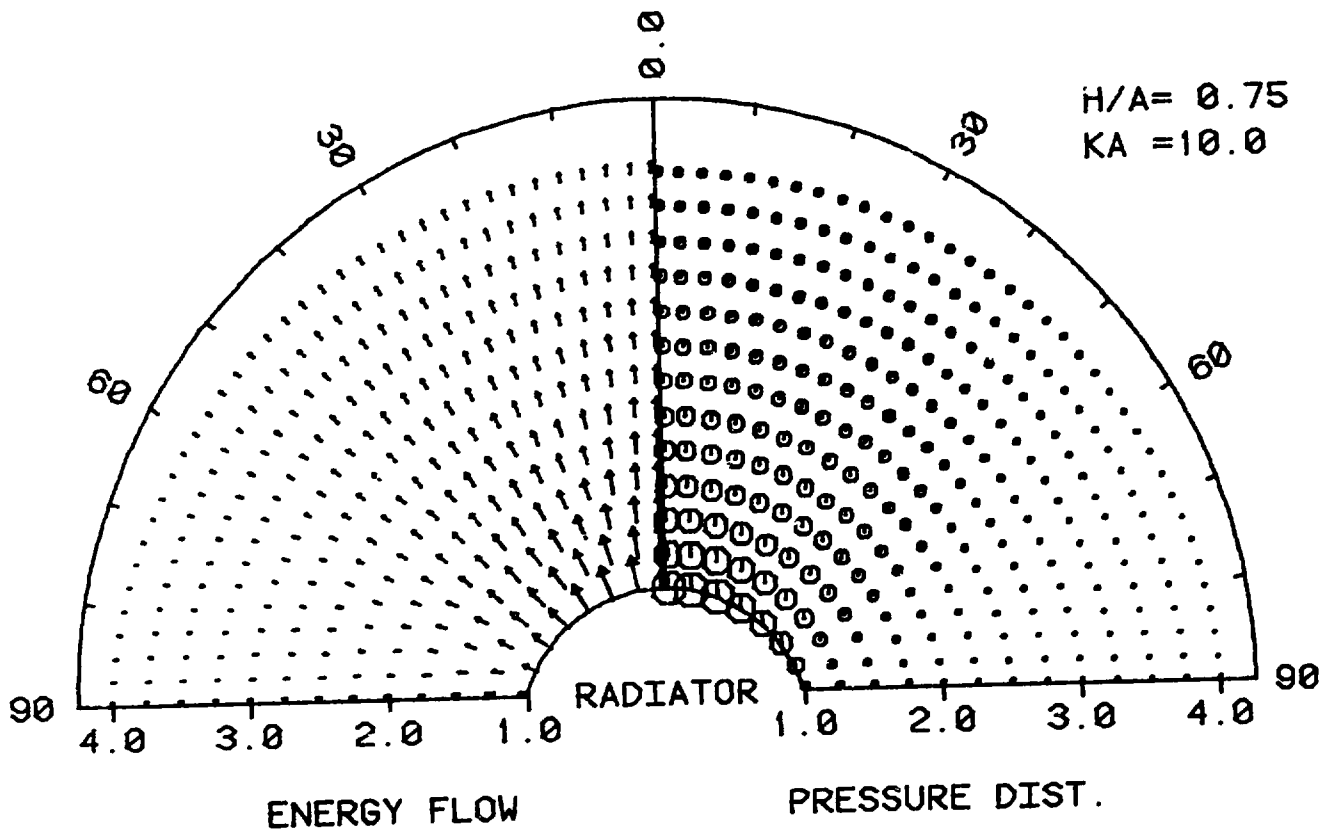

Figure 2.41 Energy flow and pressure distribution of a convex dome with H/A = 0.75 at kA = 10.0.

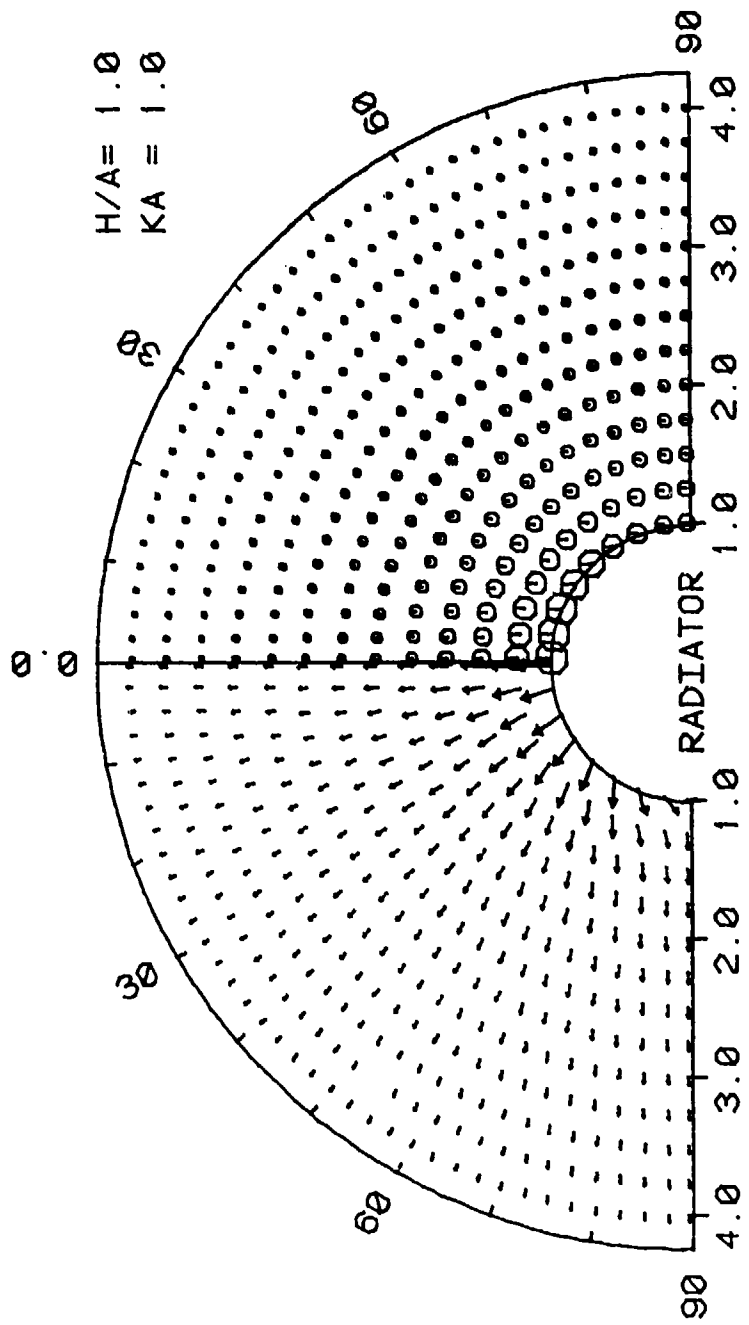

Figure 2.42 Energy flow and pressure distribution of a convex dome with H/A = 1.0 at kA = 1.0.

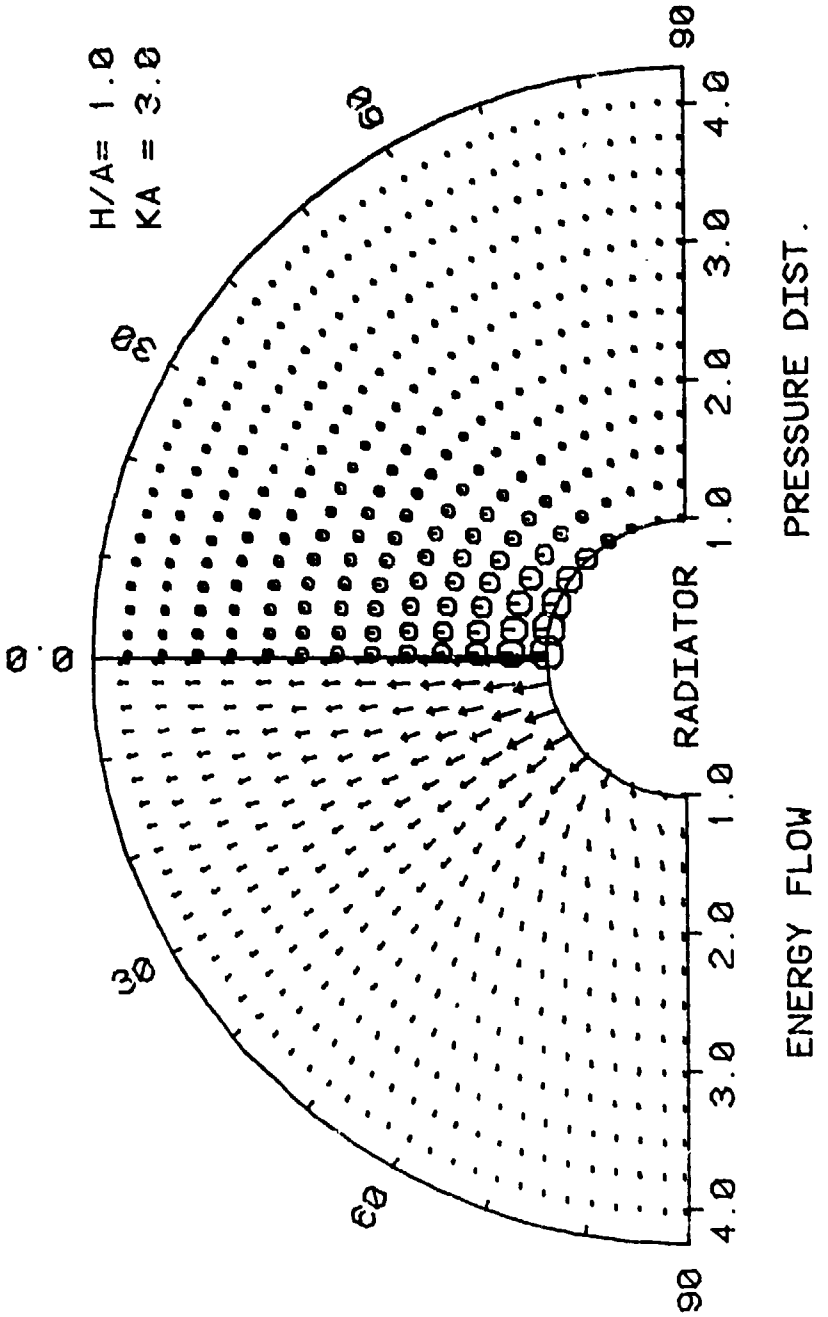

Figure 2.43 Energy flow and pressure distribution of a convex dome with H/A = 1.0 at kA = 3.0.

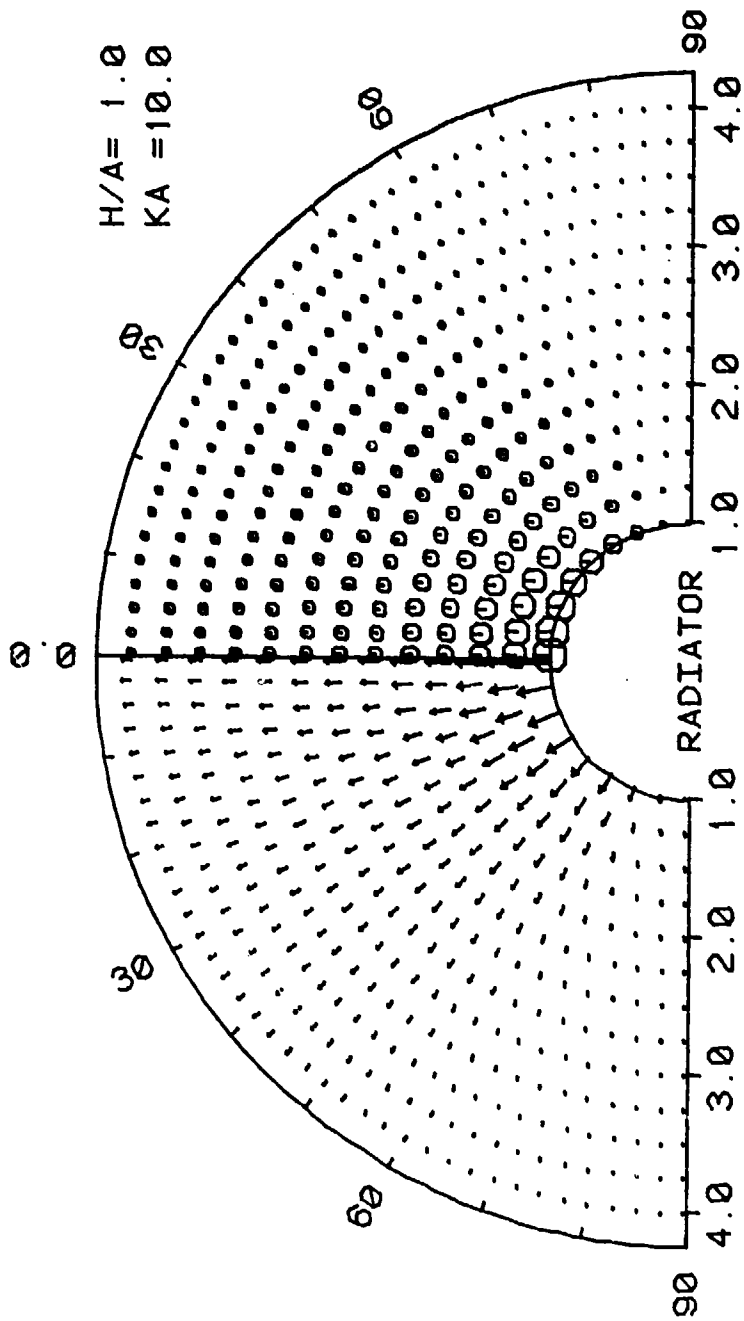

Figure 2.44 Energy flow and pressure distribution of a convex dome with H/A = 1.0 at kA = 10.0.

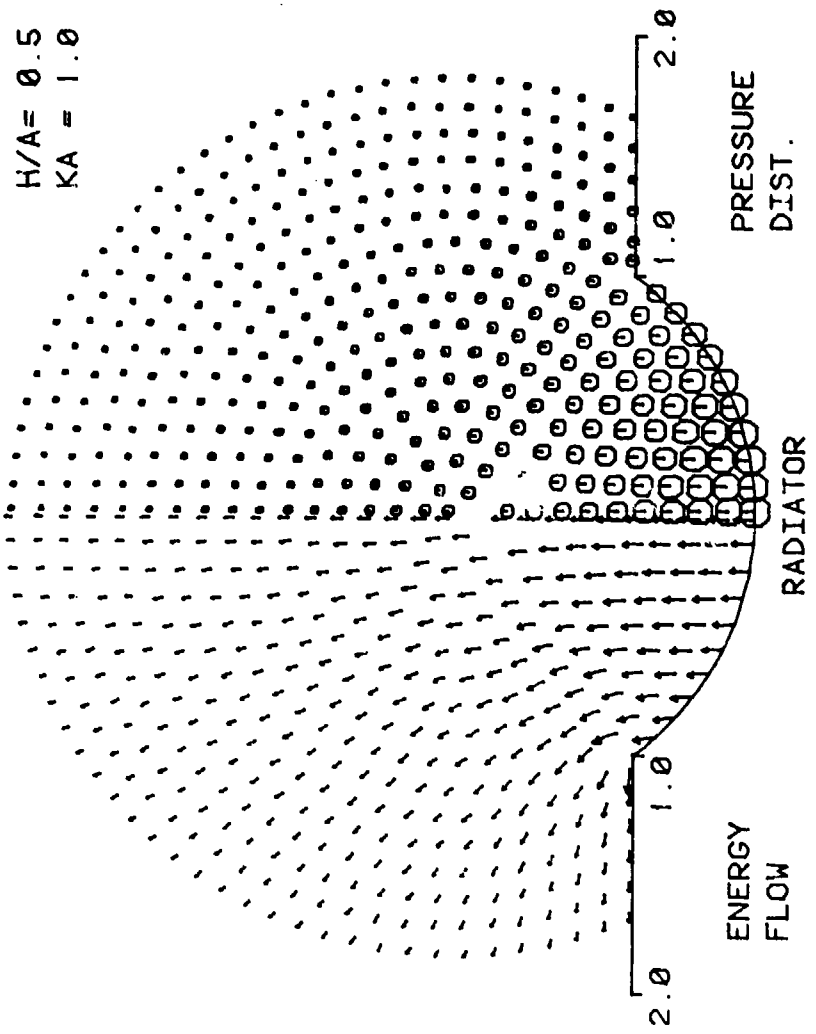

Figure 2.45 Energy flow and pressure distribution of a concave dome with H/A = 0.5 at kA 1.0.

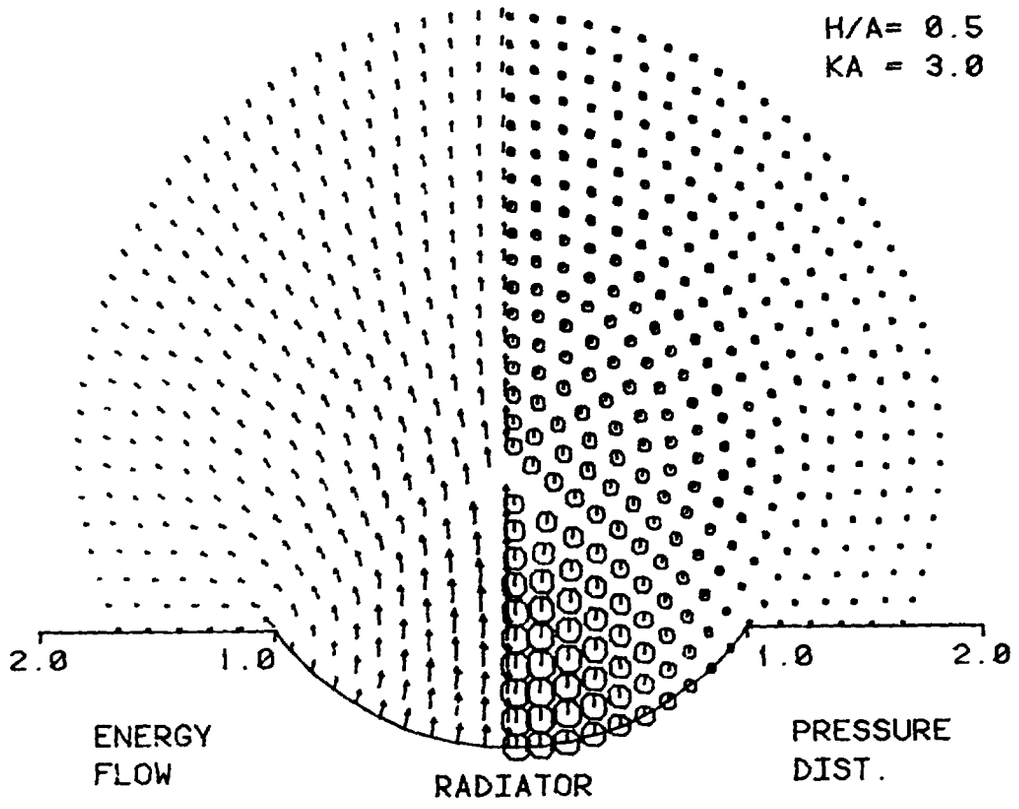

Figure 2.46 Energy flow and pressure distribution of a concave dome with H/A = 0.5 at kA = 3.0.

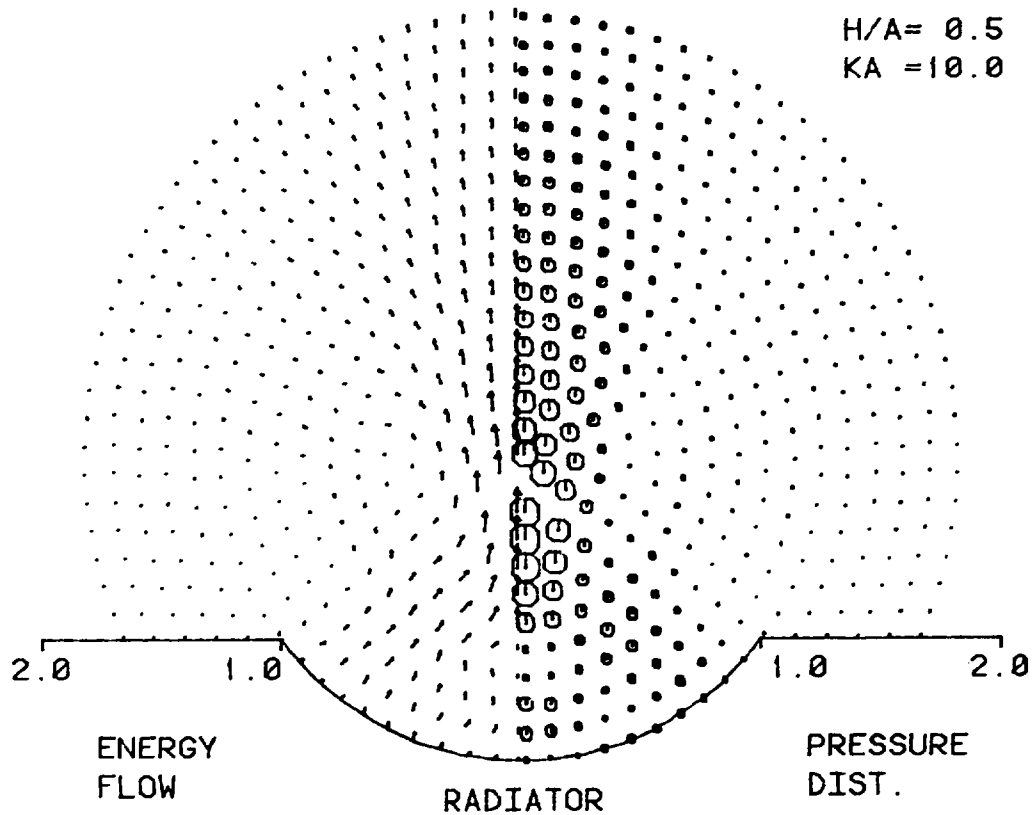

Figure 2.47 Energy flow and pressure distribution of a concave dome with H/A = 0.5 at kA = 10.0.

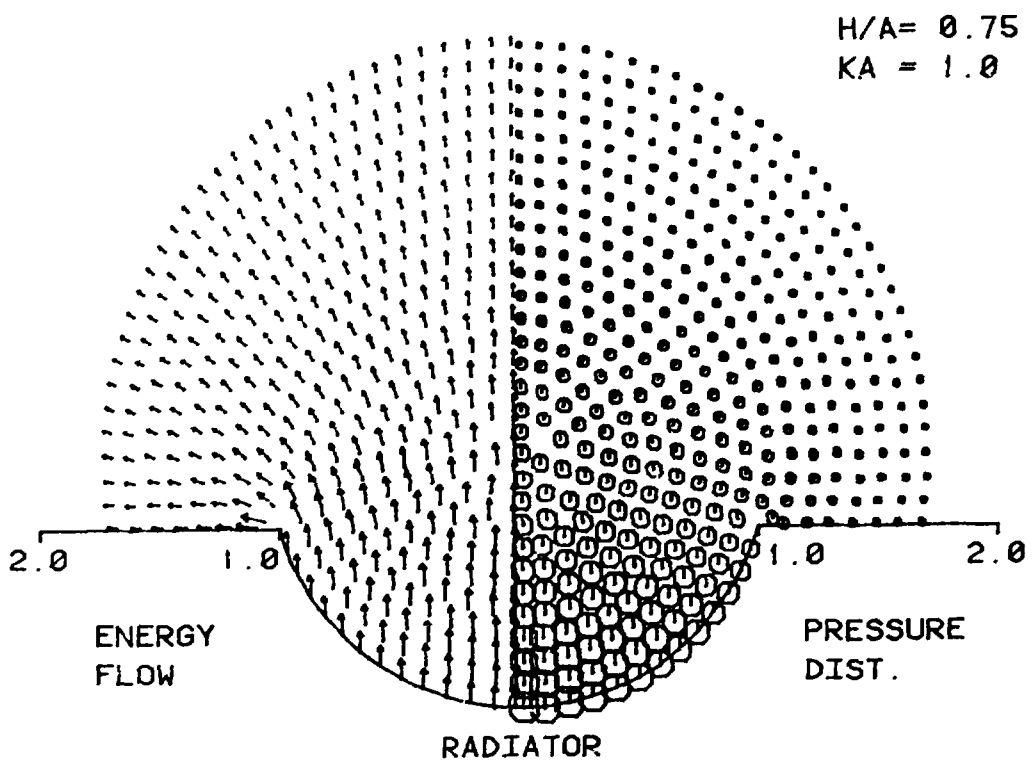

Figure 2.48 Energy flow and pressure distribution of a concave dome with H/A = 0.75 at kA = 1.0.

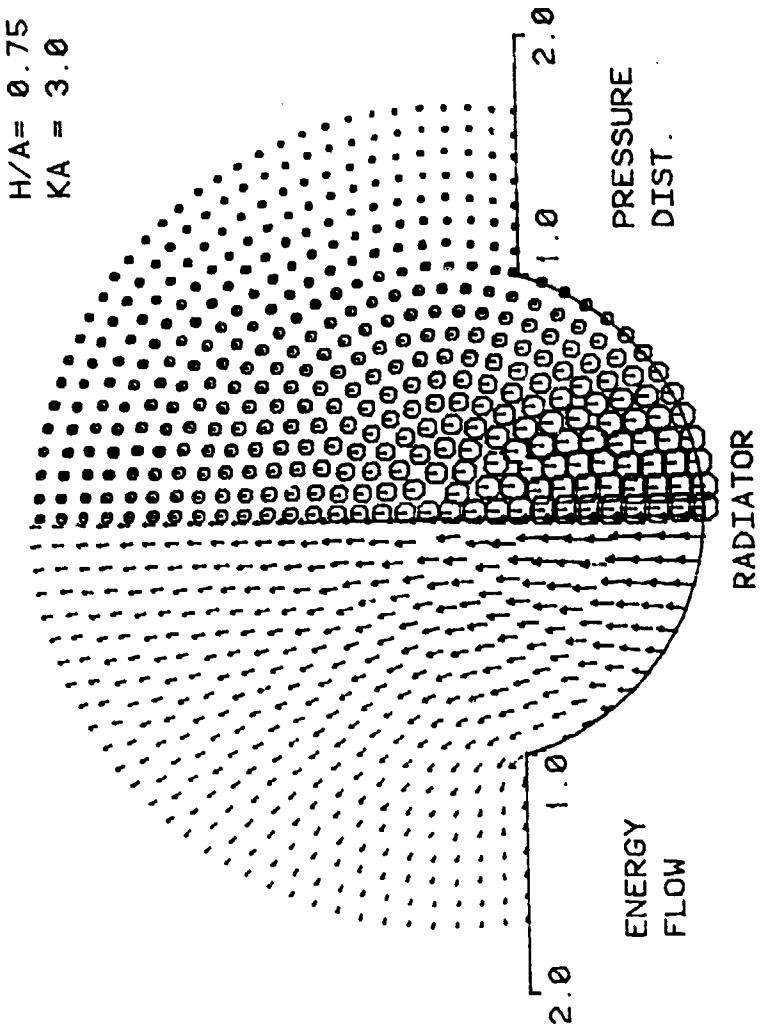

Figure 2.49 Energy flow and pressure distribution of a concave dome with H/A = 0.75 at kA = 3.0.

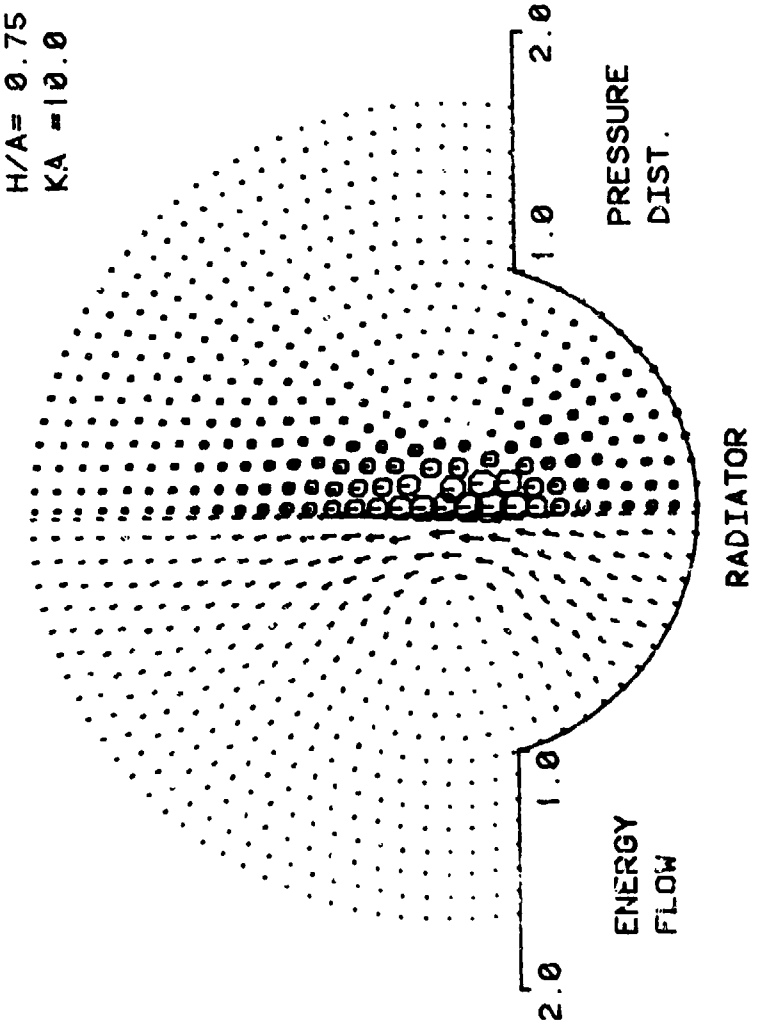

Figure 2.50 Energy flow and pressure distribution of a concave dome with H/A = 0.75 at kA = 10.0.

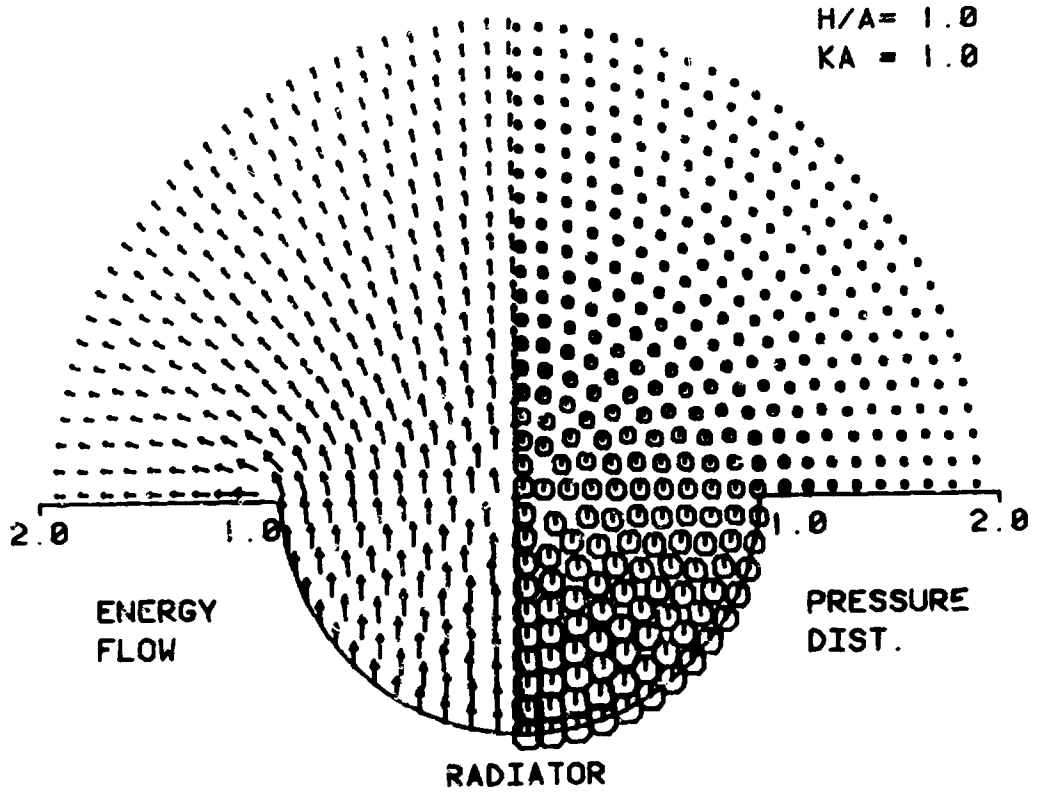

Figure 2.51 Energy flow and pressure distribution of a concave dome with H/A = 1.0 at kA = 1.0.

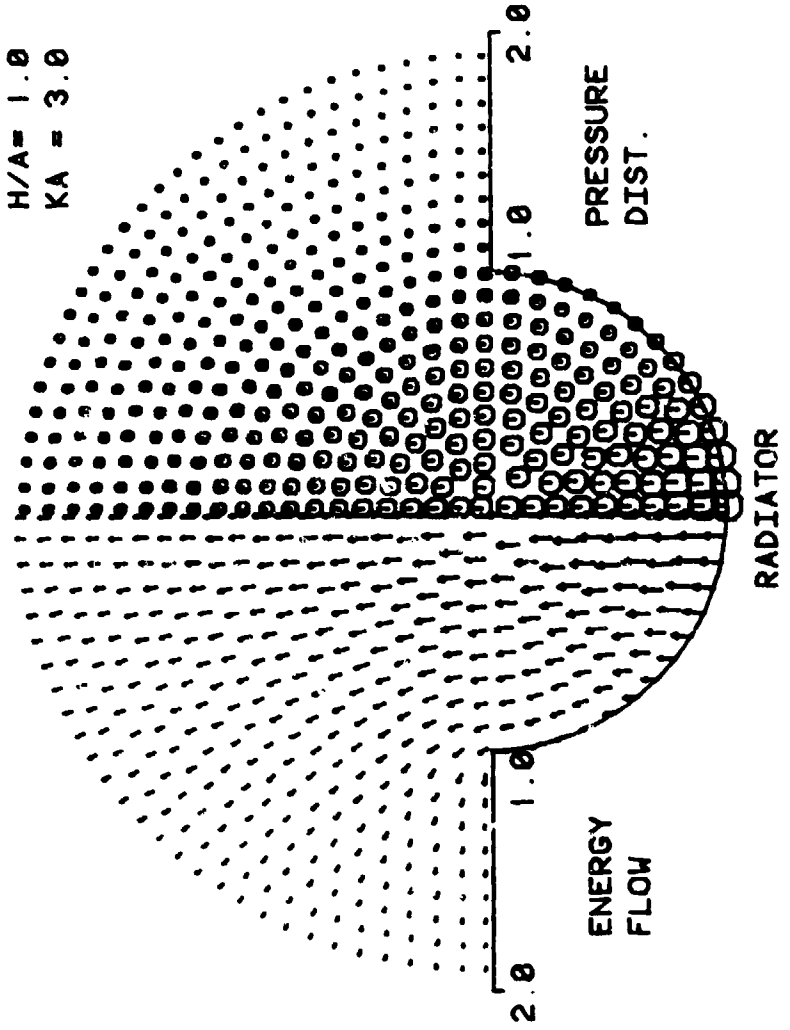

Figure 2.52 Energy flow and pressure distribution of a concave dome with H/A = 1.0 at kA = 3.0.

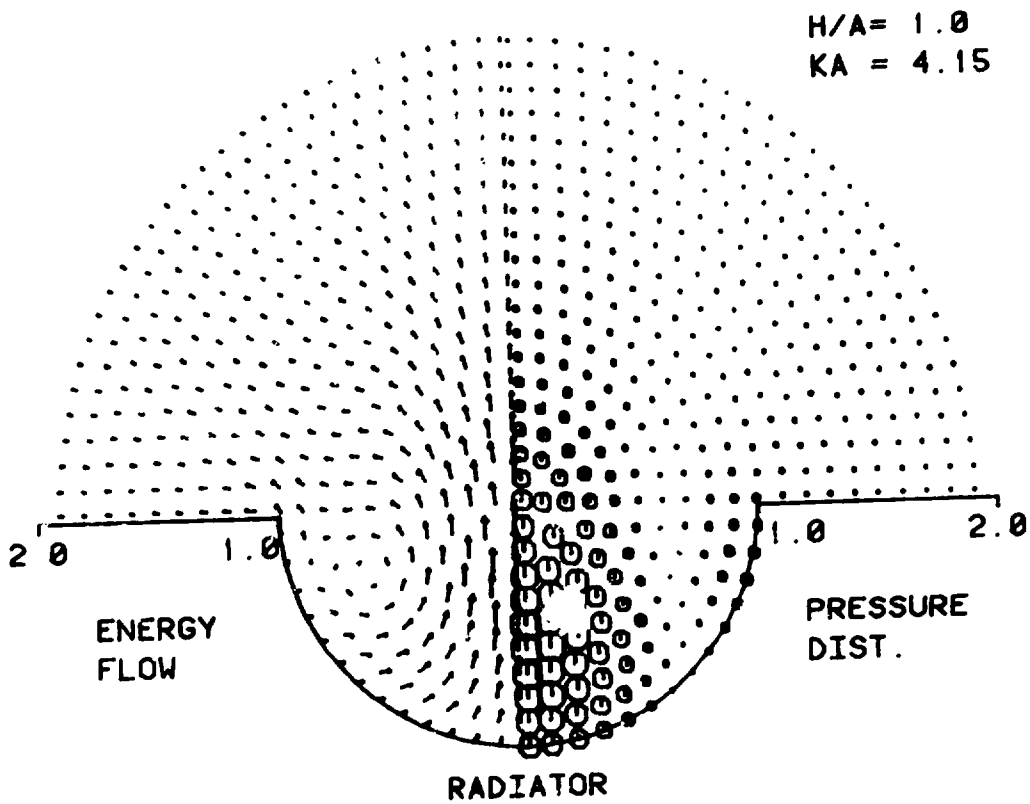

Figure 2.53 Energy flow and pressure distribution of a concave dome with H/A = 1.0 at kA = 4.15.

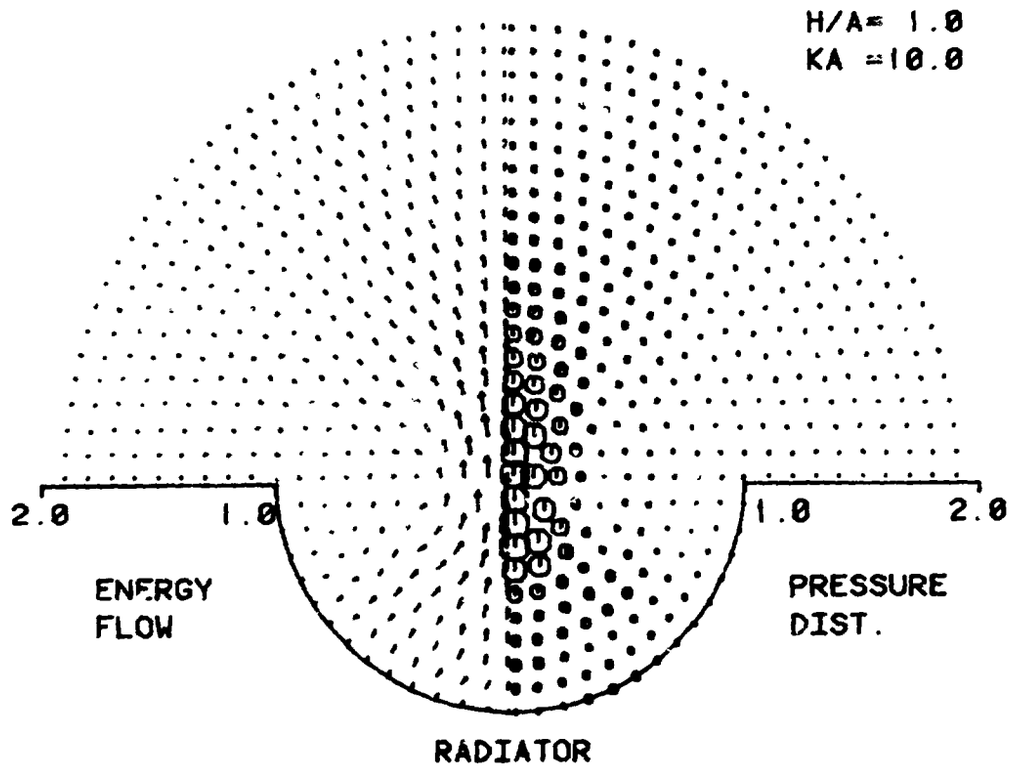

Figure 2.54 Energy flow and pressure distribution of a concave dome with H/A = 1.0 at kA = 10.0.

space from near the rim of the dome. The results of the sound pressure response and directivity pattern at this frequency are explained clearly by the energy flow and pressure distribution. At kA = 10.0 (Figure 2.54), the energy radiated normal to the radiator surface converges around the center of the sphere and then spreads out to semi-infinite space.

As was shown above, the graphical representation of the energy flow as well as the pressure distribution is a very useful tool for understanding the radiation problem.

2.3.6 Comparison of Results with other Methods

The results of the radiation and diffraction problems are compared with those obtained by different methods. As was mentioned earlier, Ikegaya [6] calculated the on-axis pressure responses of a convex dome, approximating it by an oblate spheroid for the cases of H/A = 0.2, 0.37, 0.5, and 1.0. The last case corresponds exactly to the radiation from the convex dome with H/A = 1.0. His results for H/A = 0.5, and 1.0 are plotted in Figure 2.55 along with the results obtained by the present method. Both responses for H/A = 1.0 are in good agreement with each other except the small discrepancy in the low-frequency region. The present method lacks some accuracy in this region, but is accurate enough in mid- to high-frequency regions. For H/A = 0.5, both results are significantly different from each other in the high-frequency region. This difference is considered

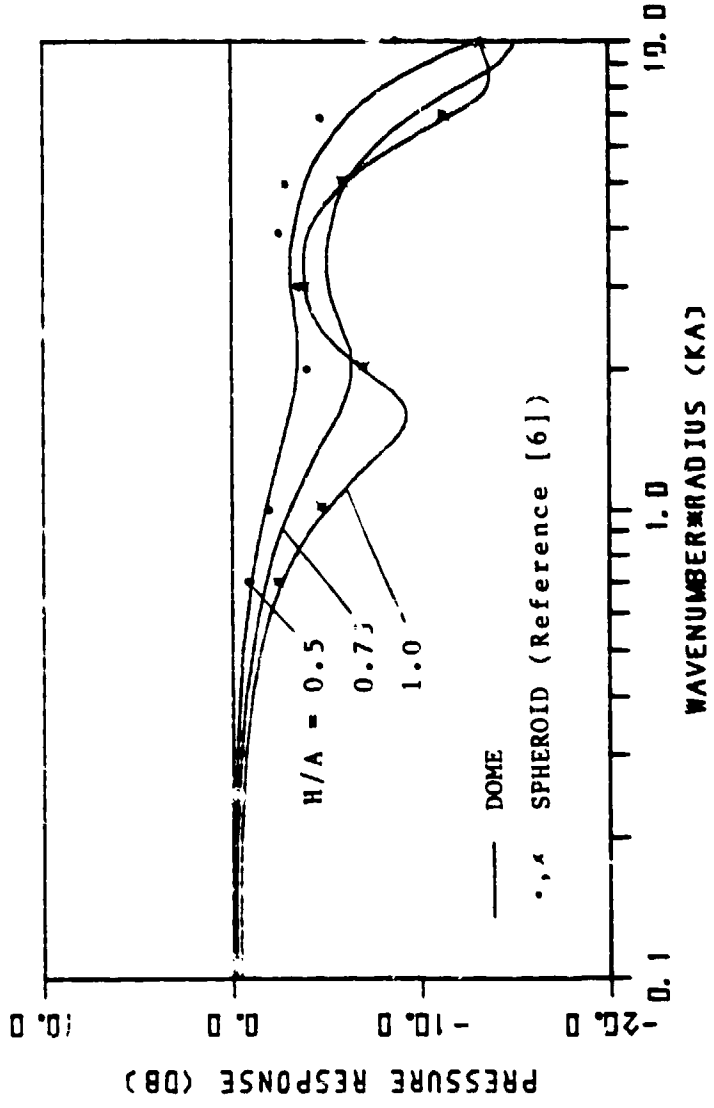

Figure 2.55 Far-field on-axis pressure responses of a convex dome and an oblate spheroid.

reasonable because the oblate spheroid has a flatter region around the z-axis than does the convex dome with the same H/A. It seems that the oblate spheroid suffers larger energy flow to the off-axis direction in the middle-frequency region since it has smaller normal velocity distribution around its rim compared with the dome.

Figure 2.56 compares the on-axis pressure responses of the concave dome obtained by our method (LSM) and by the finite element method (FEM). The programming and the calculation by the FEM were carried out by the staff of the Loudspeaker Section of Consumer Products Research Laboratory, Mitsubishi Electric Corporation in Japan, at the author's request. The number of axisymmetric triangular elements were 240, 360, and 450 for H/A = 0.5, 0.75, and 1.0, respectively. The boundary condition on the opening of the cavity was given in the form of self and mutual impedances of each mode. Inside the element, the pressure was expressed as a combination of pressures at six nodes using a shape function of quadratic form. The results of the FEM show higher resonance frequencies. But the differences of two curves for H/A = 0.5, 0.75, and 1.0 are mostly less than 1dB, respectively. The agreement of these two methods indicate that the present method is good enough for the discussion of the radiation characteristics of the concave dome radiator.

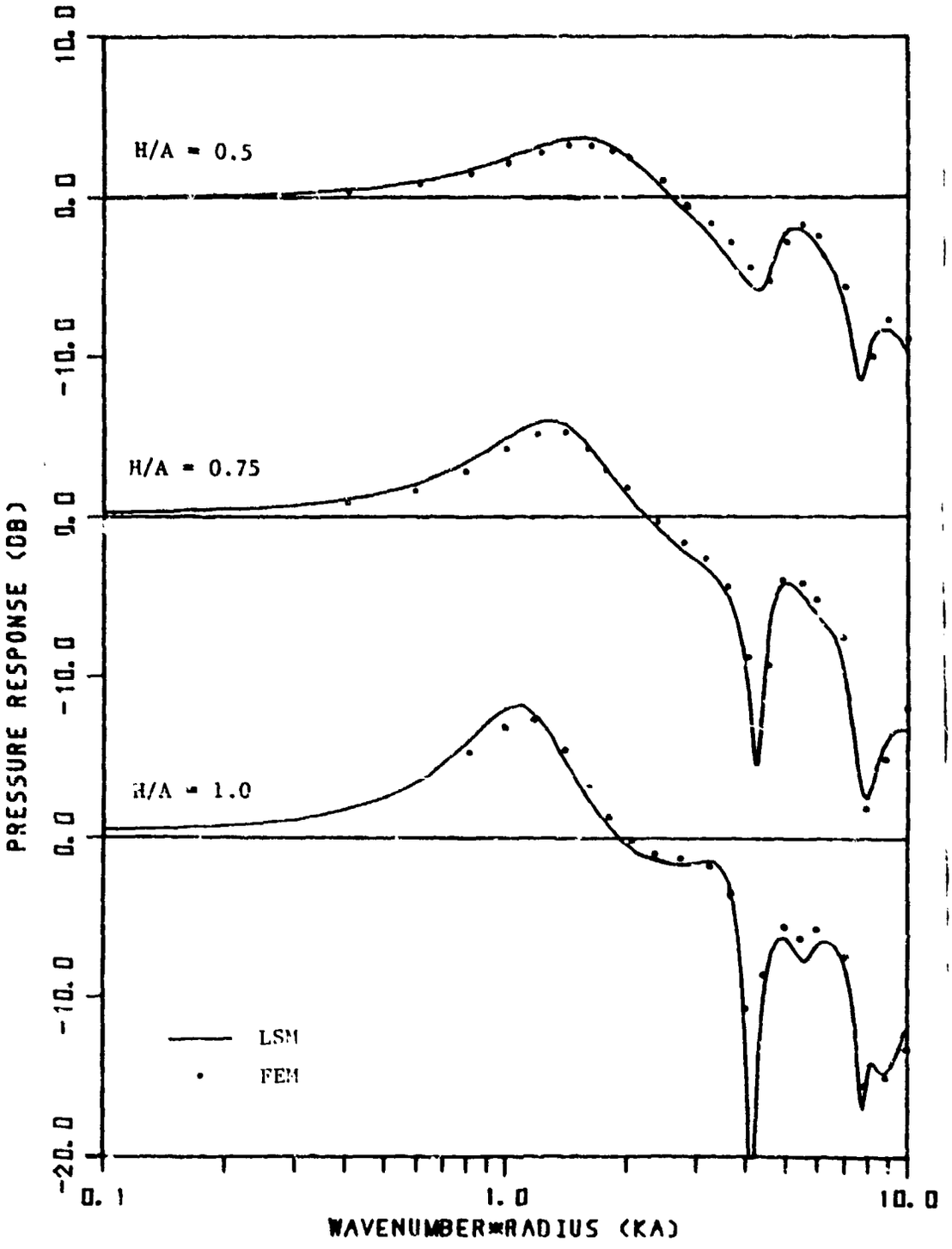

Figure 2.56 Far-field on-axis pressure responses of a concave dome obtained by the least square error method (LSM) and the finite element method (FEM).

CHAPTER III

DIFFRACTION BY CONVEX AND CONCAVE DOMES

3.1 Geometrical Model

This chapter deals with the diffraction of sound by the convex and concave domes that were used as radiators in Chapter II.

Figures 3.1 and 3.2 show ring sources with a concentric convex or a concentric concave dome in an infinite baffle, respectively. The ring source has radius A_1 and source strength $2\pi A_1 Q$. The convex and concave domes are represented as a portion of a sphere of radius R, and have height H and radius A.

The rectangular coordinate system (x,y,z) is used with the origin O. The polar coordinate system (r,θ,ϕ) is used with the origin O_1 at the center of the sphere. The surface of the convex or the concave dome, which is denoted by $S^{(1)}$, is represented by $(r = R, 0 \leq \theta \leq \theta_o, 0 \leq \phi \leq 2\pi)$ or $(r = R, \theta_o \leq \theta \leq \pi, 0 \leq \phi \leq 2\pi)$, respectively. In Figure 3.2, the opening of the cavity ($x^2+y^2 \leq A^2, z=0$) is denoted by $S^{(2)}$.

For the same reason as in Chapter II, the model shown in Figure 2.1 will be used for the diffraction problem by the convex dome; however, it does not show the ring source. The imaginary surface of the sphere with the origin O_1 is denoted by $S^{(2)}$.

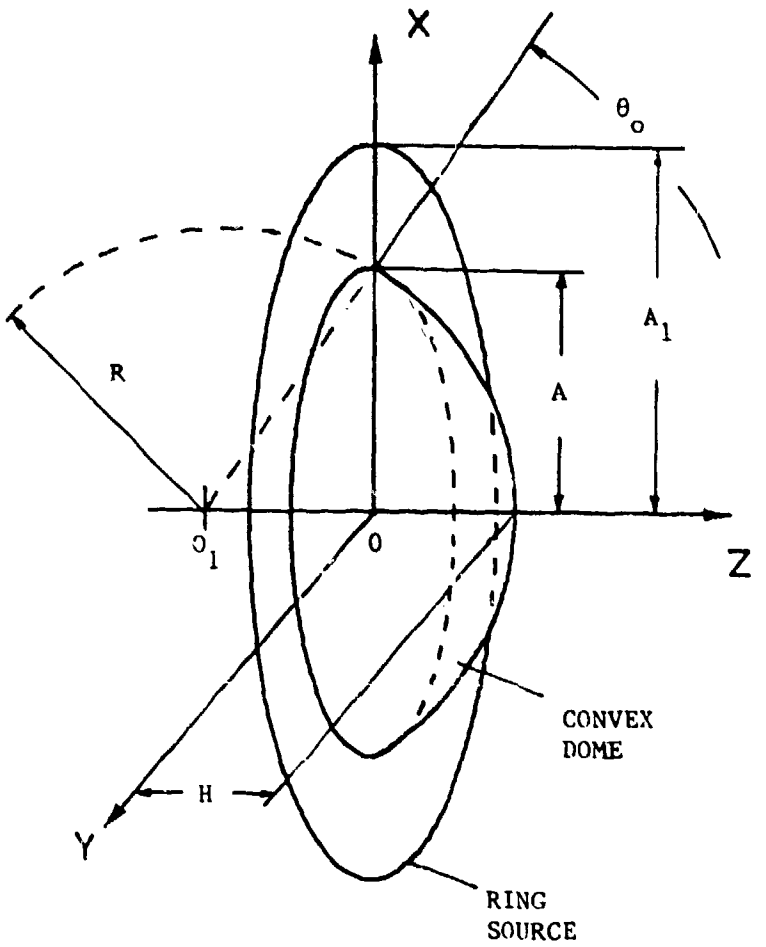

Figure 3.1 Geometry of a ring source with a concentric convex dome in an infinite baffle.

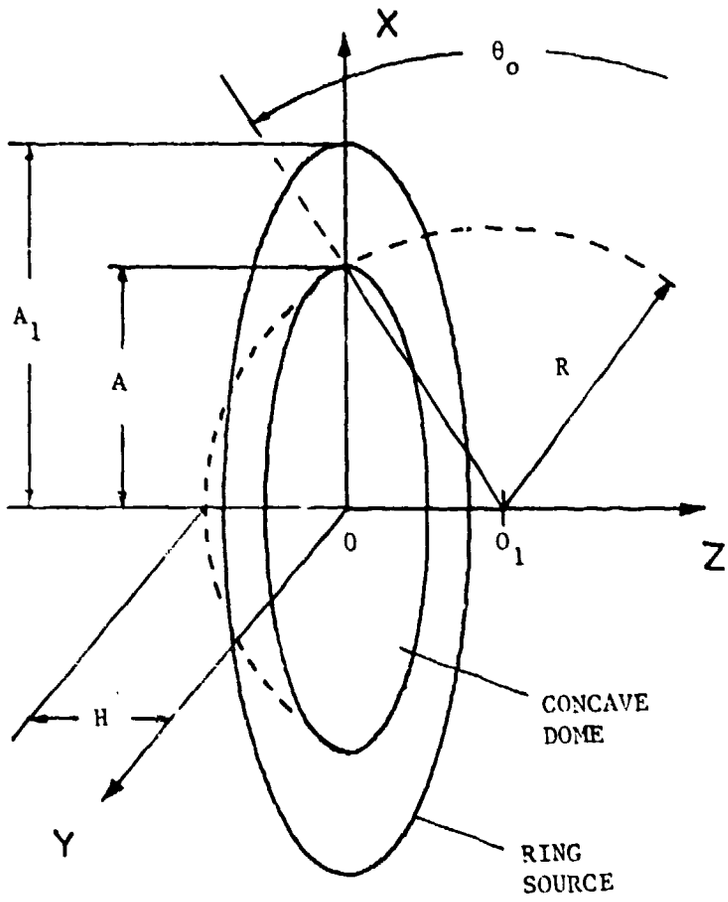

Figure 3.2 Geometry of a ring source with a concentric concave dome in an infinite baffle.

3.2 Mathematical Discussions

3.2.1 Diffraction by a Convex Dome

The present diffraction problem is actually a radiation problem from a ring source with a concentric convex or concave dome as a diffracting object. Hence, the mathematical methods described in Sections 2.2.1 and 2.2.2 are also applicable to the present problem.

In the diffraction problem of the model shown in Figure 2.1 (with the ring source missing), the center of the sphere is chosen as the origin of the coordinate system, and the boundary conditions are given on the surface of the sphere $S^{(1)}$ and $S^{(2)}$. The total velocity potential $\psi_t(\xi)$ outside the sphere can be expressed by

$$\psi_t(\xi) = \psi_s(\xi) + \psi_d(\xi) , \tag{3.1}$$

where $\psi_s(\xi)$ is the potential due to the ring source, and $\psi_d(\xi)$ is the secondarily radiated (reflected) potential by the convex dome. On the radiator surface $S^{(1)}$, $\psi_t(\xi)$ must satisfy the Neumann boundary condition,

$$[-\frac{\partial}{\partial r}\psi_t(\xi)]_{r=R} = -[\frac{\partial}{\partial r}\psi_s(\zeta) + \frac{\partial}{\partial r}\psi_d(\zeta)]_{r=R} = 0 . \tag{3.2}$$

Rewriting Eq. (3.2), one obtains

$$[-\frac{\partial}{\partial r}\psi_d(\zeta)]_{r=R} = [\frac{\partial}{\partial r}\psi_s(\zeta)]_{r=R} . \tag{3.3}$$

Thus, on the surface $S^{(1)}$, $L^{(1)}$ and $f^{(1)}(\zeta)$ are given by

$$L^{(1)} = -\frac{\partial}{\partial r} \tag{3.4}$$

and

$$f^{(1)}(\zeta) = \frac{\partial}{\partial r}\psi_s(\zeta) , \tag{3.5}$$

respectively.

The velocity potential $\psi_s(r,\theta)$ at the point $(r,\theta,0)$ is given by

$$\psi_s(r,\theta) = \frac{QA_1}{2\pi}\int_0^{2\pi}(e^{-ikd_1}/d_1)\, d\phi_1 , \tag{3.6}$$

where d_1 is the distance between the point of interest $(r,\theta,0)$, and the point of line element $A_1 d\phi_1$ of the ring source at (R_1,θ_1,ϕ_1), which is expressed by

$$d_1 = [(r\sin\theta - A_1\cos\phi_1)^2 + (A_1\sin\phi_1)^2 + (r\cos\theta - z_o)^2]^{1/2} . \tag{3.7}$$

The normal velocity distribution on the surface $S^{(1)}$ of the dome is therefore given by

$$[-\frac{\partial}{\partial r}\psi_s(r,\theta)]_{r=R} = \frac{QA_1}{2\pi}\int_0^{2\pi}[(1 + ikd_1)e^{-jkd_1}\{(R\sin\theta - A_1\cos\phi_1)\sin\theta + (R\cos\theta - z_o)\cos\theta\}/d_1^3]d\phi_1 . \tag{3.8}$$

Expressing the unknown function $\psi_d(\zeta)$ in terms of an infinite number of trial functions,

$$\psi_d(\xi) = \sum_{n=0}^{\infty} a_n h_n(kr)P_n(\cos\theta) , \qquad (3.9)$$

the function defined by Eq. (2.10) is obtained from Eqs. (3.4) and (3.9) as

$$\psi_n^{(1)}(\theta) = - kh_n'(kR)P_n(\cos\theta), \; 0 \leq\theta\leq \theta_o . \qquad (3.10)$$

The symmetry of the sound field about the xy-plane requires the symmetry of the velocity potential $\psi_d(\xi)$ itself about the xy-plane; i.e., the velocity potentials at point P $(r,\theta,0)$ and P_1 $(r_2,\theta_2,0)$ are equal to each other (potential matching). From Eq. (3.9), one obtains

$$\sum_{n=0}^{\infty} a_n\{h_n(kR)P_n(\cos\theta) - h_n(kr_2)P_n(\cos\theta_2)\} = 0 . \qquad (3.11)$$

In the case of potential matching, the operator L is not expressed explicitly. By comparing Eqs. (2.4) and (3.11), one comes to the interpretation that the operator L gives the difference between two velocity potentials at a point and its related point (in this case, symmetric point). One can define $\psi^{(2)}(\zeta)$ and $f^{(2)}(\zeta)$ as

$$\psi_n^{(2)}(\theta) = [h_n(kR)P_n(\cos\theta) - h_n(kr_2)P_n(\cos\theta_2)] \qquad (3.12)$$

and

$$f^{(2)}(\theta) = 0 . \qquad (3.13)$$

Now, applying Eqs. (3.5), (3.8), (3.10), (3.12), and (3.13)

to Eq. (2.12), one obtains

$$\sum_{n=0}^{N} a_n \left[\int_{S^{(1)}} \psi_m^{(1)*}(\theta)\psi_n^{(1)}(\theta)dS + \int_{S^{(2)}} \psi_m^{(2)*}(\theta)\psi_n^{(2)}(\theta)dS\right]$$

$$= \int_{S^{(1)}} \psi_m^{(1)*}(\theta)f^{(1)}(\theta)dS \ , \ n = 0, 1, \ldots, N \ , \qquad (3.14)$$

where $dS = 2\pi R^2 \sin\theta d\vartheta$, and Eq. (2.12) was assumed.

3.2.2 Diffraction by a Concave Dome

The diffraction problem by a concave dome is also treated here as a radiation problem from a ring source in an infinite baffle with a concentric concave dome (Figure 3.2). The velocity potential inside a sphere of radius R with the origin at O_1 is expressed by

$$\psi_t(\xi) = \psi_s(\xi) + \psi_d(\xi) \ . \qquad (3.15)$$

The potential $\psi_s(\xi)$ is the one radiated by the ring source existing only in the semi-infinite space on the right side of the xy-plane. The total potential $\psi_t(\xi)$ inside the sphere can be represented as

$$\psi_t(\xi) = \sum_{n=0}^{\infty} a_n j_n(kr)P_n(\cos\theta) \ . \qquad (3.16)$$

On the surface of the concave dome $S^{(1)}$, this must satisfy the following condition:

$$-\frac{\partial}{\partial r}\psi_t(\xi) = -\frac{\partial}{\partial r}\psi_d(\xi) = 0 \ . \qquad (3.17)$$

This defines $L^{(1)}$, $f^{(1)}(\theta)$, and $\psi_n^{(1)}(\theta)$ such as

$$L^{(1)} = -\frac{\partial}{\partial r} , \tag{3.18}$$

$$f^{(1)}(\theta) = 0 , \tag{3.19}$$

and

$$\psi_n^{(1)}(\theta) = -kj_n(kR)P_n(\cos\theta) . \tag{3.20}$$

In the region inside the sphere and outside the cavity, the total potential is divided into two components: the direct velocity potential $\psi_s(\xi)$, and the diffracted velocity potential $\psi_d(\xi)$ due to the concave dome. The potential $\psi_s(\xi)$ is given by the same equation as Eq. (3.6). The potential $\psi_d(\xi)$ is obtained by the Rayleigh integral of the normal velocity distribution $u_B(r_2,\theta_2)$ on the opening $S^{(2)}$, which is given by

$$\begin{aligned} u_B(r_2,\theta_2) &= -\left[\frac{\partial}{\partial z}\psi_t(r,\theta)\right]_{\substack{r=r_2\\ \theta=\theta_2}} \\ &= -\left[\frac{\partial}{\partial r}(\psi_t)\frac{\partial r}{\partial z} + \frac{\partial}{\partial \theta}(\psi_t)\frac{\partial \theta}{\partial z}\right]_{\substack{r=r_2\\ \theta=\theta_2}} . \end{aligned} \tag{3.21}$$

The derivatives $\partial r/\partial z$ and $\partial\theta/\partial z$ are given from the geometry by

$$\partial r/\partial z = \cos\theta \tag{3.22}$$

and

$$\partial\theta/\partial z = -\sin\theta/r . \tag{3.23}$$

From Eqs. (3.16), (3.22), and (3.23), one obtains

$$u_B(r_2,\theta_2) = -\sum_{n=0}^{\infty} a_n[k\cos\theta_2 j_n'(kr_2)P_n(\cos\theta_2) + \sin^2\theta_2 j_n(kr_2)P_n'(\cos\theta_2)/r_2] \quad . \tag{3.24}$$

Then, $\psi_d(r,\theta)$ is given by

$$\psi_d(r,\theta) = [\int_{S(2)} u_B(r_2,\theta_2)\ (e^{-ikd_2}/d_2)dS]/2\pi \quad , \tag{3.25}$$

where the coordinate of the surface element is (r_2,θ_2,ϕ_2) and

$$d_2 = [(r\sin\theta - r_2\sin\theta_2\cos\phi_2)^2 + (r_2\sin\theta_2\sin\phi_2)^2 + (r\cos\theta - r_2\cos\theta_2)^2]^{1/2} \quad . \tag{3.26}$$

From Eqs. (3.16), (3.24), and (3.25), following equation can be obtained:

$$\sum_{n=0}^{N} a_n j_n(kr)P_n(\cos\theta) = QA_1\ [\int_0^{2\pi} \{e^{-ikd_1}/d_1\}d\phi_1]/2\pi - \sum_{n=0}^{\infty} a_n\ [\int_{S(2)} \{k\cos\theta_2 j_n'(kr_2)P_n(\cos\theta_2) + \sin^2\theta_2 j_n(kr_2)P_n'(\cos\theta_2)/r_2\}\ (e^{-ikd_2}/d_2)dS]/2\pi. \tag{3.27}$$

The condition expressed by Eq. (3.27) must be satisfied everywhere in the region inside the sphere except at the cavity. But, if the imaginary surface of the sphere is chosen as the one where the condition of Eq. (3.27) is

imposed, the nonuniqueness problem occurs [see Appendix C]. With this in mind, it is chosen that the condition of Eq. (3.27) is required on the opening of the cavity $S^{(2)}$. Rewrite Eq. (3.27) such as

$$\sum_{n=0}^{\infty} a_n \psi_n^{(2)}(r,\theta) = f^{(2)}(\theta) , \tag{3.28}$$

where

$$\psi_n^{(2)}(r,\theta) = j_n(kr)P_n(\cos\theta) + \int_{S^{(2)}} \{k\cos\theta_2 j_n'(kr_2)P_n(\cos\theta_2) + \sin^2\theta_2 j_n(kr_2)P_n'(\cos\theta_2)/r_2\} (e^{-ikd_2}/d_2)dS]/2\pi \tag{3.29}$$

and

$$f^{(2)}(r,\theta) = Q\Lambda_1 \left[\int_0^{2\pi} (e^{-ikd_1}/d_1)d\phi_1\right]/2\pi \tag{3.30}$$

with the relationship between r and θ such as Eq. (2.37). Now, the unknown coefficients a_n, n = 0, 1, . . ., N are obtained from the set of (N+1) simultaneous equations with the same form as Eq. (3.14):

$$\sum_{n=0}^{\infty} a_n \left[\int_{S^{(1)}} \psi_m^{(1)*}(\theta)\psi_n^{(1)}(\theta)dS + \int_{S^{(2)}} \psi_m^{(2)*}(r,\theta)\psi_n^{(2)}(r,\theta)dS\right]$$

$$= \int_{S^{(2)}} \psi_m^{(2)*}(r,\theta)f^{(2)}(r,\theta)dS, \quad m = 0, 1, \ldots, N . \tag{3.31}$$

3.3 Results and Discussions

Corresponding to the radiation problem from a convex or a concave dome, the height/radius ratio of the dome was chosen such that H/A = 0.5, 0.75, and 1.0. In most of the cases, the radius of the ring source A_1 was equal to 1.5A. The weighting factor $q(\zeta)$ in Eq. (2.12) was kept equal to 1.0 as in Chapter II. The accuracy of the ults was confirmed by checking the error factor of Eq. (2.9) at each frequency. The maximum value of index N was 60 for kA = 40.

3.3.1 On-axis Pressure Response

The far-field on-axis pressure responses of the ring source with the convex dome are shown in Figure 3.3-3.5, where the strength of the ring source is inversely proportional to ω. The effect of the dome appears from approximately kA = 1.0, giving gradual rise to the response as the frequency increases. The height of the plateau is about 2.5dB and does not depend strongly on the H/A ratio. The differences of the levels of the peaks and dips in the high-frequency region are more than 10dB for H/A = 0.5 and 0.75. As the H/A ratio increases, the differences decrease, and the peaks and dips are shifted to higher frequencies. The results indicate that the radiat on efficiency is highly frequency dependent.

Figures 3.6-3.8 and Figures 3.9-3.11 show the on-axis pressure responses of the ring source with a concave dome for A_1/A = 1.5 and 2.0, respectively. The concave dome

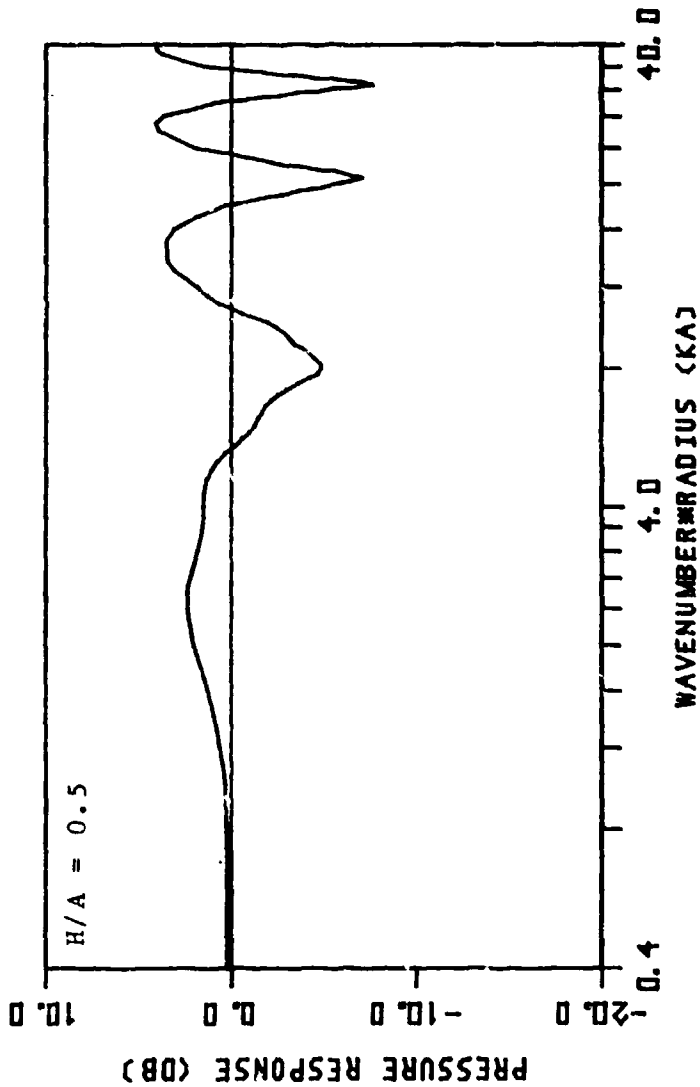

Figure 3.3 Far-field on-axis pressure responses of a ring source with a concentric convex dome for H/A = 0.5 and $A_1/A = 1.5$.

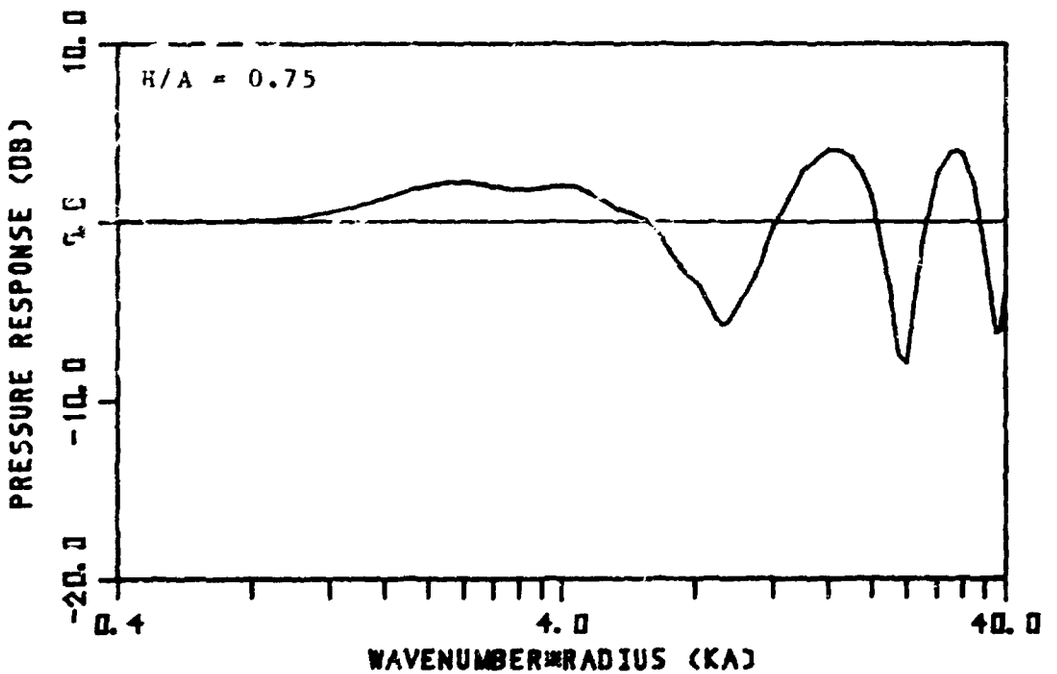

Figure 3.4 Far-field on-axis pressure responses of a ring source with a concentric convex dome with H/A = 0.75 and A_1/A = 1.5.

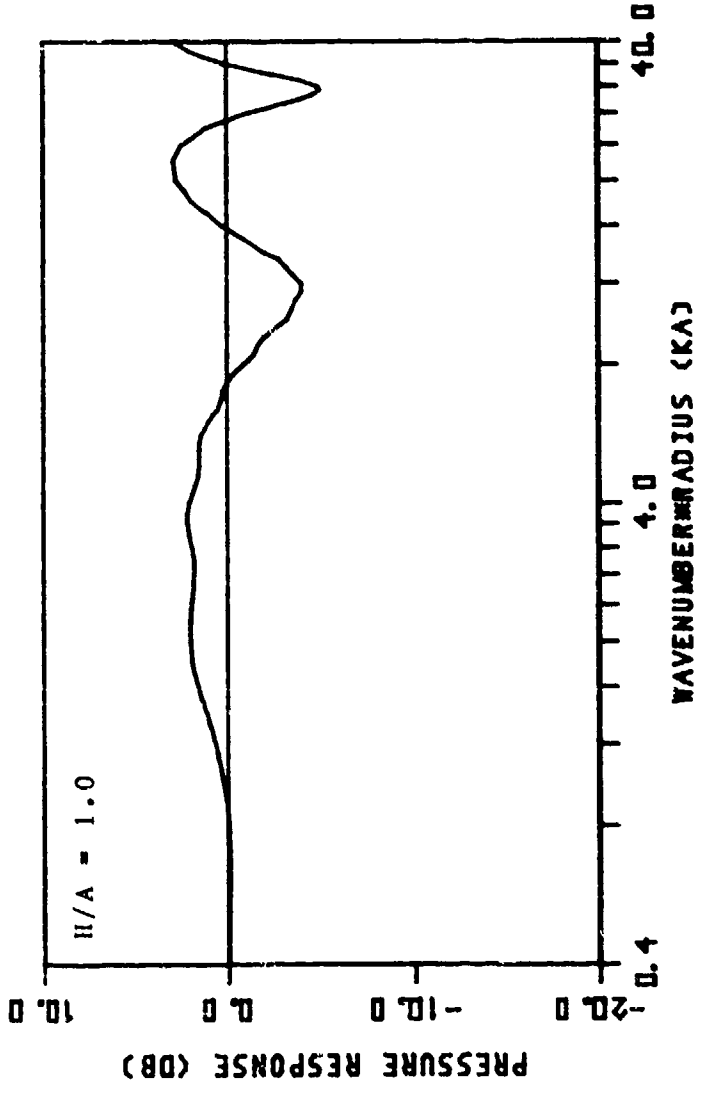

Figure 3.5 Far-field on-axis pressure responses of a ring source with a concentric convex dome with H/A = 1.0 and $A_1/A = 1.5$.

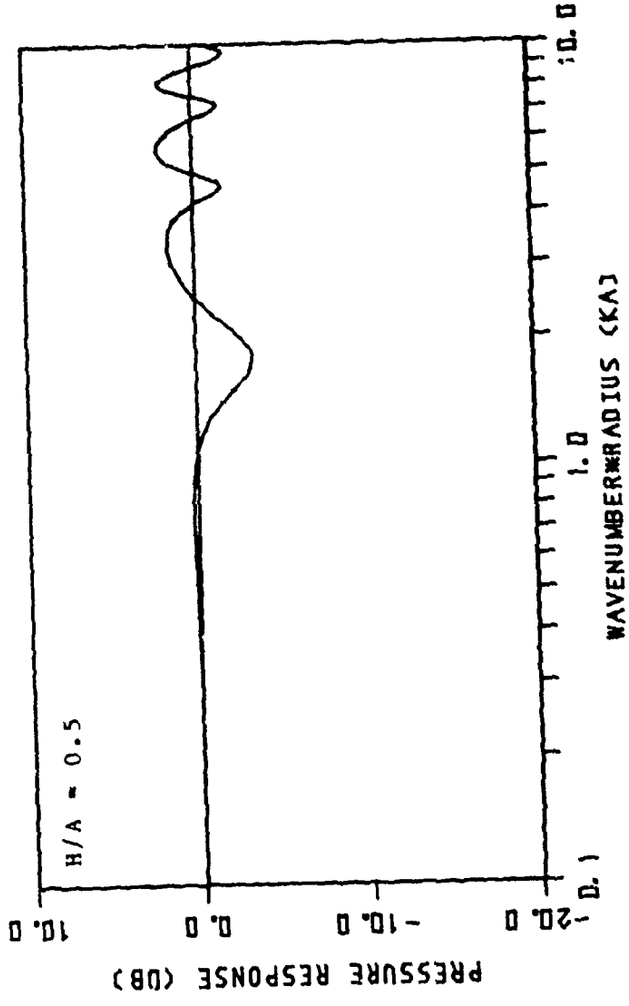

Figure 3.6 Far-field on-axis pressure responses of a ring source with a concentric concave dome with H/A = 0.5 and $A_1/A = 1.5$.

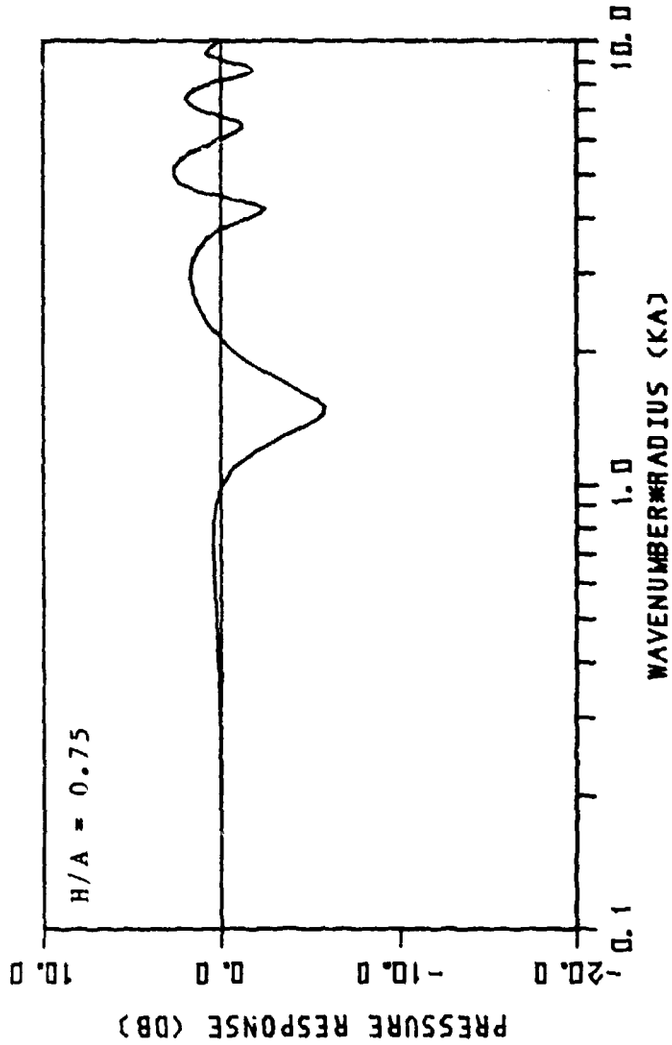

Figure 3.7 Far-field on-axis pressure responses of a ring source with a concentric concave dome with H/A = 0.75 and $A_1/A = 1.5$.

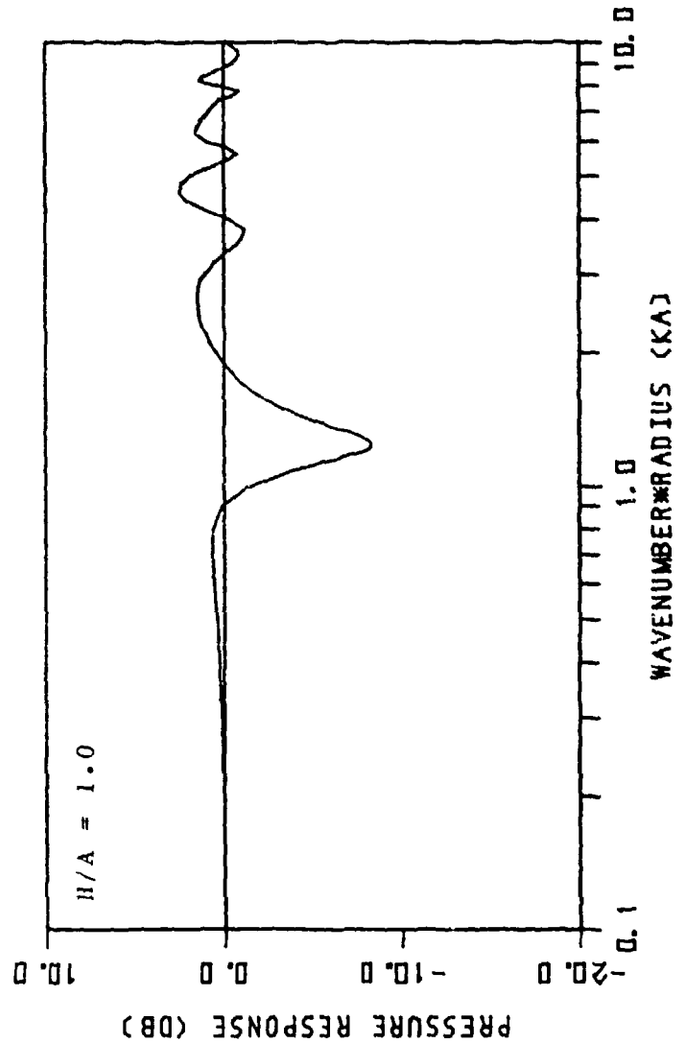

Figure 3.8 Far-filed on-axis pressure responses of a ring source with a concentric concave dome with H/A = 1.0 and A_1/A = 1.5.

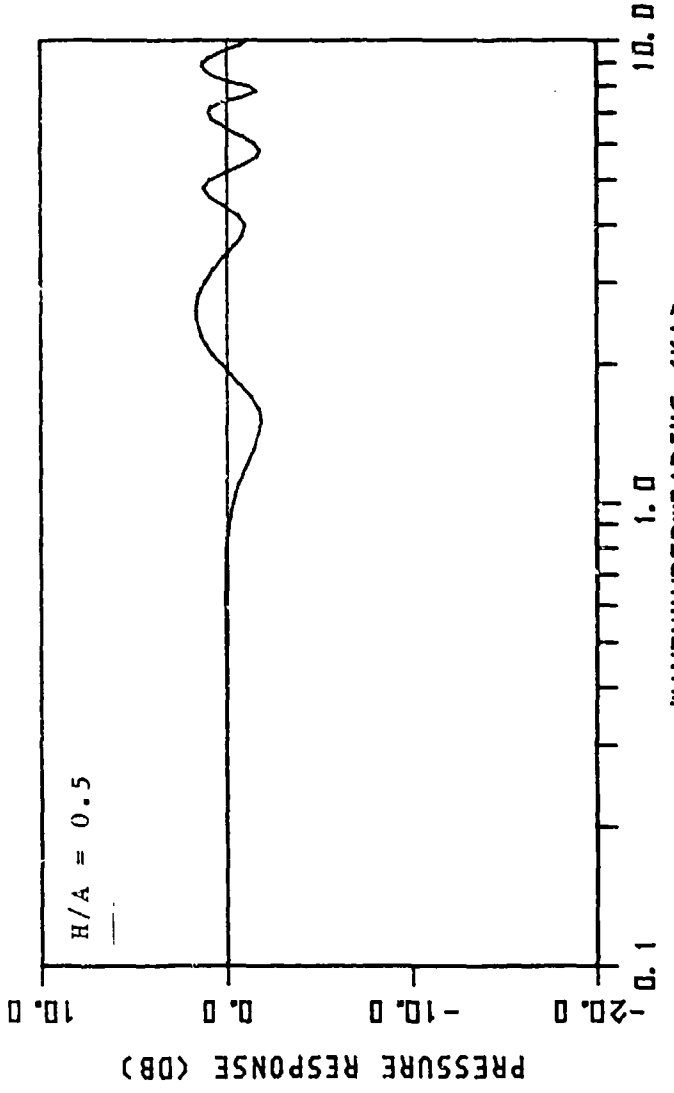

Figure 3.9 Far-field on-axis pressure response of a ring source with a concentric concave dome with H/A = 0.5 and $A_1/A = 2.0$.

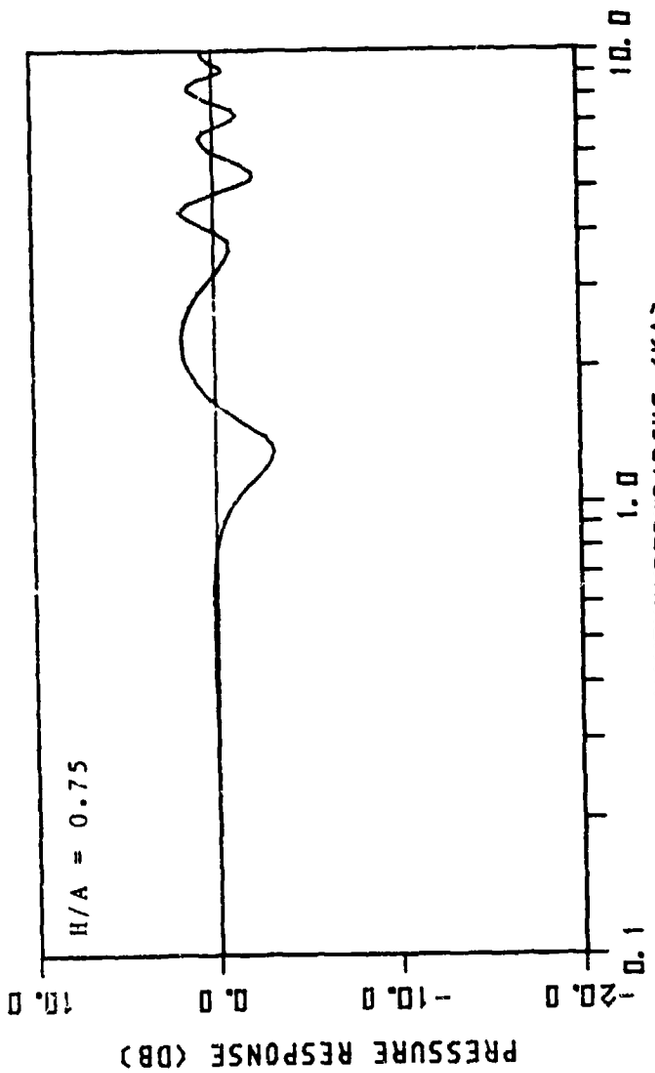

Figure 3.10 Far-field on-axis pressure responses of a ring source with a concentric concave dome with H/A = 0.75 and $A_1/A = 2.0$.

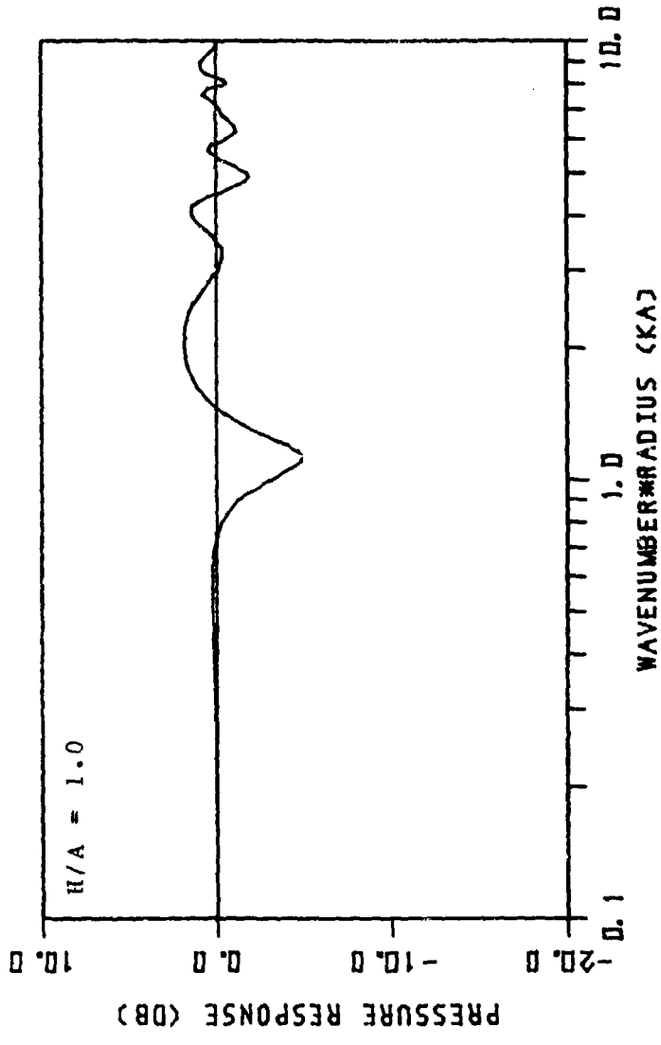

Figure 3.11 Far-field on-axis pressure responses of a ring source with a concentric concave dome with H/A = 1.0 and $A_1/A = 2.0$.

begins to have some effect on the response from about the same frequency (kA = 1.0) as the convex dome for $A_1/A = 1.5$. The first effect, however, appears as a large dip on the frequency response, contrary to the results shown in Figures 3.3-3.5. The fluctuations of the response are much smaller compared with those of the convex dome. As the H/A ratio increases, the frequencies of the peaks and dips are lowered. When the A_1/A ratio is increased (Figures 3.9-3.11), the effect of the cavity on the response decreases, and the lowest frequency at which the effect is evident also decreases.

These results show that the object (convex or concave) in the infinite baffle has a large effect on the radiation from an adjacent source. One effect of practical importance is demonstrated by Figure 3.12, which shows the difference in the response when height H is changed by $\pm 0.02A$ from H = 0.5A. For example, when A = 15cm, the change in the height is $\pm$3mm. Figure 3.12 indicates that the change of the height of the dome will produce amplitude-modulations of about -30 to -40dB at some frequencies.

3.3.2 Directivity Pattern

Directivity patterns of the ring sources are also affected by the convex or the concave object in the infinite baffle as shown in Figures 3.13-3.15 and Figures 3.16-3.18 for the case of H/A = 1.0, respectively. Figures also include some of the directivity patterns of the ring source

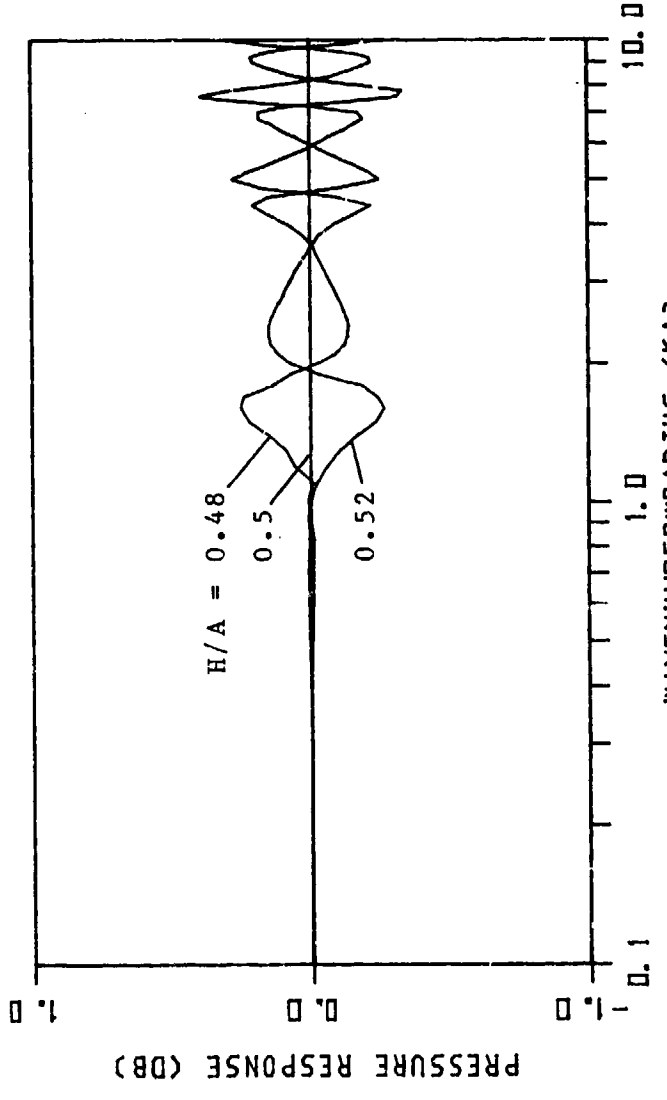

Figure 3.12 Differences of the far field on-axis pressure responses of a ring source with a concentric concave dome with $A_1/A = 1.5$ when H/A is changed by ± 0.02 from H/A = 0.5.

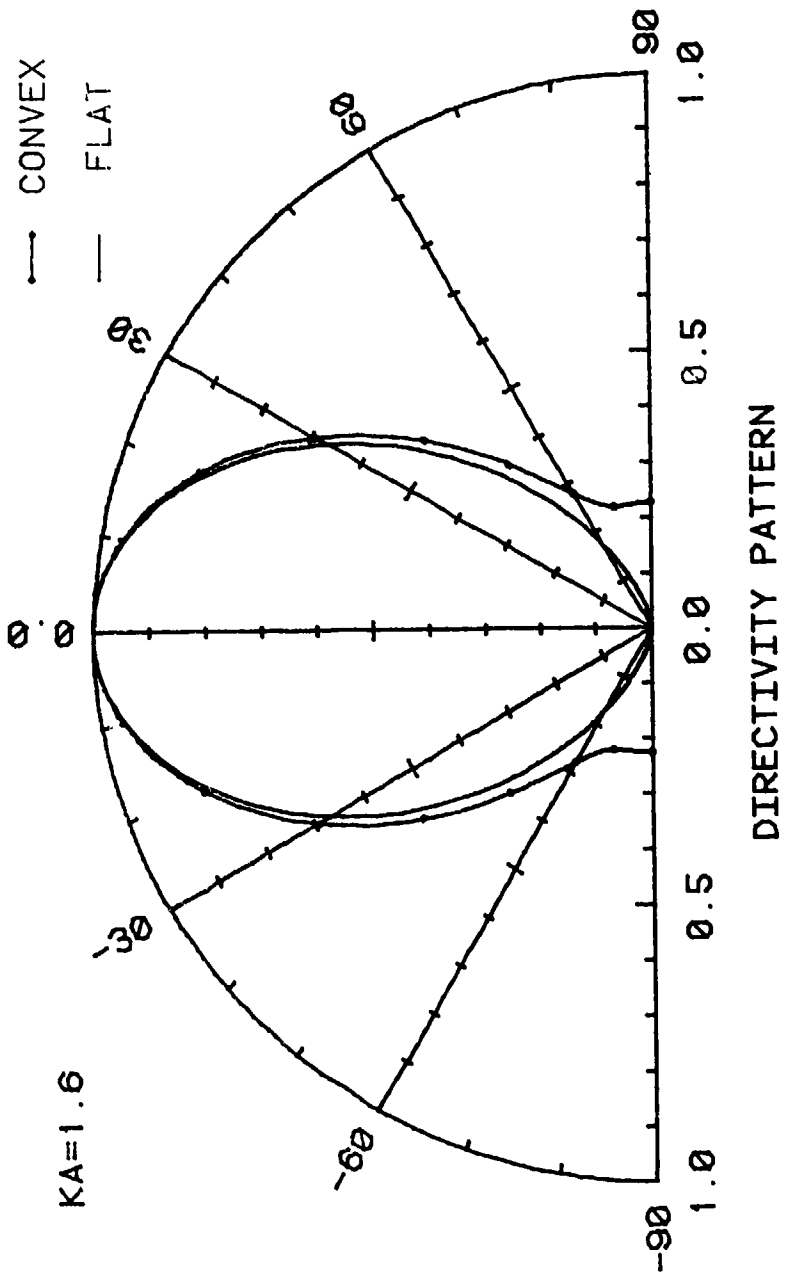

Figure 3.13 Directivity patterns of a ring source with a concentric convex dome and a flat piston for H/A = 1.0 and A_1/A = 1.5 at kA = 1.6.

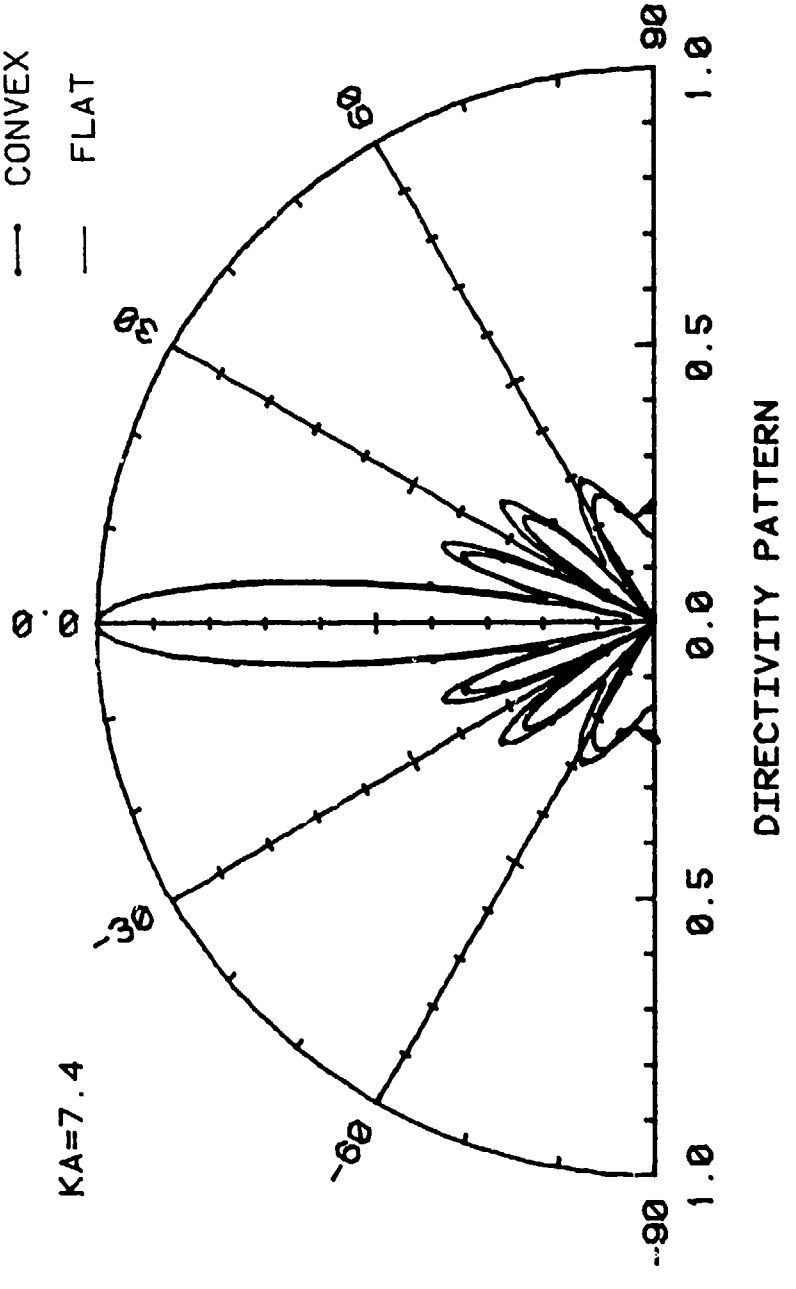

Figure 3.14 Directivity patterns of a ring source with a concentric convex dome and a flat piston for H/A = 1.0 and A_1/A = 1.5 at kA = 7.5.

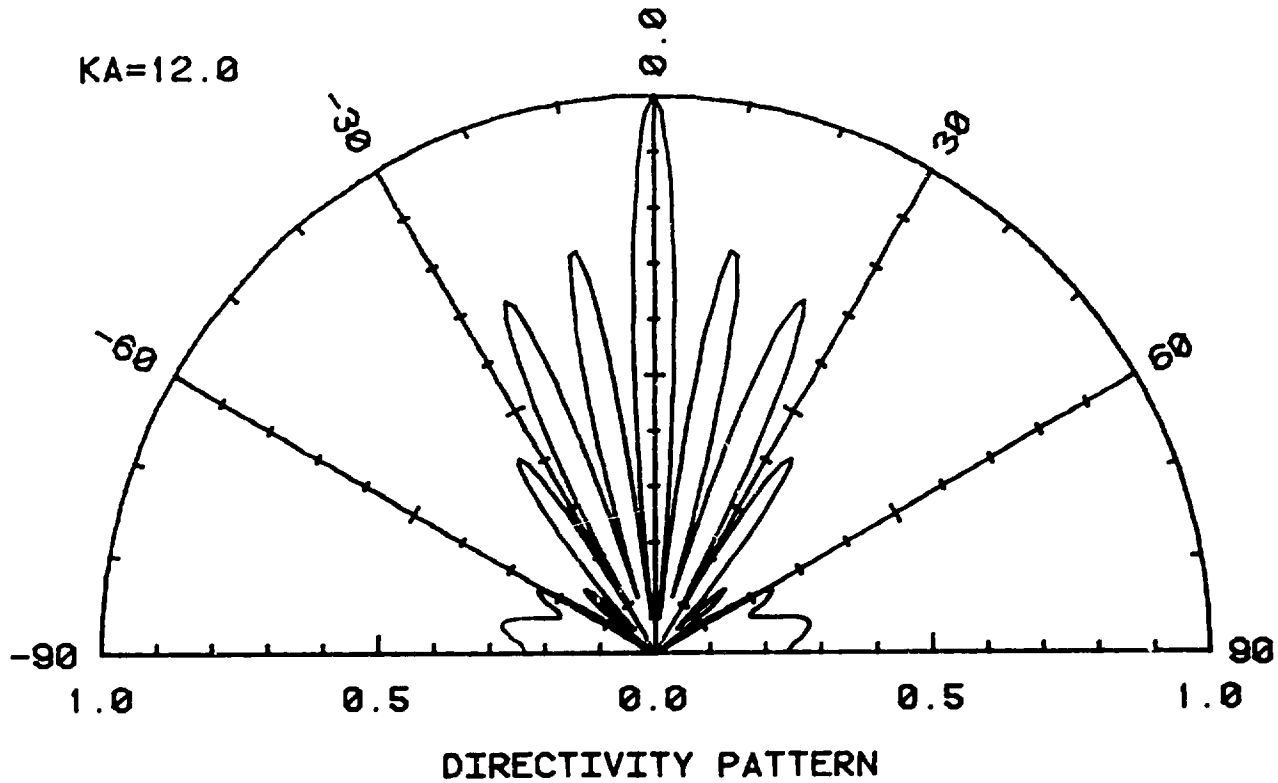

Figure 3.15 Directivity pattern of a ring source with a concentric convex dome for H/A = 1.0 and A_1/A = 1.5 at kA = 12.0.

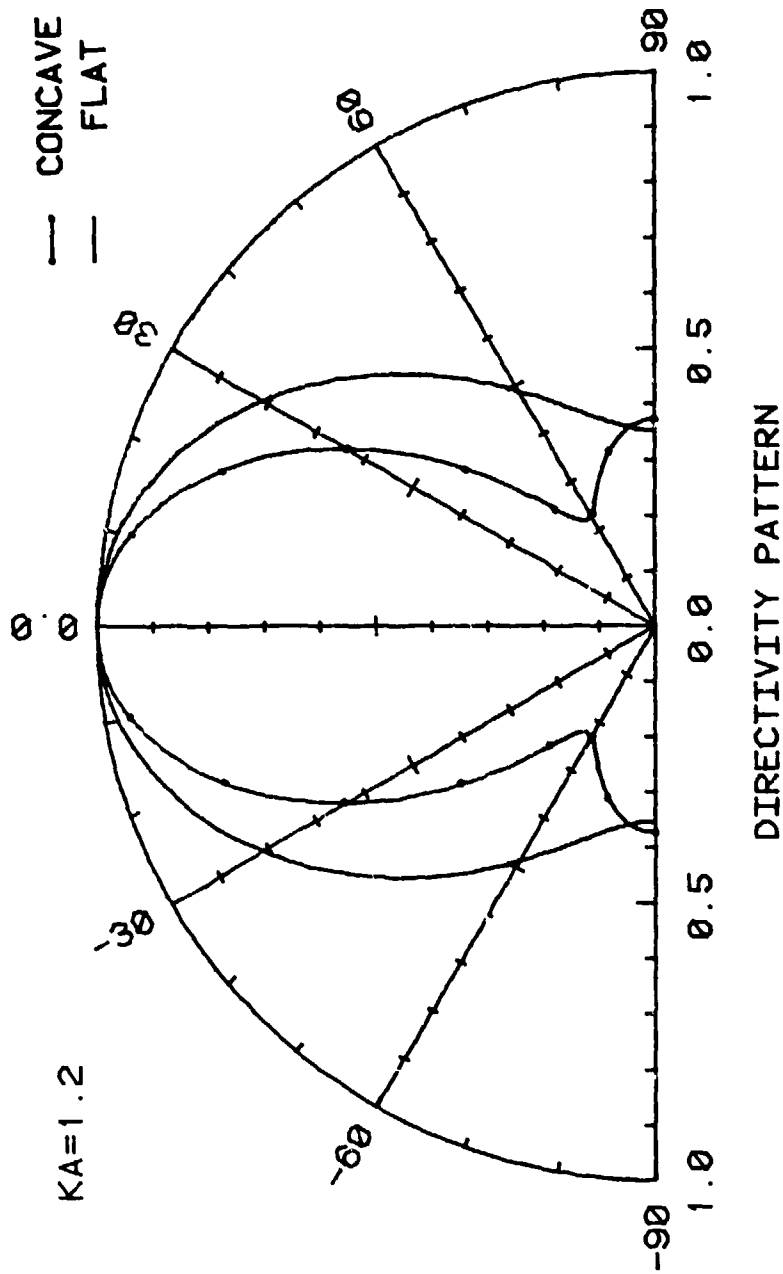

Figure 3.16 Directivity patterns of a ring source with a concentric concave dome and a flat piston for H/A = 1.0 and A_1/A = 1.5 at kA = 1.2.

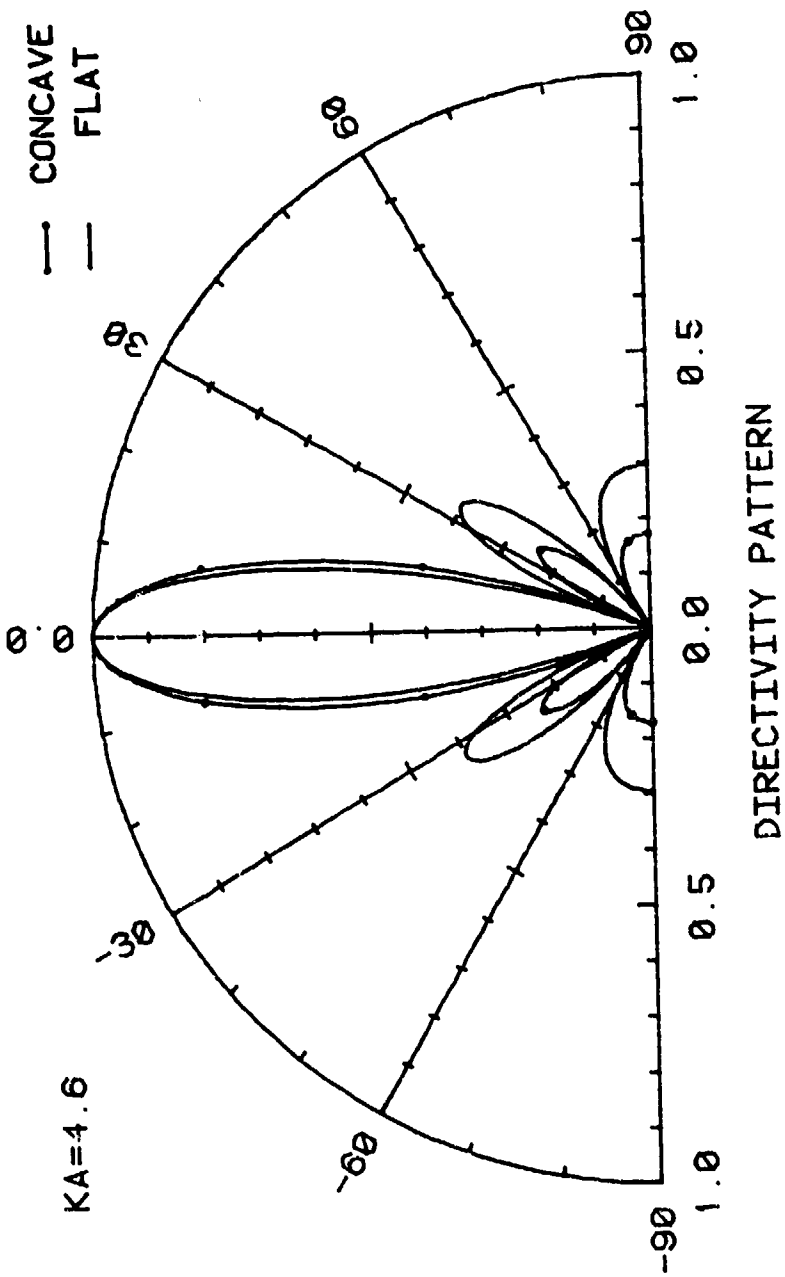

Figure 3.17 Directivity patterns of a ring source with a concentric concave dome and a flat piston for H/A = 1.0 and A_1/A = 1.5 at kA = 4.6.

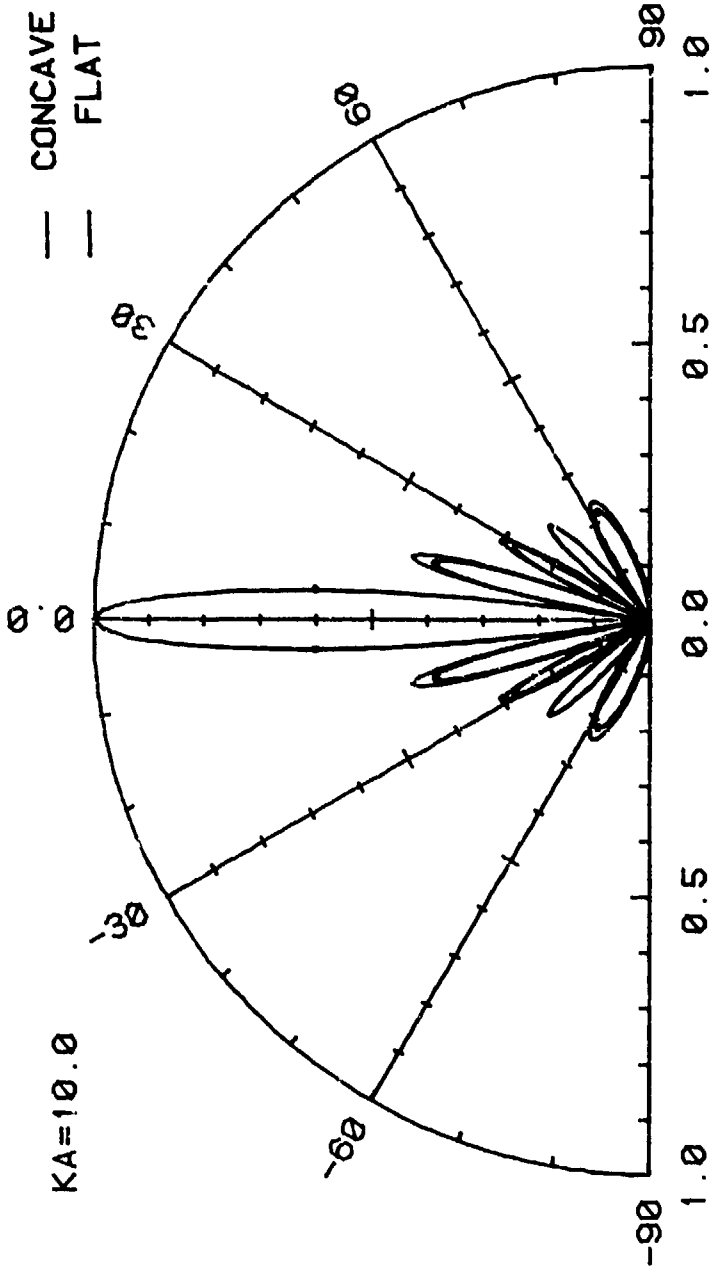

Figure 3.18 Directivity patterns of a ring source with a concentric concave dome and a flat piston for H/A = 1.0 and A_1/A = 1.5 at kA = 10.0.

only. Again, the convex and concave domes work in opposite ways. The convex dome widens the directivity pattern at kA = 1.6 as well as increases the on-axis response, resulting in a larger efficiency (Figure 3.13). The directivity pattern of the ring source with the concave dome at kA = 1.2 is much narrower than the one without the dome (Figure 3.16). In the high-frequency region, the effects of the domes are too complicated to be described simply.

3.3.3 Energy Flow and Pressure Distribution

The pressure distribution and energy flow around the source at several frequencies for H/A = 1.0 are shown in Figures 3.19-3.24. The circles indicate the relative magnitude of the pressure, and the arrows show both the direction of the energy flow and the square root of intensity. The figures show that the boundary condition of zero velocity distribution normal to the baffle and the surface of the dome is satisfied. The results in Figures 3.22-3.24 were calculated using the left-hand side of Eq. (3.27) inside the cavity, and the right-hand side of the same equation outside of it with the maximum order of n truncated at N.

The convex dome has the property that it diffracts the sound more in the high-frequency region. On the other hand, the concave dome does not have much effect in the high-frequency region. At kA = 10, the energy flows along the opening of the cavity as if there were no cavity (Figure

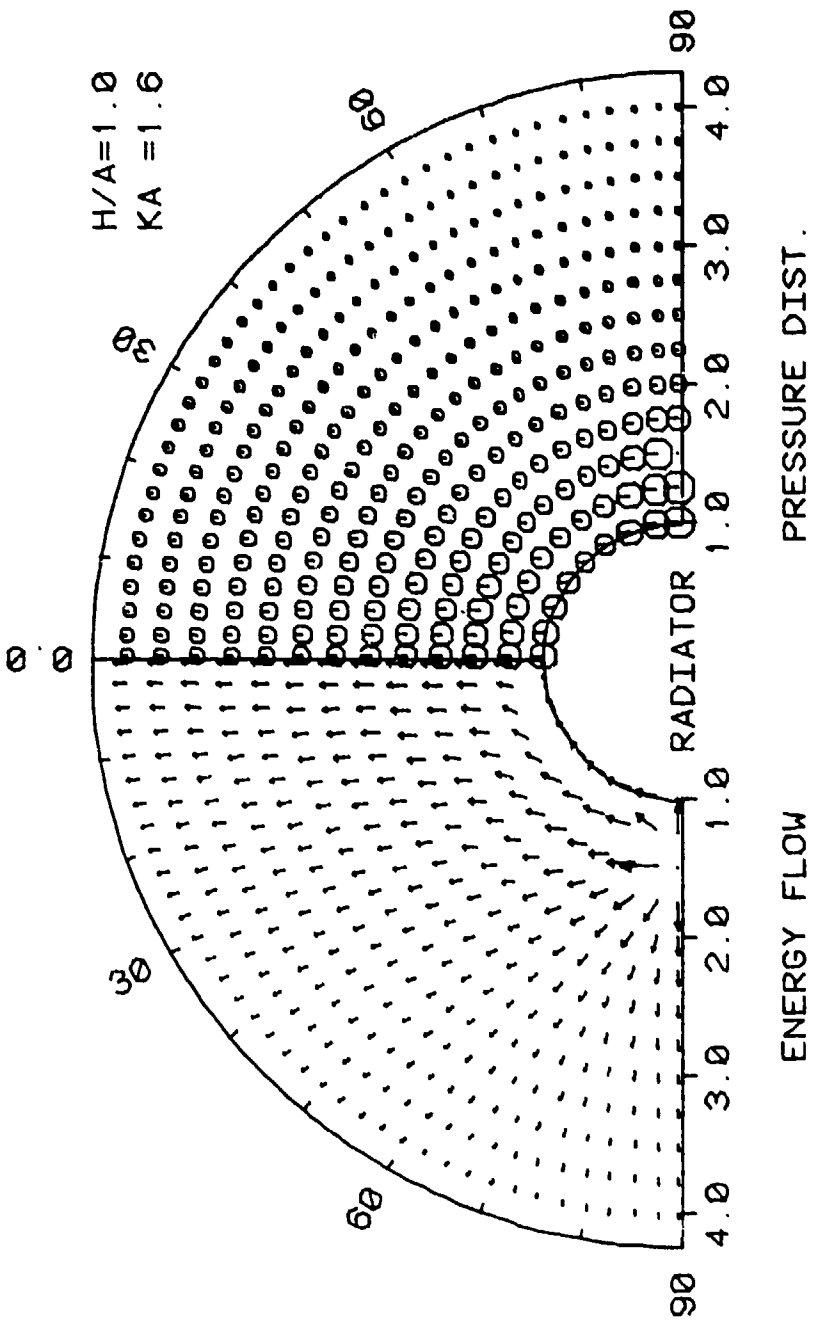

Figure 3.19 Energy flow and pressure distribution of a ring source with a concentric convex dome for H/A = 1.0 and A_1/A = 1.5 at kA = 1.6.

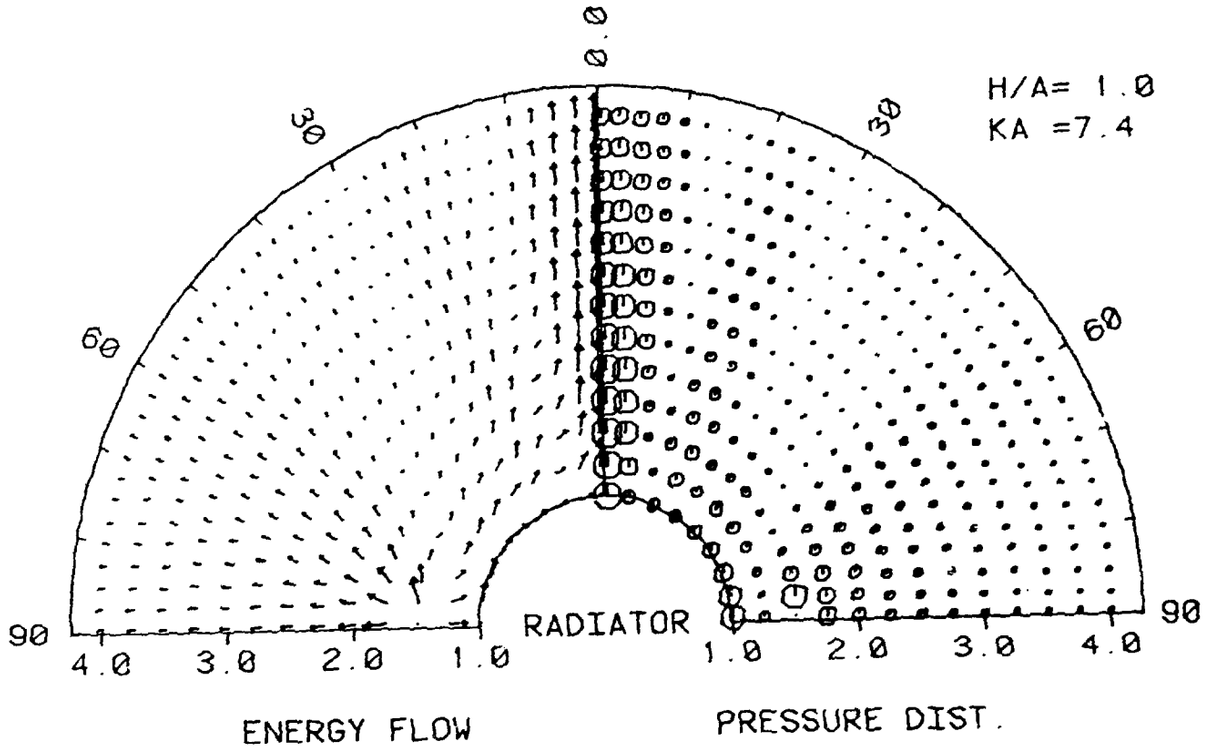

Figure 3.20 Energy flow and pressure distribution of a ring source with a concentric convex dome for H/A = 1.0 and A_1/A = 1.5 at kA = 7.4.

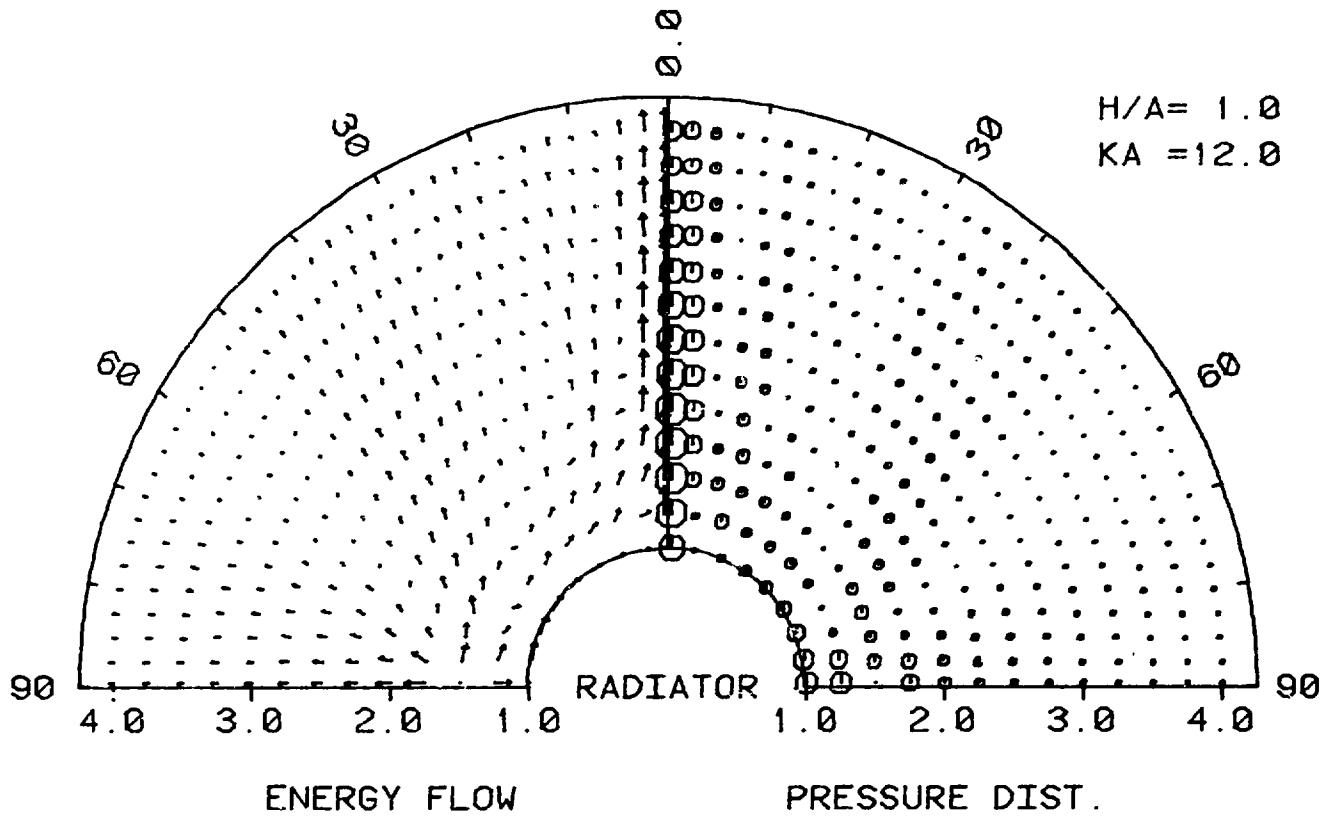

Figure 3.21 Energy flow and pressure distribution of a ring source with a concentric convex dome for H/A = 1.0 and A_1/A = 1.5 at kA = 12.0.

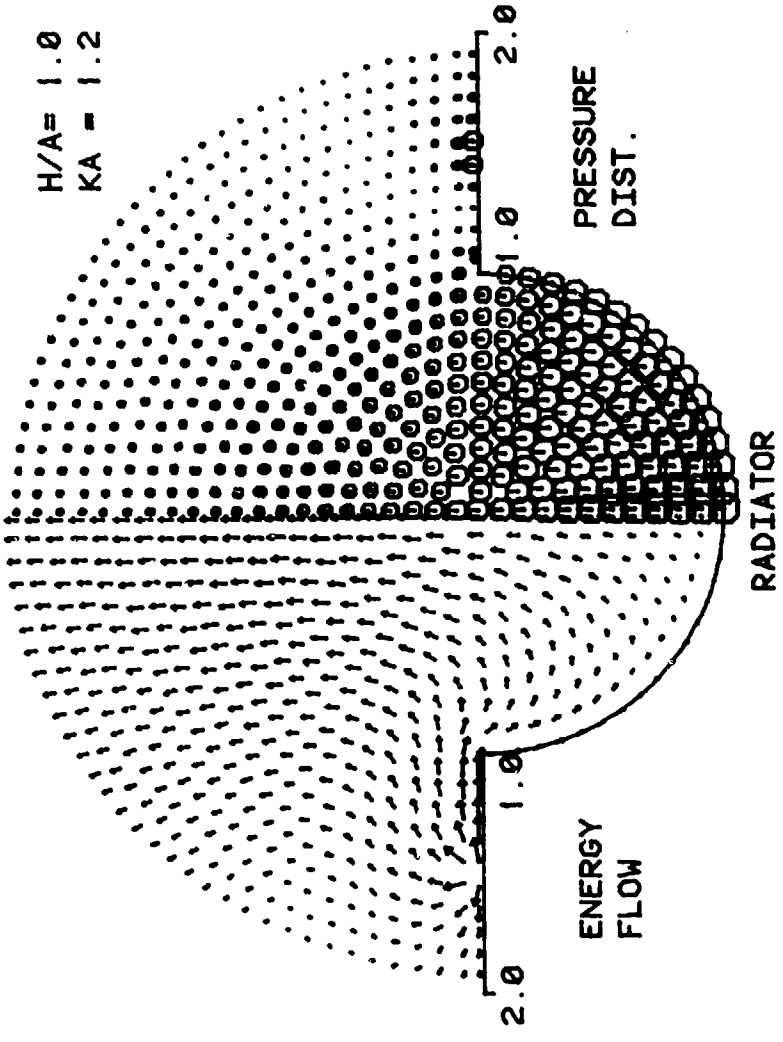

Figure 3.22 Energy flow and pressure distribution of a ring source with a concentric concave dome for H/A = 1.0 and A_1/A = 1.5 at kA = 1.2.

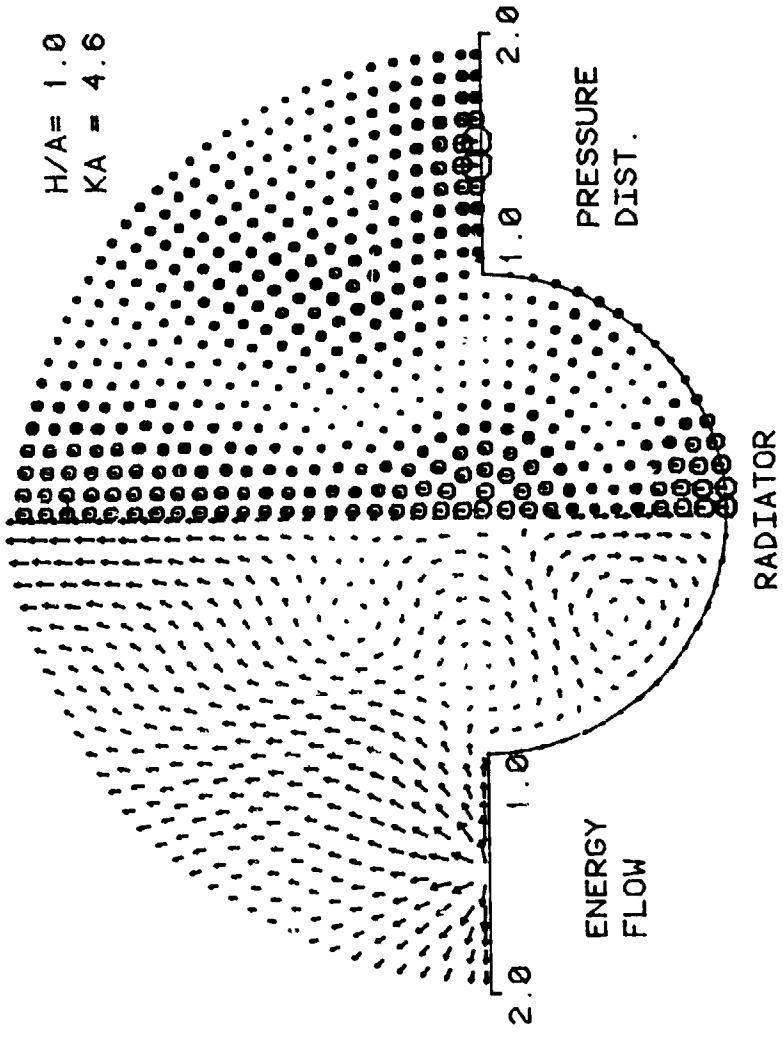

Figure 3.23 Energy flow and pressure distribution of a ring source with a concentric concave dome for H/A = 1.0 and A_1/A = 1.5 at kA = 4.6.

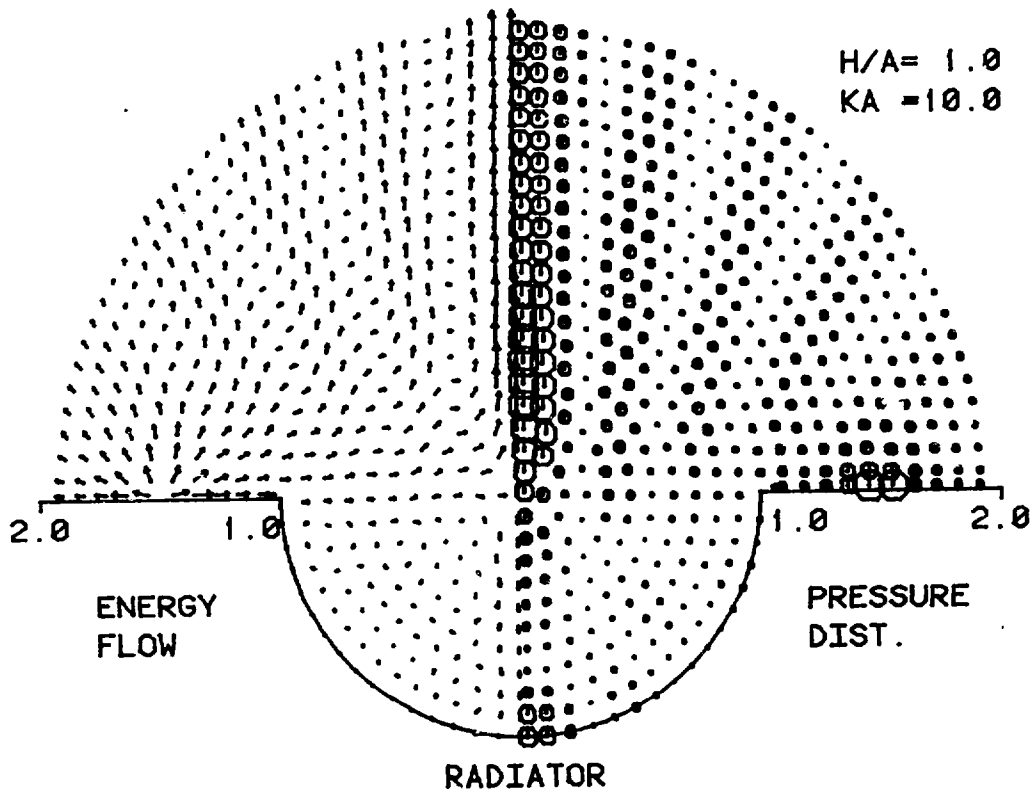

Figure 3.24 Energy flow and pressure distribution of a ring source with a concentric concave dome for H/A = 1.0 and A_1/A = 1.5 at kA = 10.0.

3.24). An interesting phenomenon is observed in Figure 3.23 which shows a couple of vortexes around the cavity at kA = 4.6. A similar phenomenon was observed by Schultz et al. in the measurement of intensity flow in a reverberant room, and he suggested as its reason a coupling between different modes [32].

Consider a sound field inside a room consisting of two tangential modes which is represented by

$$\psi(x,y) = \cos(3\pi x/l_x)\cos(\pi y/l_y) + i\cos(\pi x/l_x)\cos(2\pi y/l_y) . \tag{3.32}$$

These two modes have the same wavenumber $(35/3)^{1/2}\pi/l_x$, when $l_y/l_x = (3/8)^{1/2}$. The pressure and the particle velocity of this potential are obtained by Eqs. (2.2) and (2.3), respectively. Then, the intensity is given by Eq. (2.46).

The results calculated by Eqs. (3.32) and (2.46) are shown in Figure 3.25, which shows the circulation of energy very clearly. In the case of a single mode, there is no (time average) energy flow because the pressure and the particle velocity are 90 degrees out-of-phase with each other. If the field is of multiple modes, however, energy flows from one mode to another, causing the circulation of energy. If a semi-infinite space contains any part which is resonant, a similar phenomenon occurs. In the present case, the cavity behaves as a resonant subspace, producing a couple of vortexes of energy flow at specific frequencies.

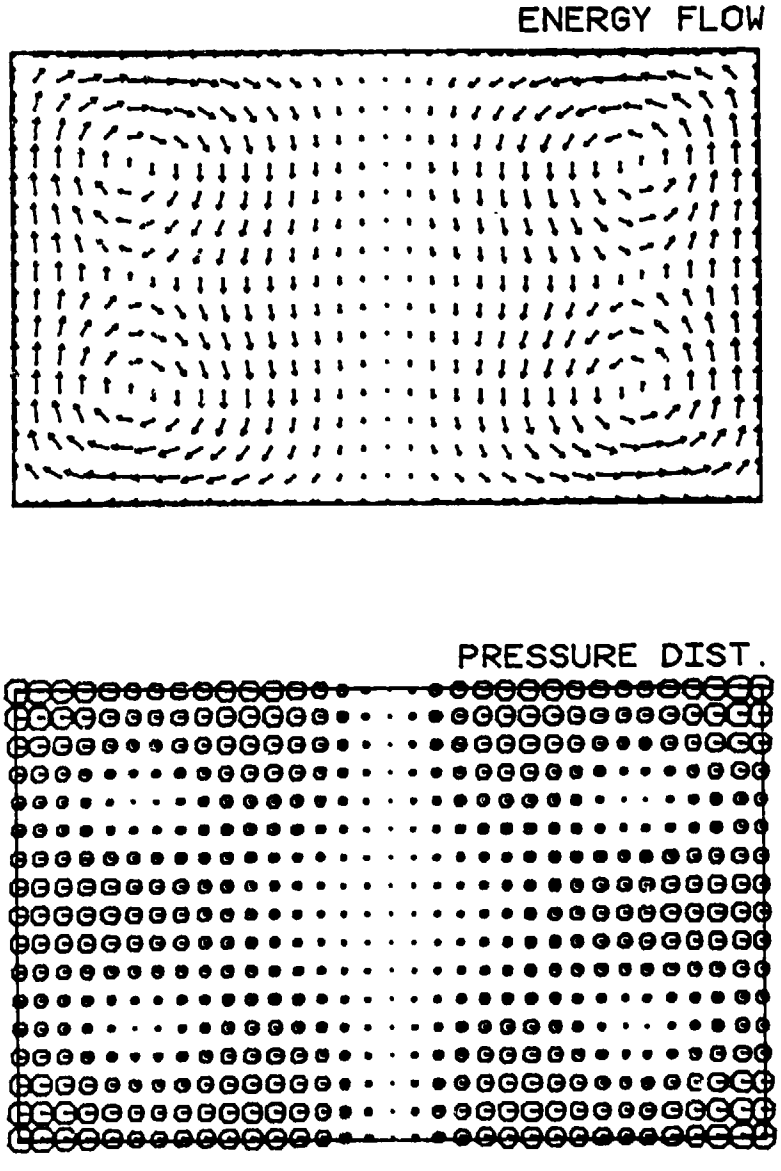

Figure 3.25 Energy flow and pressure distribution of the sound field in a rectangular room consisting of (3,1,0) and (1,2,0) modes.

CHAPTER IV

CONCLUSIONS

4.1 Remarks on the Mathematical Method

The least square error method is found to be quite successful for solving the radiation and diffraction problems. The flexibility of this method allows it to handle the complex shape of a diaphragm or a diffracting object. This was shown in the radiation and the diffraction problems by a concave dome, where the boundary condition was given on the dome surface and on the opening of the cavity. Following are the interesting techniques employed in the application of this method to the preceding problems, which worked quite well in improving the accuracy of the results:

1. The most appropriate point was chosen as the origin of the coordinates.
2. The boundary conditions were given on the imaginary surface as well as on the radiator surface.
3. New types of boundary conditions were used, which were systematically treated in the same way as the Dirichlet and Neumann boundary conditions.

The counterpart of this method is the finite element method. The advantages and disadvantages of the two methods are:

1. In this method, the sound field is expressed as a finite number of terms, each of which satisfies the wave equation. Then, the error is concentrated on the boundary surface. This may simplfy the evaluation of errors. In the finite element method, sources of error exist both on the boundary surface and in the field.
2. In this method, one must be aware of the nonuniqueness problem when he deals with a sound field including the origin. This must be avoided by a proper choice of the boundary surface. Normally, the finite element method does not have this kind of problem for radiation and diffraction problems.
3. This method is closer to the analytical method, giving better understanding of the phenomenon.
4. The largest deficiency of this method lies in the nature of the spherical Bessel and Neumann functions. One must deal with very large and very small numbers at the same time for small argument of these functions. The finite element method usually does not have this kind of problem.

4.2 Summary of Results

The main purpose of this study was to investigate the difference of radiation and diffraction phenomena due to the difference of the diaphragm shape. Using the least square error method, several important results were obtained, which may be summarized as follows:

1. The convex and concave domes have contrasting radiation and diffraction phenomena.
2. The convex dome becomes more inefficient as a radiator as H/A increases. The concave dome is more efficient for higher H/A in the range normally used for a loudspeaker.
3. The geometrical approximation method gives a good estimation of the response of the convex dome in the high-frequency region. It is a rough estimation for the concave dome in the same region.
4. The radiation resistance of the convex dome is quite smooth. The radiation resistance of the concave dome has a large peak at its first cavity resonance.
5. The radiation mass of the concave dome is equal to the sum of the mass of the fluid inside the cavity and the radiation mass of the flat piston with the same radius.
6. The radiation resistance curve closest to the +6dB/oct. line is obtained by a concave dome with H/A less than 0.5.
7. The location of the sound after the equalization of the pressure response exists at the top of the convex dome and slightly behind the opening of the cavity of the

concave dome.

8. The convex dome has a wider directivity pattern than the flat piston or the concave dome. Neither of them has any zero pressure angle, and they have similar directivity patterns in the high-frequency region.
9. The representation of sound field by the energy flow was found to be very powerful in understanding the radiation and diffraction phenomena.
10. The convex dome diffracts the sound of the concentric ring source much more than the concave dome does.
11. The results indicate that a cone-type woofer may diffract the sound emitted from a tweeter sufficiently to produce a discernible amplitude-modulated distortion.
12. In the low- to mid-frequency region, the convex dome widens the directivity pattern of the ring source, whereas the concave dome works in the opposite way.
13. The existence of vortexes of the energy flow in the resonant subspace was observed, and it was explained as the result of interaction between different modes.

4.3 Future Work

The results obtained so far are rather basic knowledge about the radiation and diffraction phenomena. For further information for the improvements of a loudspeaker, more practical aspects of the loudspeaker should be taken into account in the calculation. The following is recommended as future work.

4.3.1 Modal Vibration of the Diaphragm

The high end of the reproducing range of an actual loudspeaker is limited, mainly by the modal vibration of the diaphragm rather than the acoustical reason. The assumption of piston-like motion of the diaphragm is then not so preferable to discuss the responses in the high-frequency region of the loudspeaker. The velocity distribution of the diaphragm at its modal vibration can be obtained either by a measurement or by a theoretical calculation. Applying this velocity distribution into Eq. (2.6), the modal vibration is easily taken into account in the present method.

4.3.2 Diaphragm Shape other than a Dome

A cone-type loudspeaker usually has a straight cone with a dome-type dust cap at its center. In this case, the concave dome is not really a good approximation of the cone-type loudspeaker diaphragm. In order to investigate the radiation or the diffraction by the cone diaphragm, an exact shape must be considered, especially in the high-frequency

region. As was mentioned in Section 4.1, the present method does not necessarily depend on the dome shape. When the present method is applied to the diaphragm shape other than the convex or the concave dome, it is recommended to choose the center of a sphere as the origin of the coordinate, where the portion of the sphere represents the shape of the diaphragm most effectively.

Calculations of the characteristics of some kinds of diaphragm shapes will give the general knowledge about the relation between the diaphragm shape and several important responses such as the on-axis pressure response, radiation impedance, and directivity pattern. The interpretation of this relation will yield information about the "best" shape of the loudspeaker diaphragm, which may be different for different purposes. It is needless to say that, in the process of the evaluation of the characteristics, the psychological aspects of them must be taken into account.

4.3.3 Three-Dimensional Problem

The vibration of a diaphragm with radial modes is considered less effective on most of the radiation characteristics. Hence, the assumption of the axisymmetry of the sound field seems reasonable. When one discusses the diffraction problem, however, he should be able to deal with the problem as a three-dimensional case. The process to extend the present two-dimensional program to a three-dimensional program is rather a straightforward task. The

problems one may encounter are related to the limitation of the memory size of the central processing unit of a computer and the computation time. These limitations may be overcome by a large computer system and improved algorithms that are now available. The results will bring some more important knowledge about the diffraction phenomenon.

APPENDIX A

DERIVATION OF EQUATION (2.12) FROM EQUATION (2.11)

The condition that the variation of the functional defined by Eq. (2.9) is zero for all a_n, n=0, 1, . . ., N is the necessary and sufficient condition for the validity of Eq. (2.12). This is proved as follows:

$$J = \int_S \{\sum_{n=0}^{N} a_n \Psi_n(\zeta) - f(\zeta)\}\{\sum_{i=0}^{N} a_i^* \Psi_i^*(\zeta) - f^*(\zeta)\}dS \ . \quad (A.1)$$

Then,

$$\frac{\partial J}{\partial a_m} = \int_S \Psi_m(\zeta) \{\sum_{n=0}^{N} a_n^* \Psi_n^*(\zeta) - f^*(\zeta)\}dS \quad (A.2)$$

and

$$\frac{\partial J}{\partial a_m^*} = \int_S \Psi_m^*(\zeta) \{\sum_{n=0}^{N} a_n \Psi_n(\zeta) - f(\zeta)\}dS = \left(\frac{\partial J}{\partial a_m}\right)^* \ . \quad (A.3)$$

Hence,

$$\delta J_m = \frac{\partial J}{\partial a_m} \delta a_m + \frac{\partial J}{\partial a_m^*} \delta a_m^* = 2 \, \mathrm{Re}\{\left(\frac{\partial J}{\partial a_m}\right) \delta a_m\} \ . \quad (A.4)$$

In order for δJ_m to be zero for arbitrary δa_m, Eq. (A.2) and equivalently Eq. (A.3) must be zero. Rewriting Eq. (A.3), one obtains Eq. (2.12) [assuming $q(\zeta) = 1.0$ for simplicity].

$$\int_S \sum_{n=0}^{N} a_n \Psi_n(\zeta) \Psi_m^*(\zeta) dS = \int_S \Psi_m^*(\zeta) f(\zeta) dS$$

$$m = 0, 1, \ldots, N \ . \quad (A.5)$$

APPENDIX B

ANOTHER SOLUTION TO RADIATION PROBLEM FROM A CONVEX DOME

Another solution rather than the one discussed in Section 2.2.3 is possible. The details of this method and its deficiencies are discussed here.

The sound field is expressed in terms of the spherical Hankel functions and Legendre functions with the origin at O in Figure 2.1:

$$\psi(r',\theta') = \sum_{n=0}^{N} a_{2n} h_{2n}(kr') P_{2n}(\cos\theta') , \qquad (B.1)$$

where only the even orders of terms are used because of the symmetry of the sound field. The normal velocity distribution $\underline{u}_n(\theta)$ is obtained by differentiating Eq. (B.1) in terms of r such as

$$\underline{u}_n(\theta) = - \left(\frac{\partial\psi}{\partial r'} \cdot \frac{\partial r'}{\partial r} + \frac{\partial\psi}{\partial\theta'} \cdot \frac{\partial\theta'}{\partial r}\right) . \qquad (B.2)$$

The relationship among r′, θ', r, and θ are given by

$$r'^2 = r^2 + z_o^2 - 2rz_o\cos\theta \qquad (B.3)$$

and

$$(r\cos\theta - z_o)\tan\theta' = r\sin\theta , \qquad (B.4)$$

where

$$z_o = R\cos\theta_o \,. \tag{B.5}$$

From Eqs. (B.3) and (B.4), one obtains

$$\frac{\partial r'}{\partial r} = (r - z_o\cos\theta)/r' = \cos(\theta' - \theta) \tag{B.6}$$

and

$$\frac{\partial \theta'}{\partial r} = -\sin(\theta' - \theta)/r' \,. \tag{B.7}$$

Substitution of Eqs. (B.6) and (B.7) into Eq. (B.2) gives

$$\underline{u}_n(\theta) = -\sum_{n=0}^{N} a_{2n}[kh_{2n}(kr')P_{2n}(\cos\theta')\cos(\theta' - \theta) + h_{2n}(kr')P'_{2n}(\cos\theta')\sin\theta'\sin(\theta' - \theta)/r'] \,. \tag{B.8}$$

Now, $\Psi_{2n}(\theta)$ and $f(\theta)$ are defined such as

$$\Psi_{2n}(\theta) = -[kh_{2n}(kr')P_{2n}(\cos\theta') + h_{2n}(kr')P'_{2n}(\cos\theta')\sin\theta'\sin(\theta' - \theta)/r'] \tag{B.9}$$

and

$$f(\theta) = U_o\cos\theta. \tag{B.10}$$

Then, the unknown coefficients a_n, n = 0, 1, . . ., N are obtained by solving (N+1) simultaneous equations:

$$\sum_{n=0}^{N} a_{2n}\left[\int_0^{\theta_o} \Psi^*_{2m}(\theta)\Psi_{2n}(\theta)2\pi R^2\sin(\theta)d\theta\right] = \int_0^{\theta_o} \Psi^*_{2m}(\theta)U_o\cos(\theta)2\pi R^2\sin(\theta)d\theta$$

$$m = 0, 1, 2, \ldots, N \,. \tag{B.11}$$

This method looks simple because it does not require the introduction of the imaginary surface. But it was found that this method has two basic problems. Firstly, the convergence of Eq. (B.8) to Eq. (B.10) is very slow. This is because the origin O is not suitable for the expansion of sound field in the form of Eq. (B.1). For the radiation problem from a portion of a sphere, it seems reasonable to choose a coordinate system with its origin at the center of the sphere. Secondly, the argument kr′ becomes small near the z-axis for small H/A ratio. The real and imaginary parts of the spherical Hankel function become very small and very large, respectively, for small argument when the order n become large. This causes the underflow and overflow problem in the process of numerical computation. This nature of the spherical Hankel function prohibits from taking higher order of n when one tries to have good approximation of Eq. (B.8) to Eq. (B.11).

APPENDIX C

NONEXISTENCE AND NONUNIQUENESS PROBLEMS OF A SERIES EXPANSION OF THE SOUND FIELD

i. Radiation From a Sphere

The nonexistence and nonuniqueness properties of the solution of the sound radiation problems were discussed theoretically by Copley [11] and Schenck [12]. These properties are discussed here focussing especially on the series expansion of the sound field inside and outside the sphere.

The velocity potential outside the sphere with only an outgoing axisymmetric wave can be expressed by

$$\psi(r,\theta) = \sum_{n=0}^{N} a_n h_n(kr) P_n(\cos\theta) \ . \qquad (C.1)$$

Generally, the boundary condition is given either by the pressure distribution or by the normal velocity distribution such as $P(\theta)$ or $U(\theta)$ on the surface of the sphere. Then,

$$P(\theta) = \sum_{n=0}^{N} p_n \ . \ P_n(\cos\theta) \qquad (C.2)$$

and

$$U(\theta) = \sum_{n=0}^{N} u_n \ . \ P_n(\cos\theta) \ , \qquad (C.3)$$

where

$$p_n = (n + 1/2) \int_0^{\pi} P(\theta) P_n(\cos\theta) \sin(\theta) d\theta \qquad (C.4)$$

and

$$u_n = (n + 1/2) \int_0^{\pi} U(\theta) P_n(\cos\theta) \sin(\theta) d\theta \ . \qquad (C.5)$$

Comparing Eq. (C.1) with Eq. (C.2) or (C.3), one obtains

$$a_n = P_n / j\omega\rho h_n(kR) \qquad (C.6)$$

or

$$a_n = -u_n / kh_n'(kR) \ . \qquad (C.7)$$

Now, $h_n(x)$ and $h_n'(x)$ can never be zero for $x \neq 0$, because the real part $j_n(x)$ and imaginary part $n_n(x)$ of $h_n(x)$, and their derivatives satisfy the following equation [33]:

$$j_n(x) \cdot n_n'(x) - n_n(x) \cdot j_n'(x) = 1/x^2 \ . \qquad (C.8)$$

Thus, a_n is uniquely determined for any prescribed pressure distribution or normal velocity distribution.

But, when the velocity potential is expressed such as (corresponding to the solution by Green's function [34])

$$\psi(r,\theta) = \sum_{n=0}^{N} a_n j_n(kR) h_n(kr) P_n(\cos\theta) \ , \qquad (C.9)$$

the unknown coefficient a_n is given by

$$a_n = P_n / j\omega j_n(kR) h_n(kR) \qquad (C.10)$$

or

$$a_n = -u_n/kj_n(kR)h_n'(kR) \quad . \tag{C.11}$$

In this case, the coefficient defined by Eq. (C.10) or Eq. (C.11) does not exist at the frequencies where $j_n(kR) = 0$.

ii. Sound Field Inside a Sphere

The velocity potential inside a sphere is expressed by

$$\psi(r,\theta) = \sum_{n=0}^{N} a_n j_n(kr) P_n(\cos\theta) \quad . \tag{C.12}$$

Corresponding to Eqs. (C.6) and (C.7), a_n is given by

$$a_n = p_n/j\omega\rho j_n(kR) \tag{C.13}$$

or

$$a_n = -u_n/kj_n'(kR) \quad . \tag{C.14}$$

Then, the coefficient a_n obtained from Eq. (C.13) or Eq. (C.14) is divergent at the characteristic frequencies, where $j_n(kR) = 0$ or $j_n'(kR) = 0$ if p_n or u_n is not equal to zero, respectively. If p_n or u_n is equal to zero at the characteristic frequencies, the n^{th} term must be excluded from the series expansion. If it is included even at these frequencies, the solution is not unique since a_n can take any finite value without affecting the boundary condition. This kind of nonuniqueness or nonconvergence problem may happen if Eq. (C.12) is employed and if the boundary condition is given on the surface of the sphere.

APPENDIX D

ACOUSTIC CENTER OF A LINE SOURCE

The acoustic center of a line source which is lying in the z direction between z = 0 and z = l_o is calculated as follows.

The far-field on-axis pressure response of the source, which is normalized to a point source with the same source strength at z = 0, is given by

$$p = \frac{1}{l_o}\int_0^{l_o} e^{ikz}dz$$

$$= [\sin kl_o + i(1 - \cos kl_o)]/kl_o$$

$$= \sin(\Omega)e^{i\Omega}/\Omega \ , \qquad (D.1)$$

where $\Omega = kl_o/2$.

The imaginary part of a minimum phase network having the real part of Eq. (D.1) is obtained using the Hilbert transform such as (using the integral formula in [35])

$$I_m(p_{min}) = \int_{-\infty}^{\infty} \frac{\sin 2\Omega'}{2\Omega'} \frac{d\Omega'}{\pi(\Omega' - \Omega)}$$

$$= (\cos 2\Omega - 1)/2\Omega \ . \qquad (D.2)$$

Then, the total response of the minimum phase network is given by

$$p_{min} = \sin(\Omega)e^{-i\Omega}/\Omega. \qquad (D.3)$$

The phase response $\phi_{allpass}$ defined by Eq. (2.46) is given by the difference of phase responses of Eq. (D.1) and Eq. (D.3) such as

$$\phi_{allpass}(\Omega) = \Omega - (-\Omega) = kl_o . \qquad (D.4)$$

Dividing Eq. (D.4) by k one obtains the acoustic center l_o which is constant with respect to frequency.

REFERENCES

[1] J. W. R. Rayleigh, The Theory of Sound, Vol. 2, Dover, New York (1945).

[2] H. Lamb, Hydrodynamics, Dover, New York (1945).

[3] P. M. Morse and K. U. Ingard, Theoretical Acoustics, pp. 332-356, McGraw-Hill, New York (1968).

[4] J. A. Stratton, P. M. Morse, L. J. Chu, J. D. C. Little, and F. J. Corbato, Spheroidal Wave Functions, Wiley and Technology Press of M.I.T., New York (1956).

[5] C. Flammer, Spheroidal Wave Functions, Stanford University Press, Stanford, California (1957).

[6] K. Ikegaya, "Some characteristics of the sphere and the circular disk as models of acoustic apparatus in sound field," Electrical Communication Laboratory's Technical Journal, Nippon Telegraph and Telephone, Vol. 7, pp. 127-188 (1958, in Japanese).

[7] L. H. Chen and D. G. Schweikert, "Sound radiation from an arbitrary body," J. Acoust. Soc. Am., Vol. 35, pp. 1626-1632 (1963).

[8] J. M. McCormick and M. L. Baron, "Sound radiation from submerged cylindrical shells of finite length," Trans. A.S.M.E. Ser. B, Vol. 87, pp. 393-405 (1965).

[9] G. Chertock, "Sound radiation from vibrating surfaces," J. Acoust. Soc. Am., Vol 36, pp. 1305-1313 (1964).

[10] L. G. Copley, "Integral equation method for radiation from vibrating bodies," J. Acoust. Soc. Am., Vol. 41, pp. 807-816 (1967).

[11] L. G. Copley, "Fundamental results concerning integral representations in acoustic radiation," J. Acoust. Soc. Am., Vol. 44, pp. 28-32 (1968).

[12] H. A. Schenck, "Improved integral formulation for acoustic radiation problems," J. Acoust. Soc. Am., Vol. 44, pp. 41-58 (1968).

[13] W. Williams, N. G. Parke, D. A. Moran, and C. H. Sherman, "Acoustic radiation from a finite cylinder," J. Acoust. Soc. Am., Vol. 36, pp. 2316-2322 (1964).

REFERENCES (continued)

[14] E. Skudrzyk, The Foundations of Acoustics, pp. 400-407, Springer-Verlag, New York (1971).

[15] F. H. Fenlon, "Calculations of the acoustic radiation field at the surface of a finite cylinder by the method of weighted residuals," Proc. of the IEEE, Vol. 57, pp. 291-306 (1969).

[16] J. T. Hunt, M. R. Knittel, C. S. Nichols, and D. Barach, "Finite element approach to acoustic radiation from elastic structures," J. Acoust. Soc. Am., Vol. 55, pp. 269-280 (1974).

[17] S. Ohie, H. Suzuki, and T. Shindo, "Sound radiation from a concave radiator in an infinite baffle," J. Acoust. Soc. Jpn., Vol. 34, pp. 429-435 (1978, in Japanese).

[18] T. Shindo, N. Kyono, O. Yashima, T. Yamabuchi, and Y. Kagawa, "The role of the dust cap in the cone-type loudspeaker," Preprint for the 63rd Convention of Audio Eng. Soc., Los Angeles (1979).

[19] S. Morita, N. Kyono, S. Sakai, T. Yamabuchi, and Y. Kagawa, "Acoustic radiation of a horn loudspeaker by the finite element method - a consideration of the acoustic characteristics of horns," J. Audio Eng. Soc., Vol. 28, pp. 482-489 (1980).

[20] J. J. Faran, "Sound scattering by solid cylinders and spheres," J. Acoust. Soc. Am., Vol. 23, pp. 405-418 (1951).

[21] R. Hickering and N. M. Wang, "Scattering of sound by a rigid movable sphere," J. Acoust. Soc. Am., Vol. 39, pp. 276-279 (1966).

[22] A. J. Rudgers, "Separation and analysis of the acoustic field scattered by a rigid sphere," J. Acoust. Soc. Am., Vol. 52, pp. 234-246 (1972).

[23] M. C. Junger, "The concept of radiation scattering and its application to reinforced cylindrical shells," J. Acoust. Soc. Am., Vol. 25, pp. 899-903 (1953).

REFERENCES (continued)

[24] R. D. Doolittle and H. Uberall, "Sound scattering by elastic cylindrical shells," J. Acoust. Soc. Am., Vol. 39, pp. 272-275 (1965).

[25] R. D. Spence and S. Granger, "The scattering of sound from a prolate spheroid," J. Acoust. Soc. Am., Vol. 23, pp. 701-706 (1951).

[26] J. E. Burke, "Scattering by penetrable spheroids," J. Acoust. Soc. Am., Vol. 43, pp. 871-875 (1968).

[27] J. T. Hunt, M. R. Knittel, C. S. Nichols, and D. Barach, "Finite element approach to acoustic radiation from elastic structures," J. Acoust. Soc. Am., Vol. 57, pp. 287-299 (1975).

[28] C. H. Wilcox, "A generalization of theorems of Rellich and Atkinson," Proc. Am. Math. Soc., Vol. 7, pp. 271-276 (1956).

[29] M. Becker, The Principles and Applications of Variational Method, M.I.T. Press, Cambridge, Mass. (1964).

[30] G. Arfken, Mathematical Methods for Physicists, Academic Press, New York (1970).

[31] A. Papoulis, The Fourier Integral and Its Application, pp. 192-212, McGraw-Hill, New York (1962).

[32] T. J. Schultz, P. W. Smith Jr., and C. I. Malme, "Measurement of acoustic intensity in reactive sound field," J. Acoust. Soc. Am., Vol. 57, pp. 1263-1268 (1975).

[33] E. Skudrzyk, The Foundations of Acoustics, pp. 690-693, Springer-Verlag, New York (1971).

[34] P. M. Morse and K. U. Ingard, Theoretical Acoustics, pp. 352-353, McGraw-Hill, New York (1968).

[35] I. S. Gradshteyn and I. M. Ryzhik, Tables of Integrals, Series, and Products, p. 407, Academic Press, New York (1965).

DISTRIBUTION LIST FOR TM 81-110

Commander (NSEA 0342)
Naval Sea Systems Command
Department of the Navy
Washington, DC 20362 — Copies 1 and 2

Commander (NSEA 9961)
Naval Sea Systems Command
Department of the Navy
Washington, DC 20362 — Copies 3 and 4

Defense Technical Information Center
5010 Duke Street
Cameron Station
Alexandria, VA 22314 — Copies 5 through 10